DESIGN AND SYNTHESIS OF PHENOTHIAZINE-BASED FLUORESCENT PROBE FOR DIFFERENTIAL DETECTION OF NORMAL AND OXIDIZED BSA

Thesis submitted in partial fulfilment for the
degree of

Master of Science

as a part of the

Integrated Ph. D. program
(Chemical Science)

by

Harshit Arora

Bioorganic Chemistry Laboratory, New Chemistry Unit
Jawaharlal Nehru Centre for Advanced Scientific Research
(*A Deemed University*)
Bengaluru, India.

March 2019

DEDICATED TO PROF. T. GOVINDARAJU
AND MY LAB GROUP

Prof. T. Govindaraju
Associate Professor
Bioorganic Chemistry Laboratory
New Chemistry Unit, ICMS
Jawaharlal Nehru Centre for
Advanced Scientific Research
Bengaluru, India-560064

Email: tgraju@jncasr.ac.in
Phone: +91-080-2208-2969
http://www.jncasr.ac.in/tgraju/

CERTIFICATE

I hereby certify that the work described in this thesis entitled, "**Design and synthesis of bespoke phenothiazine-based fluorescent probe for differential detection of normal and oxidized BSA**" has been carried out by Mr. Harshit Arora under my supervision at the Bioorganic Chemistry Laboratory, New Chemistry Unit, Jawaharlal Nehru Centre for Advanced Scientific Research, Bengaluru, India and that it has not been submitted elsewhere for the award of any degree or diploma.

Prof. T. Govindaraju
(Research Supervisor)

DECLARATION

I hereby declare that the work enveloped in this thesis entitled, "**Design and synthesis of bespoke phenothiazine-based fluorescent probe for differential detection of normal and oxidized BSA**" has been the result of constant investigations carried out by me under the supervision of **Prof. T. Govindaraju** at the New Chemistry Unit, Jawaharlal Nehru Centre for Advanced Scientific Research, Bengaluru, India and the work has not been submitted elsewhere for the award of any degree or diploma.

In keeping with the general practice in reporting the scientific observations, due acknowledgement has been made whenever the work described is based on the findings of other investigators. Any omission that might have occurred due to oversight or error in judgement is regretted.

Harshit Arora

ACKNOWLEDGEMENT

It would be quite unjust if my supervisor is not thanked at the first place. ***Professor T. Govindaraju****, Bioorganic Chemistry Laboratory, New Chemistry Unit, JNCASR, has ever been a benevolent human being besides possessing a high degree of patience in keeping up as a guide to several master's and PhD students. The written thesis is a testimony of the help and the timely guidance he has been showering upon me for my period of stay at his laboratory.*

I would like to extend a heartfelt thanks to ***Professor C. N. R. Rao****, FRS for his words of wisdom at most of the academic events. His speeches are worth remembering for the stories told are full of encouragement and motivation to climb even higher ladders. His presence has always given me immense inspiration to indulge in active research. I also thank him for providing the infrastructure and facilities to carry out my research work at NCU, JNCASR.*

Professor H. Ila*,* ***my fairy godmother****, can never be re-payed just by thanking her in limited words. She is the reason why my journey at JNCASR has been so smooth and filed with laughter and happiness. I would like to thank her for her precious time that she has spent with me, advising me like a mother and guiding me whenever I had gone wrong. I have never hesitated visiting her chamber for any kind of discussion and she has ever welcomed me with open arms. I wish wherever I go in future, I get a figure like you professor.*

I am thankful to Dr. K. Rajasekhar, Miss Y. V. Suseela, Dr. Bappaditya Roy, Dr. Pardhasarthi, Dr. Lakshmipriya, Dr. Balachandra, Dr. Komala, Dr. Kalpana, Dr. Aparna, Dr. Jyotish, Dr. Mahesh, Dr. Shadab, Mr. Sumon, Mr. Saurav, Mr. Debasis, Mr. Biswanath, Mr. Ashish, Mr. Satyajeet, Dr. Madhu, Miss Shradhya, Miss Minal, Mr. Madhav, Miss Reshma, Mr. Gopal, Miss Nikita and other trainees at the Bioorganic Chemistry Laboratory for their help in various capacities, co-operation and maintaining cheerful atmosphere in the lab.

My special thanks to Miss Y. V. Suseela and Mr. Sumon Pratihar for their constant support and fruitful discussions at various points in time.

I shall be ever thankful to my Int. PhD professors; Prof. H. Ila, Prof. Aloknath Chakraborty, Prof. S. Balasubramanian, Prof. T. Govindaraju, Prof. Shridhar Rajaram, Prof. A. Sundaresan, Prof. Chandrabhas Narayana, Prof. Tapas. K. Maji, Prof. Eswaramoorthy, Prof. Jayanta Haldar, Prof. Subi J. George, Prof. Ranjani Viswanatha, Dr. Sebastian C Peter, Dr. Kanishka Biswas, Dr. Sarit S. Agasti, Dr. Premkumar for their valuable courses.

I would like to thank my Integrated Ph.D. batchmates of 2016 especially Miss Geetika Dhanda, Miss Sushmita Chandra, Miss Aditi Chiring, Mr. Amit, Miss Pragya Arora, Miss Raagya Arora, Miss Chhavi Saini, for extending their help and cooperation for the successful completion of my project work besides being a major reason for my awesome life at the JNCASR hostel and outside, in Bengaluru. Moreover, I would like to mention special regards to Mr. Shantanu Aggarwal, Miss Palak Agrawal, Miss Ananya Mishra, Miss Ekashmi, Miss Shikha, Miss Meenakshi Pahwa, Mr. Tirath Raj Dwivedi and all my close seniors for making JNCASR a beautiful experience altogether.

My thesis would have been an incomplete document if I had not received timely support from Mr. Shiv Kumar (HRMS) and Mr. Deepak and Mr. Mahesh (NMR). Furthermore, I would like to thank the library facilities for providing a peaceful and well-equipped atmosphere, especially till mid-night. I am thankful to the Hostel (NVSH and Main building) facilities for my easy stay at JNCASR.

I would like to mention my gratitude for ***Dr. Satish Kumar****, St. Stephen's College for supporting me in every case,* ***Miss Archana Khare*** *for motivating me to pursue chemistry at City Montessorie School,* ***Mrs. Kanika Malik*** *for being the coolest teacher and an endearing friend, and all the teachers at school and undergraduate levels for ever standing beside me.*

My family has been my spinal cord while my MS program at JNCASR. Hence, I owe my success and every moment of achievement to them. Especially, my mother; ***Mrs. Geeta Arora*** *without whom I would never have accomplished even the slightest of what I have today. I am deeply indebted to her for my entire life and possibly, would be in more lives to come. My father* ***Mr. Ramesh Kumar Arora****, a person so deeply rooted in moral values. I have learnt a lot from him while growing up and I wish I can practice his good qualities and carry forward to the generations to come. 'I love you Ma and Papa'*

*Besides, I would like to thank **Mrs. Ruby Malik** for being the nicest sister, **Miss Khushi Malik** for her lovely existence in my life. Particularly, I would like to thank **Mr. Harish Kumar Wadhwa**, **Mrs. Rita Wadhwa**, **Miss Aditi Wadhwa** and my brother, **Mr. Ankur Wadhwa** with whom I shall be pursuing my future endeavors in a foreign land.*

*The acknowledgement would be complete only when I thank some of the dearest members of my extended family particularly my lovely aunties namely, **Mrs. Tarun Sikka** and **Mrs. Gurmeet Kaur**, my fatherly uncles; **Mr. Anil Sikka** and '**Kali Chacha'**, lastly, the most interesting character; **Mrs. Gurbani Gujral Sikka** for teaching me business and street-smart behavior.*

Harshit Arora

PREFACE

This thesis entitled, "**Design and synthesis of bespoke phenothiazine-based fluorescent probe for differential detection of normal and oxidized BSA**" has been divided in three chapters

Chapter One: **Introduction**

Brief overview of fluorescence and basic underlying mechanisms that are studied while developing a fluorescent probe for imaging biological or biologically potential analytes.

Chapter Two: **Design and syntheses of phenothiazine-based molecular probes**

Describes the set of reaction schemes followed for the simple syntheses of the phenothiazine-based fluorescent probes. The reactions are chosen to be simple for their real-time applications in any industrial organization or for later developing as potential imaging tools in clinics.

Chapter Three (part A): **A red-NIR selective fluorescent molecular sensor for BSA**

Spectroscopic investigations of the designed probe for its photophysical properties in solution. Moreover, the chapter particularly highlights the probe's selective interactions with BSA.

Chapter Three (part B): **Differential sensing of oxidized BSA from BSA in far red-NIR window**

Spectroscopic investigations of the designed probe for its differential interactions with pristine BSA and oxidized form of BSA. The chapter is an inspiration from Domingues. et al. reported work and is hypothesized based on the facts presented in their report.

CONTENTS

Introduction

Chapter One

1.1 Introduction

Our universe is a complex collection of several different elements, ionic species, organic-inorganic molecules etc. that are in continuous equilibrium of chemical reactions. Living organisms and their surrounding environment communicate with each other via numerous principle chemical pathways namely, transfer of electron, acid-base chemistries, metal-ligand interactions and catalytic transformations. Understanding the abovementioned phenomena by which the living organisms communicate and survive is not only an interesting challenge but also an opportunity for the chemists worldwide to develop novel tools to study the dynamism of the biological relationships at cellular level. In this regard, organic chemists in association with chemical biologists have been trying to develop simple and effective analytical methods which would allow real-time examination of the intact biological systems with spatial as well as temporal control.[1] Molecular imaging has been defined as an in vivo characterization technique to measure biological phenomena at cellular and molecular level exploiting the advantages of the synthetic molecular probe design besides the per se imaging instrumentation.[2] This technology enables us to visualize bio-macromolecules and ions in the cells, tissues and organisms with the basic aim of acquiring information about the biological effects of the analytes under interest. Molecular probes contain a recognition site and a conjugated signaling subunit in their structure, both of which work in symbiosis to yield a specific read out signal from the system under study.[3] The primary purpose of the binding unit is to recognize a target analyte and bind the entire molecule to the recognized target. This is achieved either of the several mechanisms including ionic interactions, covalent interactions, van der Waals interactions or hydrophobic interactions.[4-5] As a consequence, these interactions predispose the molecular structure to yield either an electronic or optical signal which is further displayed either through colorimetrically, fluorometrically or electrochemically.[6] An efficient molecular probe must be highly selective and sensitive towards a characteristic target with respect to the others in the proximity. Hence, to achieve these qualities in a probe, it is essential to combine the recognition process with a smart photophysical behavior from a reporting unit.

Fluorescence imaging techniques have become very useful among the pool of existing technologies to monitor several biological phenomena, ranging from simple to complex processes. Moreover, fluorescent molecular probes are preferred owing to their simplicity and

high sensitivity per se, for probing different biologically important species like metal ions, anions, reactive radicals (ROS and RNS), proteins, nucleic acids (NAs), organelles etc. *in vitro* and *in vivo*.[7-8] The modern-day spectroscopy and the growing advancements in the existing bioimaging techniques such as fluorescence light microscopy, two-photon microscopy and confocal microscopy have ever been motivating the scientist to continue developing and modifying their designs for monitoring intra- and extracellular events with high chemo-selectivity.[9-11] Colorimetric molecular probes have gained a great impetus for these allow 'naked-eye' detection in a simplistic and economical manner, providing qualitative and quantitative information.[12-13] A fluorescent or colorimetric molecular probe can be defined as a probe which undergoes structural or electronic reorganization upon binding to a target analyte thereby generatig either fluorescence or color change in response to the interaction. The underlying principle of the molecular probe design is to optimize signal to background ratio. This is important because in certain cases background signal might be mistaken for the receptor-analyte signal owing to their higher intensity than the one from receptor-analyte interaction. Therefore, certain optimizations are required to be done at organism, organ, cellular and atomic levels to minimize the effect of the background fluorescence.[14-15] Moreover, near-infrared (NIR) molecular probes have been a much sought-after tools these days because they suffer the least from the background emission signal which happens to be at lower wavelength than the near-infrared emission from the receptor-analyte interactions.[1, 16-17]

1.2 Real-time spectral window for fluorescence imaging

Optical detection and imaging depend on photons ranging in the wavelength from the visible (450 nm) to the near-infrared (1500 nm).[18-19] This broad spectral range can easily be compartmentalized for different applications. The shorter wavelength spectral profile, ranging from 400 nm to 600 nm is basically limited to imaging surface or intermediary subsurface phenomena. On the opposite side, the longer wavelength spectral profile, also called as NIR profile is the most appropriate spectral window for the visualization of the sample's deeper structure i.e. it can penetrate deeper into the tissues (Figure 1).[20] The reason is simple, human skin is comprised of a range of chromophores which scatter in a highly wavelength dependent manner. The scattering properties of tissue are due to attenuation properties intrinsic to the

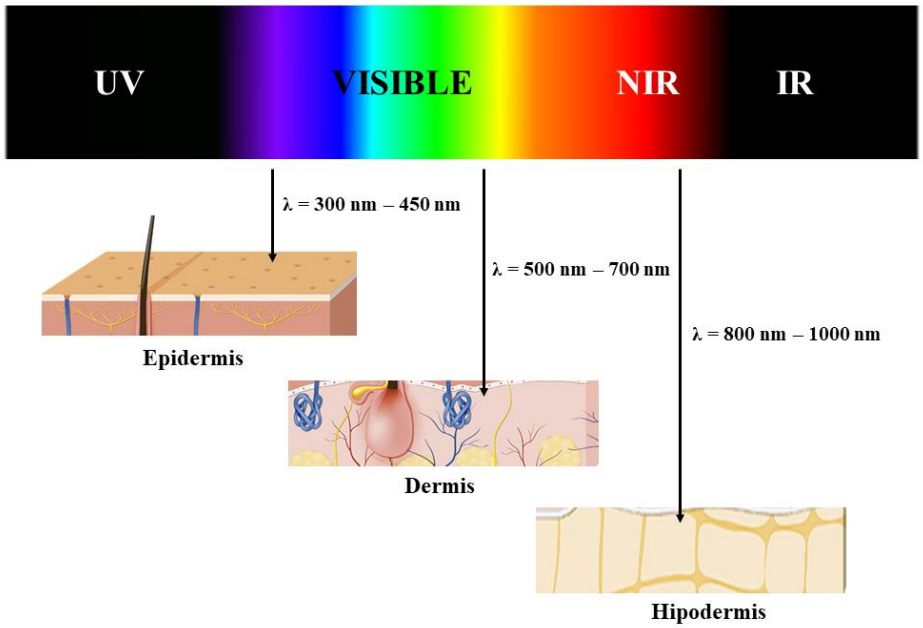

Figure 1. Schematic representation of the spectral profile, ranging from UV to IR wavelength and their characteristic tissue penetration power

chromophore and to the size of the particles within the tissue which also governs the type of scattering that occurs, namely Mie or Rayleigh scattering. Scattering leads to light dispersion in the tissue and the eventual reduction in the energy density with increasing depth. To validate, it has well been looked by several simulations and theoretical studies that increasing the wavelength of the source, enhances its tissue penetration in various biological samples.

1.3 Biologically potential targets

Till date, there have been multiple reports on the syntheses of several imaging agents for numerous bio-active targets.[21] These targets are mainly selected on the basis of their critical functions in several important biological cycles. While the basic targets remain the metal ions, anions, ROS and RNS, the most important biological targets include functional proteins, enzymes and NAs. These are of paramount importance because many of these targets are either associated directly with a biological dysfunctional cycle or directly involved in the malfunctioning of a healthy life cycle. Some of the potential targets are listed below (Figure 2).

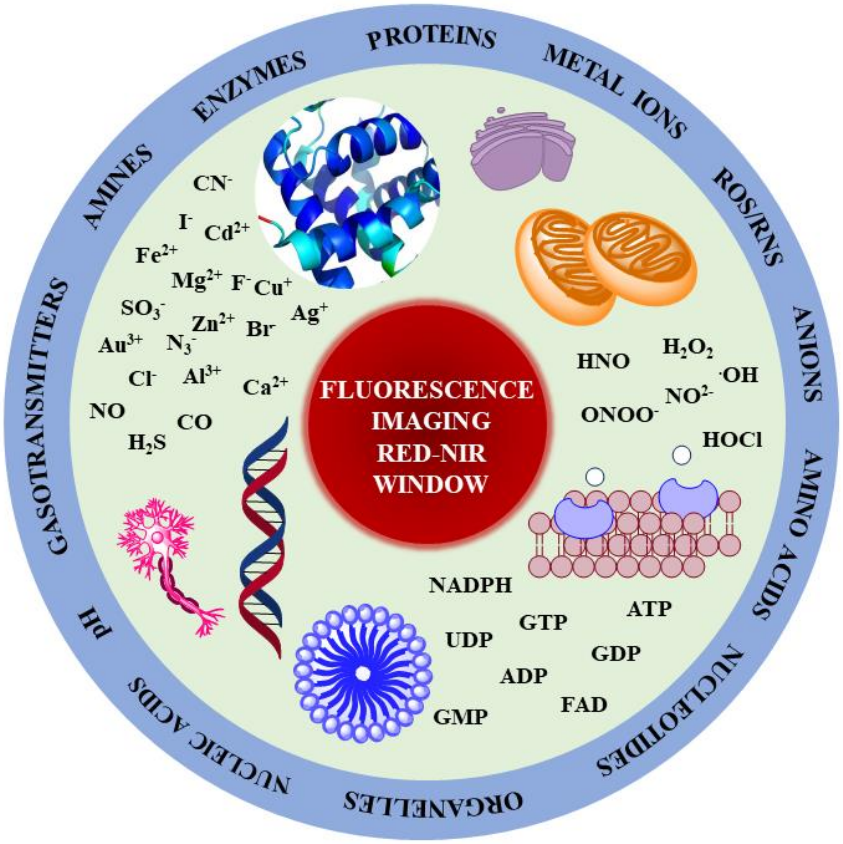

Figure 2. Illustration of the pool of biological or biologically potential analytes which can be probed with fluorescence imaging

1.4 Fluorophores

As it is already mentioned, a fluorescent molecular probe is comprised of two units, (i) receptor unit, responsible for binding to the characteristic targets and (ii) fluorophore, for read out signal yielded either as a direct or indirect consequence of one of the several pertinent interactions between the receptor unit and the analyte.[22] Fluorophores can be broadly compartmentalized into two major categories, intrinsic and extrinsic. Intrinsic fluorophores occur naturally like aromatic amino acids, NADH, flavins, chlorophyll etc. while the extrinsic fluorophores are synthesized biomimetically to probe various phenomena when none of the naturally occurring fluorophore works well. Examples of the latter category are uncountable but to mention, dansyl, fluorescein, rhodamine are some among many.

1.4.1 Intrinsic fluorophores

Intrinsic protein fluorescence originates with the aromatic amino acids like tryptophan (W), tyrosine (Y), and phenylalanine (F).[23] The reason for the innate fluorescence in tryptophan is due to its indole groups while for tyrosine, it is its phenolic moiety. Emission from the phenylalanine is observed only when the sample protein lacks both tyrosine and tryptophan residues.

The emission due to these intrinsic fluorophores is highly sensitive to their microenvironment. Any change due to any external or internal factor can easily be probed by monitoring the absorbance or emission bands due to these structures. These changes can be ligand binding to the protein, protein-protein interactions, denaturation of nascent protein etc. One such essential example of the intrinsic type fluorophore is NADH.[24-25] NADH is highly fluorescent, with absorption and emission maxima at 340 nm and 460 nm, respectively. The oxidized form, NAD^+, is nonfluorescent due to the positive charge on the nicotinamide ring. The lifetime of the NADH in aqueous buffer is 0.4 ns. Upon binding to the proteins, the quantum yield of the NADH generally increases fourfold and the lifetime increases to about 1.2 ns. However, the increment or decrement in the emission intensity of the NADH depends on the kind of interaction with the external protein. For instance, when the enzyme, 17β-hydroxysteroid dehydrogenase (17β-HSD), a catalyst in the biosynthesis of estradiol from estrogen, binds to NADH as its cofactor, the emission intensity of the NADH moiety increases as compared to its free state in aqueous solution.[26] This is because the enzyme, 17β-HSD prevents the quenching of the reduced nicotinamide by the adenine group.

1.4.2 Extrinsic fluorophores

Oftentimes, the molecules of interest are nonfluorescent, or the intrinsic fluorescence is not at all adequate for the desired experiment. For instance, DNA and lipids are essentially devoid of intrinsic fluorescence. In these cases, useful fluorescence is obtained by labeling the molecules with extrinsic probes. Till now, the number of the designed and tested extrinsic fluorescent probes has grown colossal. For an ideal extrinsic fluorophore, following criteria should be satisfied:[1, 27] (i) high optical brightness in order to reduce the amount of probe needed for the experiments, (ii) non-toxic and highly bio-compatible, (iii) excitation and emission profile

should fall in the visible or mostly preferred, in the NIR region to prevent any interference from autofluorescence from the sample itself, (iv) excellent photostability and (v) a balanced structural design (hydrophobic : hydrophilic ratio) to confer membrane permeability, cellular retention and water solubility (Figure 3). Some of the commonly employed extrinsic fluorophores are discussed below.[28]

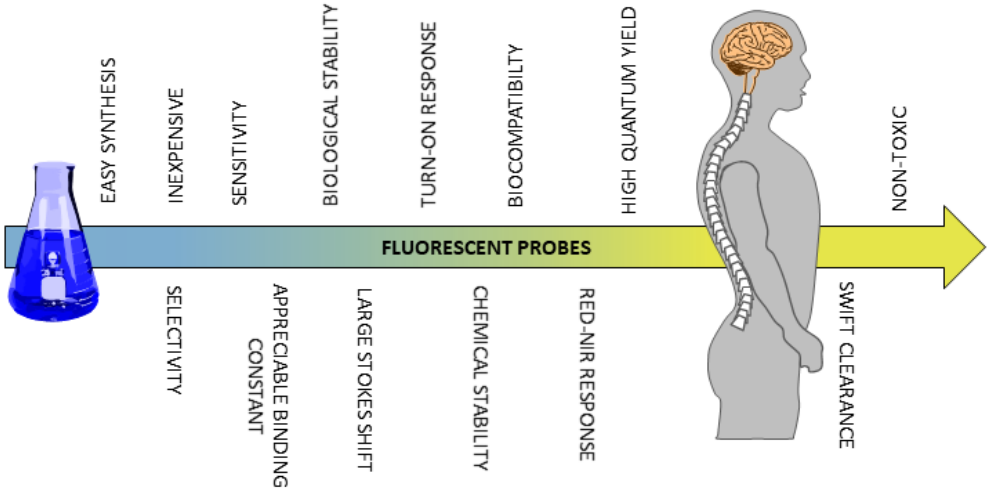

Figure 3. Ideal characteristics of a fluorescent probe

1.4.2.1 Fluorescein and Rhodamine and their derivatives

Fluorescein and rhodamine class of dyes are widely employed as extrinsic tools for bioimaging (Figure 4).[28-30] These dyes have favorably long absorption maxima near 480 nm and 600 nm and emission wavelengths from 510 nm to 615 nm, respectively. In contrast to other dyes, these are sensitive to polar solvents. An additional reason for their widespread use is their high molar extinction coefficients near 80,000 $M^{-1}cm^{-1}$. One common use of fluorescein and rhodamine is for labeling of the antibodies. A wide variety of fluorescein- and rhodamine-labeled immunoglobulins are commercially available, and these proteins are frequently used in fluorescence microscopy and in immunoassays.

1.4.2.2 BODIPY and its derivatives

The BODIPY dyes have been introduced as replacements for fluorescein and rhodamines. These dyes are basically based on an unusual boron-containing fluorophore (Figure 5).[28, 31] Depending on the precise structure, a wide range of emission wavelengths can be obtained, from 510 nm to 675 nm. The BODIPY dyes have the additional advantage of displaying high quantum yields approaching unity, extinction coefficients near 80,000 $M^{-1}cm^{-1}$, and insensitivity to the solvent polarity and pH.

The emission spectra are narrower than those of fluorescein and rhodamines, so that more of the light is emitted at the peak wavelength, possibly allowing more individual dyes to be resolved. A disadvantage of the BODIPY dyes is very small Stokes shift. As a result, the dyes transfer to each other with a Forster distance near 57 Å.

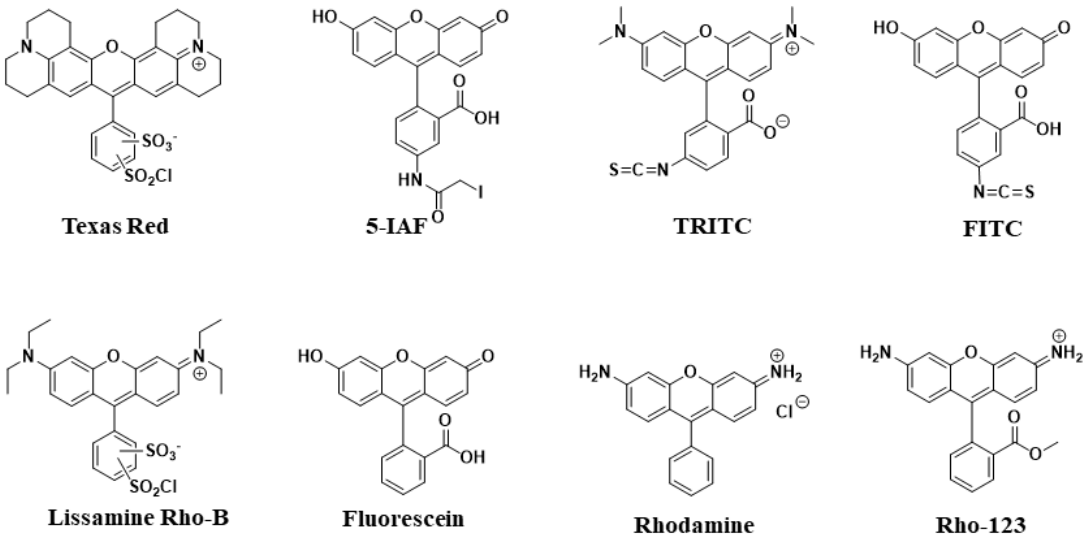

Figure 4. Rhodamine and fluorescein-based fluorescent probe

1.4.2.3 Cyanine and its derivatives

Cyanine fluorophores such as Cy-3, Cy-5 and Cy-7 have proven to be very important (Figure 5).[28, 32] While their quantum yields are typically low (≤0.25), their very high extinction coefficients make them among the brightest known fluorophores. They were some of the earliest dyes developed that gave red/NIR emission and remain highly popular for this reason.

A significant limitation is the ease with which they are oxidized. This is not limited to the problematic photo-oxidation common in many fluorophores. Derivatives of Cy-5 and Cy-7, undergo background oxidation with O_2, and even the minute amounts of O3 present in the atmosphere. This makes it difficult to use these fluorophores in studies that require long measurement periods. However, new cyanine derivatives have been developed with increased quantum yields and improve oxidation resistance.[33] Most of these improvements are based on an understanding of the origins of excited state deactivation and oxidative degradation. This underscores the value of mechanistic analysis in moving the fluorescent probe field forward.

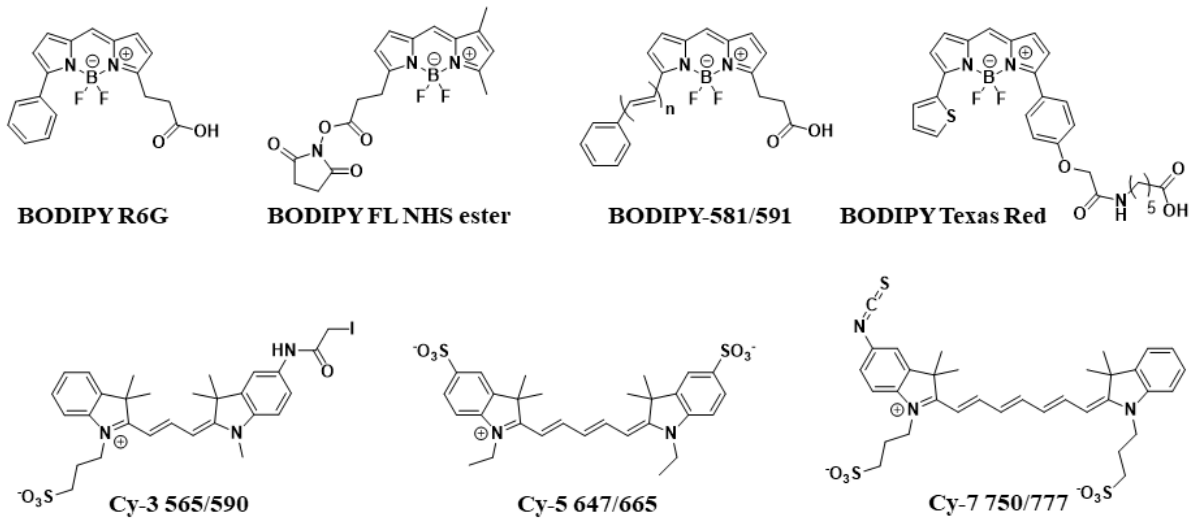

Figure 5. BODIPY and cyanine-based fluorescent probe

1.4.2.4 Coumarin and its derivatives

Coumarins are among the oldest and most easily synthesized fluorophores (Figure 6). They usually have short wavelength (UV) excitation, making them non-ideal for cellular assays or imaging.[28, 34-35] However, they are useful as FRET probes, especially in enzyme assays. Such assays are valuable for the discovery of new enzyme inhibitors. Coumarins have limited brightness, because they do not absorb strongly, due to the relatively minimal fluorescence scaffold. However, they are very photostable. That is, continued excitation leads to minimal fluorophore degradation. In addition, as ICT fluorophores, they have very large Stokes shifts.[36]

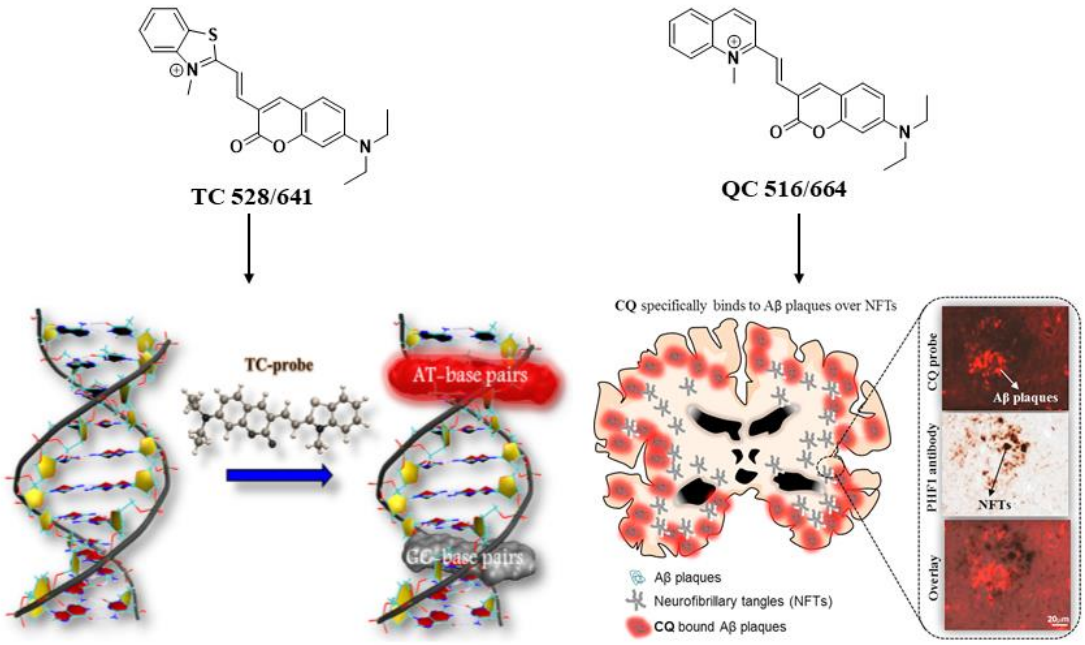

Figure 6. Schematics of TC (left) and QC (right) as coumarin-based fluorescent probes and their applications

1.4.2.5 Phenothiazine and its derivatives

The phenothiazine (PTZ) core scaffold is a class of electron-rich tricyclic nitrogen–sulfur heterocycles, which exhibits relatively intense luminescence, high photo-conductivities and undergoes reversible oxidation processes.[37-38] In general, PTZ derivatives (PTZs) have a low oxidation potential and a high propensity to form stable radical cations. Moreover, the well-defined electron-donating properties of PTZs can be partially associated with electrophores to alter the oxidation potentials of PTZs, especially electronic substitutions in the 3- or 3, 7-positions. Thus, because of its ground state intramolecular charge transfer (ICT) and excited-state photoinduced electron transfer (PET) properties, PTZs are widely used as fluorescent dyes for several biological (chemosensors and NIR dyes) and material (organic light-emitting diodes (OLED), semiconductors and solar cells) applications.[39-41]

However, most of these applications use the protected PTZ structure with covalent substitutions on the nitrogen atom at the 10-position (10N–H becomes 10N–R). There is an example, such as the methylene blue (MB) derivatives, the important pharmacological

applications of PTZs are attributed to its stable radical cation heterocyclic form, which can be used for photodynamic therapy and exhibit near infrared fluorescence.[42] In this case, the proton 10N–H of PTZ is indispensable in the formation of a stable radical cation, but this leads to certain limitations for structural modifications. An example of the phenothiazine-based imaging probe is shown below (Figure 7a and 7b). On one side, the trifluoro modified phenothiazine-based molecule is employed in fluorescent imaging of a calmodulin protein[43] while the other azure B binds to DNA in an intercalation mode to yield a turn-on emission signal.[44]

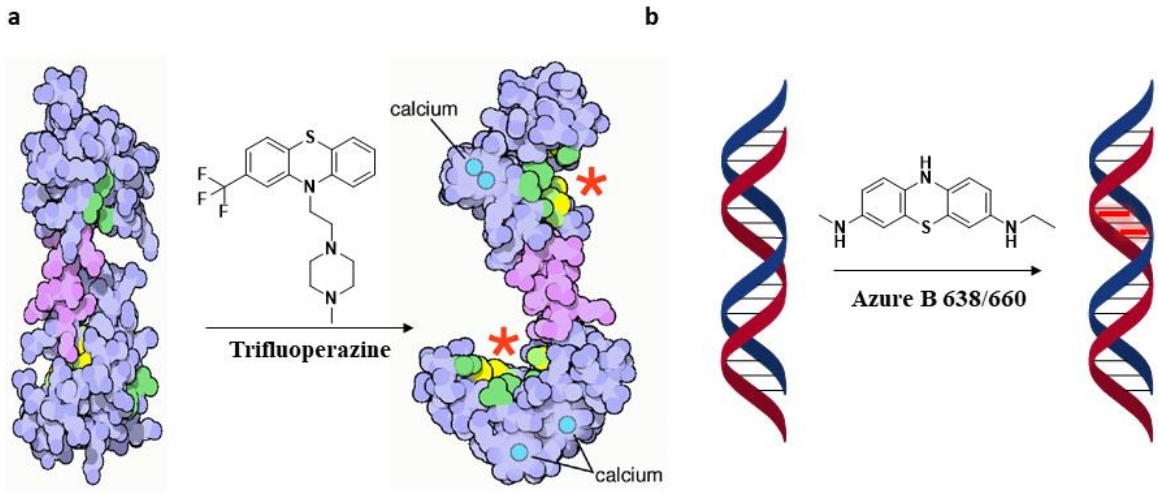

Figure 7. Sensing applications of phenothiazine-based fluorescent probes, (a) trifluoperazine and (b) azure B

1.5 Signal transduction mechanisms

The fluorescence of organic molecules is closely associated with delocalized electronic structure. Conjugated π systems absorb UV or visible light. Deletion of specific absorbed wavelengths from reflected visible light leads to our perception of color. However, a very small fraction of conjugated systems converts the absorbed energy into re-emission of light-fluorescence.[45] For most organic π systems, the non-radiative internal conversion (IC) and/or inter system crossing (ISC) processes are much faster than fluorescence emission, which is why most molecules do not fluoresce. IC involves mechanical dissipation of energy. This makes it conceptually inaccessible to most organic and biomolecular chemists.[46] Hence, most of the fluorescent probes are based on the mechanisms different than IC and ISC by which fluorescence emission can be controlled.

These mechanisms are: suppression of photoinduced electron transfer (PET), modulation of intramolecular charge transfer (ICT) and Förster resonance energy transfer (FRET). Moreover, recently several new rationales, such as metal ion coordination inhibited excited state intramolecular proton transfer (ESIPT) and aggregation-induced emission (AIE) have also been explored to devise fluorescent probes.

1.5.1 Photoinduced electron transfer (PET)

Suppression of photoinduced electron transfer (PET) is one of the most commonly used methods for converting a non-fluorescent molecule into a fluorescent molecule.[47] PET involves electron transfer from a donor (D) to the excited state of a fluorophore (Figure 8). A requirement is that, energetically, the donor electron's energy must lie between the energies of the π and π* orbitals. PET lowers the net energy of the excited state and blocks the π* → π relaxation that leads to fluorescence.

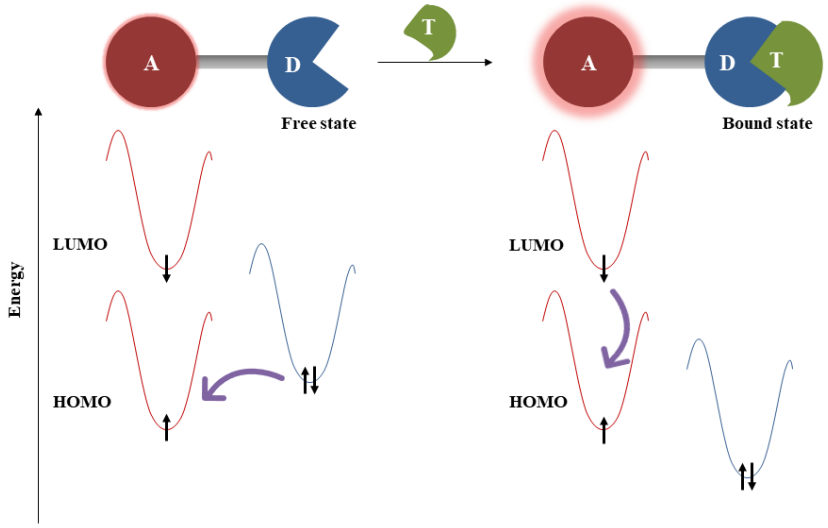

Figure 8. Schematic representation of PET process in fluorescence sensing mechanism

1.5.2 Intramolecular charge transfer (ICT)

Along with suppression of PET, modulation of intramolecular charge transfer (ICT) is one of the most common signaling mechanisms used in fluorescent probe design. Fluorophores that alter

their emission via changes in ICT usually have an electron donor (D) on one end of the fluorophore, and an electron acceptor (A) on the other end (Figure 9).[48-50] In some cases, the fluorophore itself serves as the donor or the acceptor. That is, the fluorophore bears only a donor or an acceptor group. The excited state of ICT systems most often has a stronger dipole moment than the ground state. The architectures (D-π-A) may also twist about a bond and form twisted ICT (TICT) in solutions.[51-52]

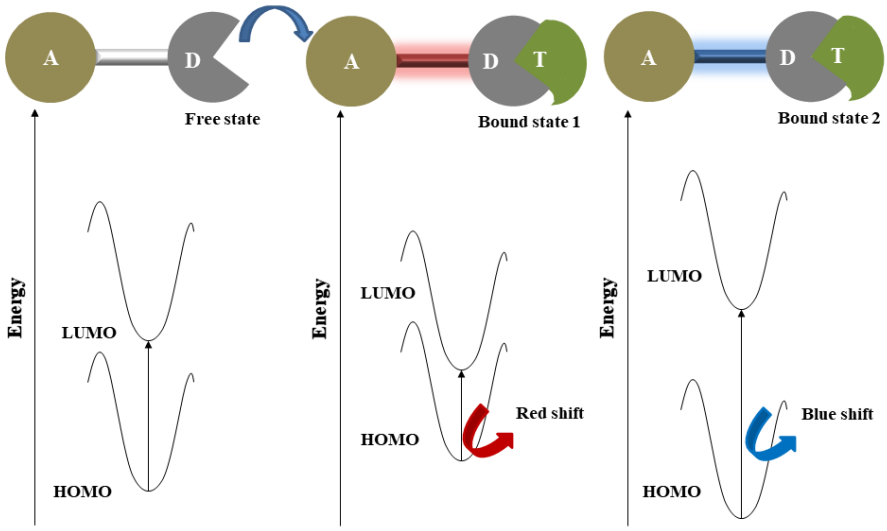

Figure 9. Schematic representation of ICT or TICT process in fluorescence sensing mechanism

1.5.3 Förster resonance energy transfer (FRET)

Förster resonance energy transfer (FRET) is based on the ability of a donor fluorophore to transfer its excited state energy to an acceptor fluorophore with a lower energy excited state, if there is a matching acceptor excited state vibrational level available (Figure 10).[53] This energy transfer is not a photon emission/absorption phenomenon and is thus a non-radiative process. Rather, it can be thought of as transfer of donor excited state energy to the acceptor. This energy transfer "calls up" a ground state acceptor electron to the excited state level into which the donor energy is transferred. Following rapid vibrational relaxation of the acceptor excited state; this represents a reduction of the total energy of the system.

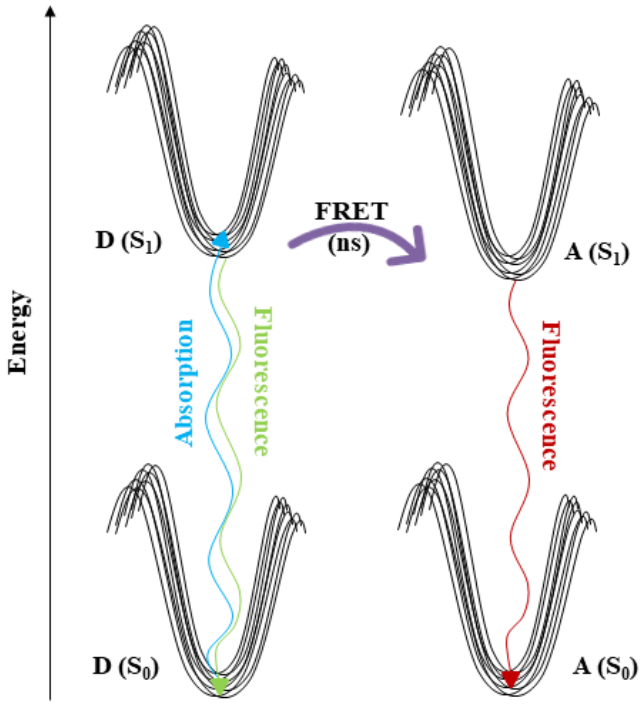

Figure 10. Schematic representation of FRET process in fluorescence sensing mechanism

For a utilitarian understanding of FRET, one can focus on two essential factors that determine FRET efficiency: the distance between the donor and acceptor molecules strongly influences the efficiency of FRET, which scales with 1/r6, where r is the average spatial separation; and, the "spectral overlap" of the "spectral overlap" of donor emission and acceptor absorption, which controls the degree to which the excited states can "talk to each other".[54] The final brightness of the FRET pair is also controlled by the intrinsic brightness of the donor and acceptor fluorophores.[55] Because the donor and acceptor have different absorption and emission maxima, selective excitation and emission measurements allow separate measurement of the "FRET state" (donor-acceptor emission) and the "non-FRET state," in the form of donor-only or acceptor-only emission. This in turn increases the precision with which fluorescence changes can be measured.

1.5.4 Excited state intramolecular proton transfer (ESIPT)

Excited state intramolecular proton transfer (ESIPT) is a process in which photoexcited molecules relax their energy through tautomerization by transfer of protons.[56-57] Some kinds of

molecules could have different minimum-energy tautomers in different electronic states, and if the molecular structure of minimum-energy tautomer in the excited state is proton-transferred geometry between neighboring atoms, proton transfer in excited state can occur (Figure 11).[58-60] The tautomerization often takes the form of keto-enol tautomerism.

Since a proton-transferred geometry is usually the minimum-energy tautomer only in the excited state and relatively unstable in the ground state, molecules that have ESIPT character may show extraordinarily larger Stokes shift than common fluorescent molecules, or exhibit dual fluorescence that shorter-wavelength one comes from the original tautomer and longer-wavelength one from proton-transferred tautomer.[61] However, there are some exceptional cases where ESIPT molecules have no dual luminescence or significantly red-shifted emission from proton-transferred tautomer, from various reasons.

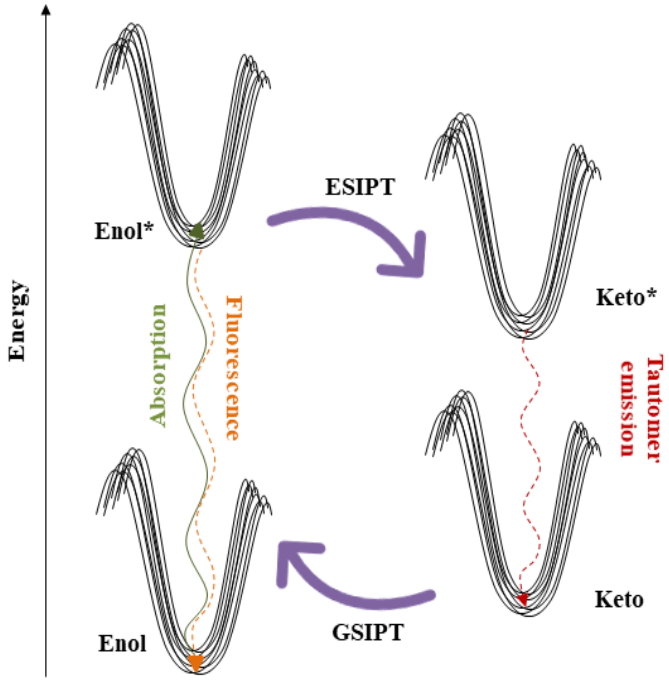

Figure 11. Schematic representation of ESIPT and GSIPT processes in fluorescence sensing mechanism

1.5.5 Aggregation-induced emission (AIE)

Aggregation-induced emission (AIE) is an abnormal phenomenon that is observed with certain organic luminophores (fluorescent dyes).[62] Most organic compounds have planar structures and

higher photoemission efficiencies in solution than in the solid state. Otherwise said, these fluorophores or fluorescent dyes are much more emissive in solution compared to just the solid form, in that the intensity of their emission is greater in solution. However, some organic luminophores have freely-rotating groups (rotational degrees of freedom), when these molecules are excited instead of releasing that energy as light they relax back down through these rotations (Figure 12).[63] When these luminophores aggregate or crystallize, which restricts those rotations, they can become very fluorescent or emissive, and the photoluminescence efficiency (i.e. quantum yield) increases.

In view of such an uncanny fluorescence behavior, AIE have been progressively utilized in designing sensitive and selective chemosensors.[64-65] The aggregation of AIE molecules can be altered by any guest molecules (can be solvent of different polarity) through electrostatic interactions, coordination interaction, hydrophobic interaction, steric hindrance, mercapto reaction, or change in the polarity or viscosity.

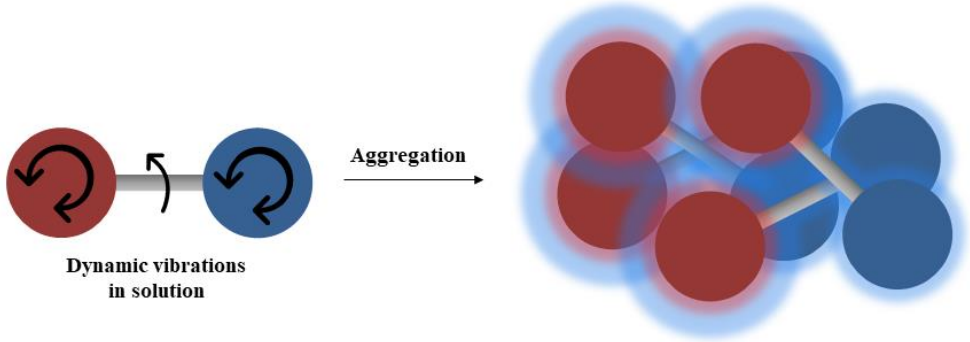

Figure 12. Schematic representation of AIE process in fluorescence sensing mechanism

1.6 Design strategies for molecular fluorescent probes

Considering the abovementioned fluorescence mechanisms, several probe design strategies have been exploited to enhance the probe's signal intensity upon any favorable interaction with the desired analyte. Some of these strategies are discussed below.

1.6.1 Typical conjugation of donor with acceptor (D-π-A)

The prototypal fluorescent molecular probes contain a donor unit (ionophore) conjugated to the accep[66]tor unit (fluorophore). In the normal 'off' state, the molecule is nonfluorescent due to the PET from the ionophore to the fluorophore. Upon binding to the appropriate analyte, the ionophore transforms its structural conformation with respect to the analyte and PET is arrested. Consequently, the molecule achieves its 'on' state and fluoresces in the given condition.[67] The strategy is just a classic example for various modern strategies. However, it encompasses a lot of assumptions beforehand which is quite difficult in designing a probe. Detailed discussion has been done in chapter two.

1.6.2 Chemical reaction-induced fluorescence

The host-guest interactions between the ionophore and the targeted analyte (more like a lock-key model) can be studied to develop a novel design strategy for targeted designing of the molecular probe.[11] The probes can be engineered in such a way that upon its proximal interactions with the target analyte, it undergoes a simple yet effective chemcial transformation through a reaction. The reaction can be of any kind namely, nucleophilic or electrophilic addition or substitution or simple acid-base reaction. Some of the examples may include oxidative cycloaddition[68], oxidative cleavage[69], reductive cleavage[70], tandem displacement[71], metal-ligand substitution[72], metal-mediated redox addition or cleavage[73], organometallic reactions[74] etc. Thus, studying various diverse categories of the analytes and their function in normal biological processes, we can design synthetic probes for monitoring these essential analytes (Figure 13).

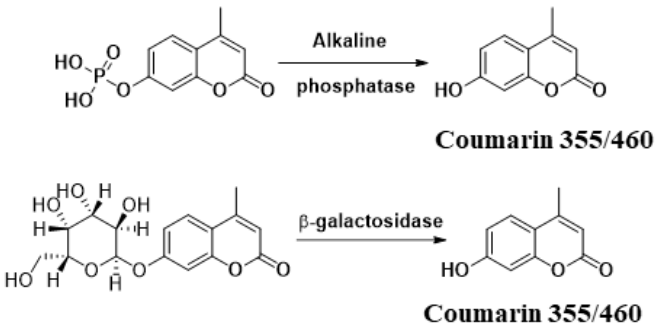

Figure 13. Reaction-based coumarin fluorescent probes

1.7 Conclusion

Brightness, photostability, background, toxicity, spectral overlap, ion sensitivity, and structural and cellular effects on the targeted partner are all important issues to consider when choosing a fluorescent molecular probe for imaging of bioactive analytes. Year by year, new fluorescent probes with improved properties are being developed for a variety of target molecules. In addition, the scope of targets addressed by the fluorescent probes is rapidly expanding. For example, probes based on fluorescent proteins have allowed specific measurements of closely related biomolecules, such as lipids, which would be difficult, if not impossible, to achieve with small-molecular probes. Nonetheless, there is no single answer to which probe or method will provide the best signal for all imaging applications. The development and refinement of fluorescent probes for imaging is progressing rapidly and the molecular toolkit continues to grow.

1.8 References

1. Suseela, Y. V.; Narayanaswamy, N.; Pratihar, S.; Govindaraju, T., Far-red fluorescent probes for canonical and non-canonical nucleic acid structures: current progress and future implications. *Chem. Soc. Rev.* **2018,** *47* (3), 1098-1131.

2. Ueno, T.; Nagano, T., Fluorescent probes for sensing and imaging. *Nat. Meth.* **2011,** *8*, 642.

3. Lemke, E. A.; Schultz, C., Principles for designing fluorescent sensors and reporters. *Nat. Chem. Biol.* **2011,** *7*, 480.

4. Lavigne, J. J.; Anslyn, E. V., Sensing A Paradigm Shift in the Field of Molecular Recognition: From Selective to Differential Receptors. *Angew. Chem. Int. Ed.* **2001,** *40* (17), 3118-3130.

5. Hovius, R.; Vallotton, P.; Wohland, T.; Vogel, H., Fluorescence techniques: shedding light on ligand–receptor interactions. *Trends Pharmacol. Sci.* **2000,** *21* (7), 266-273.

6. New, E. J., Tools to study distinct metal pools in biology. *Dalton Trans.* **2013,** *42* (9), 3210-3219.

7. Terai, T.; Nagano, T., Fluorescent probes for bioimaging applications. *Curr. Opin. Chem. Biol.* **2008,** *12* (5), 515-521.

8. Terai, T.; Nagano, T., Small-molecule fluorophores and fluorescent probes for bioimaging. *Eur. J. Physiol.* **2013,** *465* (3), 347-359.

9. Kim, H. M.; Cho, B. R., Two-Photon Probes for Intracellular Free Metal Ions, Acidic Vesicles, And Lipid Rafts in Live Tissues. *Acc. Chem. Res.* **2009,** *42* (7), 863-872.

10. De Silva, A. P.; Gunaratne, H. Q. N.; Gunnlaugsson, T.; Huxley, A. J. M.; McCoy, C. P.; Rademacher, J. T.; Rice, T. E., Signaling Recognition Events with Fluorescent Sensors and Switches. *Chem. Rev.* **1997,** *97* (5), 1515-1566.

11. Chan, J.; Dodani, S. C.; Chang, C. J., Reaction-based small-molecule fluorescent probes for chemoselective bioimaging. *Nat. Chem.* **2012,** *4*, 973.

12. Merino, E., Synthesis of azobenzenes: the coloured pieces of molecular materials. *Chem. Soc. Rev.* **2011,** *40* (7), 3835-3853.

13. Zhou, Y.; Xu, Z.; Yoon, J., Fluorescent and colorimetric chemosensors for detection of nucleotides, FAD and NADH: highlighted research during 2004–2010. *Chem. Soc. Rev.* **2011,** *40* (5), 2222-2235.

14. Urano, Y.; Asanuma, D.; Hama, Y.; Koyama, Y.; Barrett, T.; Kamiya, M.; Nagano, T.; Watanabe, T.; Hasegawa, A.; Choyke, P. L.; Kobayashi, H., Selective molecular imaging of viable cancer cells with pH-activatable fluorescence probes. *Nat. Med.* **2008,** *15*, 104.

15. Kamiya, M.; Kobayashi, H.; Hama, Y.; Koyama, Y.; Bernardo, M.; Nagano, T.; Choyke, P. L.; Urano, Y., An Enzymatically Activated Fluorescence Probe for Targeted Tumor Imaging. *J. Am. Chem. Soc.* **2007,** *129* (13), 3918-3929.

16. Frangioni, J. V., In vivo near-infrared fluorescence imaging. *Curr. Opin. Chem. Biol.* **2003,** *7* (5), 626-634.

17. Ntziachristos, V.; Bremer, C.; Weissleder, R., Fluorescence imaging with near-infrared light: new technological advances that enable in vivo molecular imaging. *Eur. Radiol.* **2003,** *13* (1), 195-208.

18. Kobayashi, H.; Longmire, M. R.; Ogawa, M.; Choyke, P. L., Rational chemical design of the next generation of molecular imaging probes based on physics and biology: mixing modalities, colors and signals. *Chem. Soc. Rev.* **2011,** *40* (9), 4626-4648.

19. Mitsunaga, M.; Ogawa, M.; Kosaka, N.; Rosenblum, L. T.; Choyke, P. L.; Kobayashi, H., Cancer cell–selective in vivo near infrared photoimmunotherapy targeting specific membrane molecules. *Nat. Med.* **2011,** *17*, 1685.

20. Ash, C.; Dubec, M.; Donne, K.; Bashford, T., Effect of wavelength and beam width on penetration in light-tissue interaction using computational methods. *Lasers Med. Sci.* **2017,** *32* (8), 1909-1918.

21. Du, W.; Wang, Y.; Luo, Q.; Liu, B.-F., Optical molecular imaging for systems biology: from molecule to organism. *Anal. Bioanal. Chem.* **2006,** *386* (3), 444.

22. Blázquez-Castro, J. C. S. A., *Fluorescence Microscopy in Life Sciences*. Bentham Science Publishers: 2017; pp 61-95

23. Protein Fluorescence. In *Principles of Fluorescence Spectroscopy*, Lakowicz, J. R., Ed. Springer US: Boston, MA, 2006; pp 529-575.

24. Ince, C.; Coremans, J. M. C. C.; Bruining, H. A., In Vivo NADH Fluorescence. In *Oxygen Transport to Tissue XIV*, Erdmann, W.; Bruley, D. F., Eds. Springer US: Boston, MA, 1992; pp 277-296.

25. Blacker, T. S.; Mann, Z. F.; Gale, J. E.; Ziegler, M.; Bain, A. J.; Szabadkai, G.; Duchen, M. R., Separating NADH and NADPH fluorescence in live cells and tissues using FLIM. *Nat. Commun.* **2014,** *5*, 3936.

26. Breton, R.; Housset, D.; Mazza, C.; Fontecilla-Camps, J. C., The structure of a complex of human 17β-hydroxysteroid dehydrogenase with estradiol and NADP+ identifies two principal targets for the design of inhibitors. *Structure* **1996,** *4* (8), 905-915.

27. Qian, X.; Xiao, Y.; Xu, Y.; Guo, X.; Qian, J.; Zhu, W., "Alive" dyes as fluorescent sensors: fluorophore, mechanism, receptor and images in living cells. *Chem. Commun.* **2010,** *46* (35), 6418-6436.

28. Fu, Y.; Finney, N. S., Small-molecule fluorescent probes and their design. *RSC Adv.* **2018,** *8* (51), 29051-29061.

29. Zheng, H.; Zhan, X.-Q.; Bian, Q.-N.; Zhang, X.-J., Advances in modifying fluorescein and rhodamine fluorophores as fluorescent chemosensors. *Chem. Commun.* **2013,** *49* (5), 429-447.

30. Shivaprasad, M.; Govindaraju, T., Rhodamine based bright red colourimetric and turn-on fluorescence chemosensor for selective detection of Cu2+. *Mater. Technol.* **2011,** *26* (4), 168-172.

31. Kowada, T.; Maeda, H.; Kikuchi, K., BODIPY-based probes for the fluorescence imaging of biomolecules in living cells. *Chem. Soc. Rev.* **2015,** *44* (14), 4953-4972.

32. Altman, R. B.; Terry, D. S.; Zhou, Z.; Zheng, Q.; Geggier, P.; Kolster, R. A.; Zhao, Y.; Javitch, J. A.; Warren, J. D.; Blanchard, S. C., Cyanine fluorophore derivatives with enhanced photostability. *Nat. Meth.* **2011,** *9*, 68.

33. Maity, D.; Govindaraju, T., A turn-on NIR fluorescence and colourimetric cyanine probe for monitoring the thiol content in serum and the glutathione reductase assisted glutathione redox process. *Org. Biomol. Chem.* **2013,** *11* (13), 2098-2104.

34. Narayanaswamy, N.; Kumar, M.; Das, S.; Sharma, R.; Samanta, P. K.; Pati, S. K.; Dhar, S. K.; Kundu, T. K.; Govindaraju, T., A Thiazole Coumarin (TC) Turn-On Fluorescence Probe for AT-Base Pair Detection and Multipurpose Applications in Different Biological Systems. *Sci. Rep.* **2014,** *4*, 6476.

35. Rajasekhar, K.; Narayanaswamy, N.; Murugan, N. A.; Viccaro, K.; Lee, H.-G.; Shah, K.; Govindaraju, T., Aβ plaque-selective NIR fluorescence probe to differentiate Alzheimer's disease from tauopathies. *Biosens. Bioelectron.* **2017,** *98*, 54-61.

36. Maity, D.; Govindaraju, T., A differentially selective sensor with fluorescence turn-on response to Zn2+ and dual-mode ratiometric response to Al3+ in aqueous media. *Chem. Commun.* **2012,** *48* (7), 1039-1041.

37. Massie, S. P., The Chemistry of Phenothiazine. *Chem. Rev.* **1954,** *54* (5), 797-833.

38. Bloor, J. E.; Gilson, B. R.; Haas, R. J.; Zirkle, C. L., Electron-donating properties of phenothiazine and related compounds. *J. Med. Chem.* **1970,** *13* (5), 922-925.

39. Aizawa, N.; Tsou, C.-J.; Park, I. S.; Yasuda, T., Aggregation-induced delayed fluorescence from phenothiazine-containing donor–acceptor molecules for high-efficiency non-doped organic light-emitting diodes. *Polym. J.* **2016,** *49*, 197.

40. Marszalek, M.; Nagane, S.; Ichake, A.; Humphry-Baker, R.; Paul, V.; Zakeeruddin, S. M.; Grätzel, M., Tuning spectral properties of phenothiazine based donor–π–acceptor dyes for efficient dye-sensitized solar cells. *J. Mater. Chem.* **2012,** *22* (3), 889-894.

41. Dao, P.; Ye, F.; Liu, Y.; Du, Z. Y.; Zhang, K.; Dong, C. Z.; Meunier, B.; Chen, H., Development of Phenothiazine-Based Theranostic Compounds That Act Both as Inhibitors of β-Amyloid Aggregation and as Imaging Probes for Amyloid Plaques in Alzheimer's Disease. *ACS Chem. Neurosci.* **2017,** *8* (4), 798-806.

42. Jori, G.; Fabris, C.; Soncin, M.; Ferro, S.; Coppellotti, O.; Dei, D.; Fantetti, L.; Chiti, G.; Roncucci, G., Photodynamic therapy in the treatment of microbial infections: Basic principles and perspective applications. *Lasers Surg. Med.* **2006,** *38* (5), 468-481.

43. Haußer, I.; Herth, W.; Reiss, H.-D., Cllmodulin in tip-growing plant cells, visualized by fluorescing calmodulin-binding phenothiazines. *Planta* **1984,** *162* (1), 33-39.

44. Paul, P.; Suresh Kumar, G., Spectroscopic studies on the binding interaction of phenothiazinium dyes toluidine blue O, azure A and azure B to DNA. *Spectrochim. Acta A Mol. Biomol. Spectrosc.* **2013,** *107*, 303-310.

45. Steehler, J. K., Book Review of Principles of Molecular Photochemistry—An Introduction. *J. Chem. Educ.* **2010,** *87* (12), 1298-1301.

46. Wu, J.; Liu, W.; Ge, J.; Zhang, H.; Wang, P., New sensing mechanisms for design of fluorescent chemosensors emerging in recent years. *Chem. Soc. Rev.* **2011,** *40* (7), 3483-3495.

47. Daly, B.; Ling, J.; de Silva, A. P., Current developments in fluorescent PET (photoinduced electron transfer) sensors and switches. *Chem. Soc. Rev.* **2015,** *44* (13), 4203-4211.

48. Huss, A. S.; Pappenfus, T.; Bohnsack, J.; Burand, M.; Mann, K. R.; Blank, D. A., The Influence of Internal Charge Transfer on Nonradiative Decay in Substituted Terthiophenes. *J. Phys. Chem. A* **2009,** *113* (38), 10202-10210.

49. Maity, D.; Govindaraju, T., Highly Selective Visible and Near-IR Sensing of Cu2+ Based on Thiourea–Salicylaldehyde Coordination in Aqueous Media. *Chem. Eur. J.* **2011,** *17* (5), 1410-1414.

50. Maity, D.; Govindaraju, T., Conformationally Constrained (Coumarin−Triazolyl−Bipyridyl) Click Fluoroionophore as a Selective Al3+ Sensor. *Inorg. Chem.* **2010,** *49* (16), 7229-7231.

51. Wang, Y.; Eisenthal, K. B., Picosecond dynamics of twisted internal charge transfer phenomena. The role of the solvent. *J. Chem. Phys.* **1982,** *77* (12), 6076-6082.

52. Bosch, L. I.; Mahon, M. F.; James, T. D., The B–N bond controls the balance between locally excited (LE) and twisted internal charge transfer (TICT) states observed for aniline based fluorescent saccharide sensors. *Tetrahedron Lett.* **2004,** *45* (13), 2859-2862.

53. Yuan, L.; Lin, W.; Zheng, K.; Zhu, S., FRET-Based Small-Molecule Fluorescent Probes: Rational Design and Bioimaging Applications. *Acc. Chem. Res.* **2013,** *46* (7), 1462-1473.

54. Fan, J.; Hu, M.; Zhan, P.; Peng, X., Energy transfer cassettes based on organic fluorophores: construction and applications in ratiometric sensing. *Chem. Soc. Rev.* **2013,** *42* (1), 29-43.

55. Maity, D.; Karthigeyan, D.; Kundu, T. K.; Govindaraju, T., FRET-based rational strategy for ratiometric detection of Cu2+ and live cell imaging. *Sens. Actuators B Chem.* **2013,** *176*, 831-837.

56. Zhao, J.; Ji, S.; Chen, Y.; Guo, H.; Yang, P., Excited state intramolecular proton transfer (ESIPT): from principal photophysics to the development of new chromophores and applications in fluorescent molecular probes and luminescent materials. *Phys. Chem. Chem. Phys.* **2012,** *14* (25), 8803-8817.

57. Kwon, J. E.; Park, S. Y., Advanced Organic Optoelectronic Materials: Harnessing Excited-State Intramolecular Proton Transfer (ESIPT) Process. *Adv. Mater.* **2011,** *23* (32), 3615-3642.

58. Demchenko, A. P.; Tang, K.-C.; Chou, P.-T., Excited-state proton coupled charge transfer modulated by molecular structure and media polarization. *Chem. Soc. Rev.* **2013,** *42* (3), 1379-1408.

59. Maity, D.; Govindaraju, T., Naphthaldehyde–Urea/Thiourea Conjugates as Turn-On Fluorescent Probes for Al3+ Based on Restricted C=N Isomerization. *Eur. J. Inorg. Chem.* **2011,** *2011* (36), 5479-5485.

60. Maity, D.; Kumar, V.; Govindaraju, T., Reactive Probes for Ratiometric Detection of Co2+ and Cu+ Based on Excited-State Intramolecular Proton Transfer Mechanism. *Org. Lett.* **2012,** *14* (23), 6008-6011.

61. Zhang, Y.; Wang, J.-H.; Zheng, W.; Chen, T.; Tong, Q.-X.; Li, D., An ESIPT fluorescent dye based on HBI with high quantum yield and large Stokes shift for selective detection of Cys. *J. Mater. Chem. B* **2014,** *2* (26), 4159-4166.

62. Luo, J.; Xie, Z.; Lam, J. W. Y.; Cheng, L.; Chen, H.; Qiu, C.; Kwok, H. S.; Zhan, X.; Liu, Y.; Zhu, D.; Tang, B. Z., Aggregation-induced emission of 1-methyl-1,2,3,4,5-pentaphenylsilole. *Chem. Commun.* **2001,** (18), 1740-1741.

63. Tseng, N.-W.; Liu, J.; Ng, J. C. Y.; Lam, J. W. Y.; Sung, H. H. Y.; Williams, I. D.; Tang, B. Z., Deciphering mechanism of aggregation-induced emission (AIE): Is E–Zisomerisation involved in an AIE process? *Chem. Sci.* **2012,** *3* (2), 493-497.

64. Ding, D.; Li, K.; Liu, B.; Tang, B. Z., Bioprobes Based on AIE Fluorogens. *Acc. Chem. Res.* **2013,** *46* (11), 2441-2453.

65. Hong, Y., Aggregation-induced emission—fluorophores and applications. *Methods Appl. Fluoresc.* **2016,** *4* (2), 022003.

66. Karton-Lifshin, N.; Albertazzi, L.; Bendikov, M.; Baran, P. S.; Shabat, D., "Donor–Two-Acceptor" Dye Design: A Distinct Gateway to NIR Fluorescence. *J. Am. Chem. Soc.* **2012,** *134* (50), 20412-20420.

67. De Silva, A. P.; Moody, T. S.; Wright, G. D., Fluorescent PET (Photoinduced Electron Transfer) sensors as potent analytical tools. *Analyst* **2009,** *134* (12), 2385-2393.

68. Song, B.; Wang, G.; Tan, M.; Yuan, J., A Europium(III) Complex as an Efficient Singlet Oxygen Luminescence Probe. *J. Am. Chem. Soc.* **2006,** *128* (41), 13442-13450.

69. Lippert, A. R.; Van de Bittner, G. C.; Chang, C. J., Boronate Oxidation as a Bioorthogonal Reaction Approach for Studying the Chemistry of Hydrogen Peroxide in Living Systems. *Acc. Chem. Res.* **2011,** *44* (9), 793-804.

70. Lin, V. S.; Chang, C. J., Fluorescent probes for sensing and imaging biological hydrogen sulfide. *Curr. Opin. Chem. Biol.* **2012,** *16* (5), 595-601.

71. Xu, Z.; Chen, X.; Kim, H. N.; Yoon, J., Sensors for the optical detection of cyanide ion. *Chem. Soc. Rev.* **2010,** *39* (1), 127-137.

72. Wu, Z.; Zhang, Y.; Ma, J. S.; Yang, G., Ratiometric Zn2+ Sensor and Strategy for Hg2+ Selective Recognition by Central Metal Ion Replacement. *Inorg. Chem.* **2006,** *45* (8), 3140-3142.

73. Lim, M. H.; Xu, D.; Lippard, S. J., Visualization of nitric oxide in living cells by a copper-based fluorescent probe. *Nat. Chem. Biol.* **2006,** *2*, 375.

74. Zhou, Z.; Fahrni, C. J., A Fluorogenic Probe for the Copper(I)-Catalyzed Azide−Alkyne Ligation Reaction: Modulation of the Fluorescence Emission via 3(n,π*)−(π,π*) Inversion. *J. Am. Chem. Soc.* **2004,** *126* (29), 8862-8863.

Design and syntheses of phenothiazine-based molecular probes

Chapter Two

2.1 Introduction

Small molecular fluorescent probes are the molecules which exhibit characteristic changes in their fluorescence emission profile because of a responsive binding event, chemical reaction, or change in their immediate microenvironment. These molecular tools have been widely exploited in various scientific regimes namely, drug discovery, bioimaging, environmental analysis, and various medical applications. Among diverse reasons for their usefulness are; fluorescence emission can be monitored with precision and great sensitivity, fluorescence microscopy allows remarkable spatial and temporal resolution in cellular imaging and, many fluorophores are now readily accessible.[1] There are validated precedents for the vast applicative index of fluorescent molecular probes thus, fluorescent probes have been dominating the field of spectroscopy in comparison to other spectroscopic characterizations. A simplistic design of a fluorescent molecular probe comprises of a donor unit (D) and a complementary acceptor unit (A). These units can be conjugated either directly through a covalent C-C/ C-C type bond or conjugated with a network of pi (π) electron cloud; double bond(s) (Figure 1).[2-5] Over the last decade, several (D) and (A) moieties have been explored and synthesized. For an optimal fluorescence signal transduction, it is essential for the two units namely, (D) and (A) to be well conjugated in order to yield high intensity emission resulting from the extended conjugation in the structure itself.[6] Based on posteriori understanding of the fluorescent probes through several scientific reports and reviews, we can at least comment that in a prototypal case of D-π-A architecture, benzothiazoles, quinaldine, dicyanomethychromene and BODIPY form a good acceptor subunit while amino and several alkylated amino groups provide excellent donor properties due to its free lone pair and moderate electronegativity.

Inspired by such a library of fluorescent molecular structures, we have exploited a similar alkylated amino group as a (D) unit and benzothiazole as a (A) unit in our current work (Figure 2). The (D) group comes from a well-known structure; phenothiazine which is a unique design of two aromatic rings joined together by a non-aromatic six-membered ring containing both the nitrogen (N) and sulfur (S) atoms, placed trans to each other.[7]

Phenothiazine was first prepared by Bemthsen in 1883 in the course of proof of structure studies on methylene blue.[8] Since then it has played an important role in dye chemistry as the parent compound of the thiazine dyes. In the last decade phenothiazine and its derivatives have found

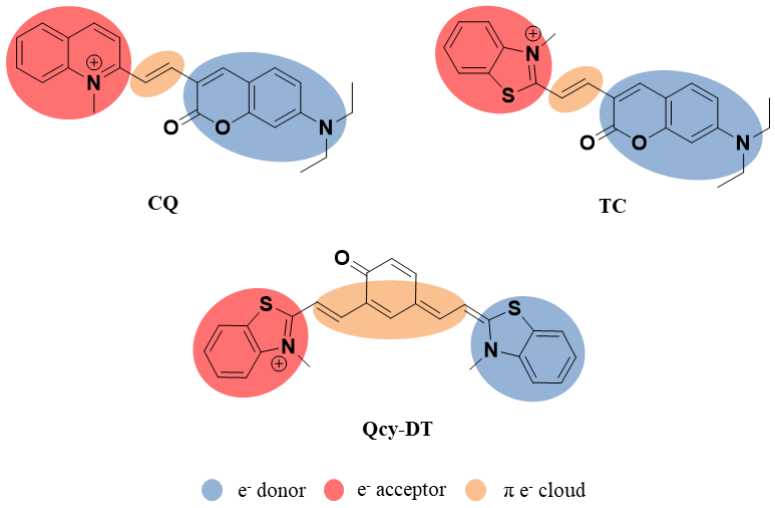

Figure 1. Schematic representation of a D-π-A architecture. Reported by Govindaraju et al.

numerous applications in numerous fields, and this has stimulated further research on these compounds. The chemical structure of phenothiazine provides a most valuable molecular template for the development of agents able to interact with a wide variety of biological processes.[9-10] Synthetic phenothiazines (with aliphatic, methylpiperazine, piperazine-ethanol, piperazine-ethyl, or piperidine side-chain) and/or phenothiazine-derived agents e.g., thioxanthenes, benzepines, imonostilbenes, tricyclic antidepressants, dimetothiazine, and cyproheptadine have been effective in the treatment of several medical conditions with widely different etiology. These include various currently clinically used drugs for their significant antihistamic, antipsychotic, anticholinergic (antiparkinson), antipruritic, and/or antiemetic properties. They are also employed, although to a minor extent, as antidepressants, antispasmodics, analgesics, and antiarrhythemics. Some of these agents are also useful as anti-inflammatory, coronary vasodilator, radioprotective, sedative, antitussive, and skeletal muscle-relaxing medication. Still, others show different degrees of effectiveness as antibacterials, anthelmintics, antimalarials, or local anesthetics; a few are valuable in the control of acute migraine attacks and intractable hiccough. Adding to the seemingly ever-expanding therapeutic use of phenothiazine derivatives, a number of ‘‘old’’ and newly synthesized compounds e.g., ‘‘half-mustard-type’’ and benzo[alpha]phenothiazines, appear to be helpful as multidrug resistance modifiers, a property of particular importance in cancer chemotherapy. Some phenothiazines inhibit human plasmatic leucine-enkephalin aminopeptidase(s), enzymes known to regulate the turnover rate of a wide range of bioactive substances. A critical examination of these findings could lead to the design of

new therapeutic or theranostic (if phenothiazine is used in fluorescent architecture) treatment modalities for conditions such as Alzheimer's and Creutzfeldt-Jakob disease.

2.2 Objective of the work

The objective behind undertaking this work has been to develop simple and targeted small organic fluorescent molecules. As it is already mentioned, fluorescent probes are the new strategy to imaging potential biological targets like proteins, nucleic acids (NAs), enzyme and several biological cycles. For a good fluorescent probe, it is essential that its synthesis should be easy and simple. Thus, we have employed a facile route following the Knoevenagel condensation reaction to synthesize the final fluorescent molecules. This is very important from application point of view in any industrial organization for an effective molecule is the one which is both biologically active and as well as chemically straightforward.

2.3 Design strategy

We have extensively exploited a facile route towards the synthesis of the reported phenothiazine-based fluorescent molecular probes by employing simple Knoevenagel condensation reactions.[11] A Knoevenagel reaction is a condensation reaction between an active methylene group (potent nucleophile under mild basic conditions) and any compatible electrophile (eg. carbonyl group). Since in our syntheses the potential nucleophile is an active methyl group, we have called it as Knoevenagel-type condensation reaction. Particularly, we have selected benzothiazole or quinaldine moieties as (A) subunit in our molecular skeletons. The otherwise unmethylated benzothiazole is a poor acceptor of electron and hence, not at all or weakly fluorescent when conjugated with a donor subunit.

This has been validated by synthesizing the unmethylated analog of already reported thiazole-coumarin (TC).[2] For a (D) moiety, we have selected N-methylated phenothiazine carboxaldehyde. Finally, these subunits have been condensed to yield fluorescent active molecular probes.

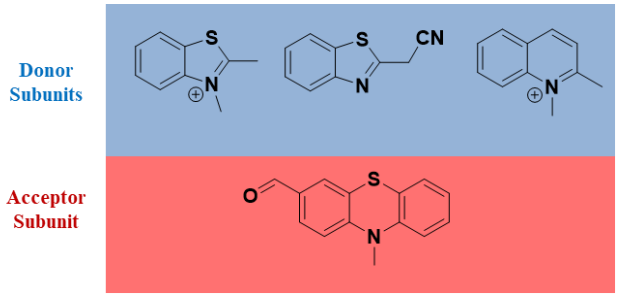

Figure 2. Schematic representation of the selected D and A subunits employed in the current work

2.4 Synthesis of benzothiazole-phenothiazine condensed fluorescent molecular probes

The (A) subunit; N-methylbenzthiazolium iodide (**1**) was synthesized by a quantitative methylation of the N atom of the benzothiazole moiety (Scheme 1). The Menshutkin reaction[12] (quaternization/ methylation of tertiary amine group) was carried out in a sealed tube (also referred to as high pressure reaction tube) using acetonitrile (MeCN) as a solvent. The active reagent chosen for the methylation of the benzothiazole N atom was methyl iodide (MeI). The facile reaction goes through a unimolecular electrophilic substitution (S_N1) reaction mechanism wherein the methyl carbocation is formed first in the solvent followed by the bond formation between the benzothiazole N and the methyl carbocation. The reaction was carried out at 40°C with constant stirring for a period of 24 h. Importantly, the above reaction depends on the selection of the right solvent. While the reaction does not occur in non-polar solvent, some polar solvents are also restricted for example, dichloromethane (DCM). DCM is a commonly used solvent for many reactions nonetheless, for Menshutkin reaction, it is not at all suitable owing to its tendency to act as a potent electrophile for the incoming nucleophile (benzothiazole N atom in our case). Hence, we observe a competition between the desired electrophile (methyl carbocation) and the unwanted electrophile (DCM) which has been avoided in our case by replacing DCM with MeCN.

Similar protocol was followed for synthesizing N-methylquinaldinium iodide (**3**). Interestingly, 2-(benzothiazol-2-yl) acetonitrile (**2**) could not be methylated using similar protocol. This can be reasoned out well by critically examining its structure.

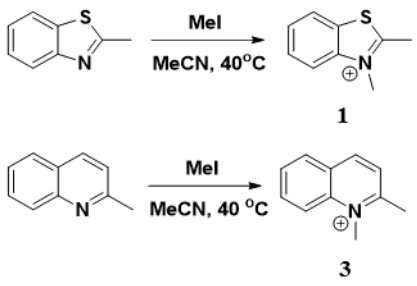

Scheme 1. Synthetic route to generate N-methylbenzothiazolium cation (**1**) and N-methylquinaldinium cation (**2**) respectively

The cyano group attached to the benzothiazole ring devoid it of enough electron density to undergo an electrophilic addition reaction. Nonetheless, (**2**) was condensed as it is with phenothiazine carboxaldehyde.

For the synthesis of the (A) subunit; phenothiazine carboxaldehyde (**5**), commercially available phenothiazine was methylated at N position in the middle ring to yield N-methylphenothiazine (**4**) (Scheme 2). The reaction was done by employing sodium hydride (NaH) as a deprotonating agent followed by the conventional MeI as a simple methylating agent. The sensitive reaction was performed in dry dimethylformamide (DMF) at ice-cold temperature to minimize the formation of hydrogen gas (H_2) bubbles. Consequently, MeI was introduced into the reaction mixture and the reaction was stirred at 40 °C for 24 h. For the next step, a formyl group was introduced at the C3 position in structure (**4**) (Scheme 2).

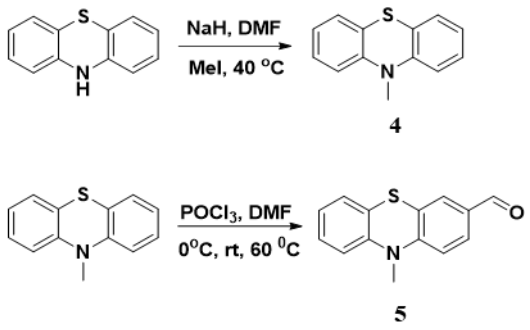

Scheme 2. Synthetic route to generate N-methylphenothiazine (**4**) and N-methylphenothiazine-3-carbaldehyde (**5**)

This was achieved via a facile Vilsmeier-Haack formylation reaction. First, (**4**) was stirred in dry DMF with stoichiometric amount of phosphorus oxychloride ($POCl_3$) at 0 ℃ for 30-40 min under N_2 atmosphere (ice maintained constantly for this time). Consequently, the reaction mixture was further stirred at room temperature (rt) for 20-30 min before it was heated at 60 ℃ for 3 h. After the completion of the reaction, the reaction mixture was poured in ice-cold distilled water to yield a solid product (**5**). Some important notes for the above reaction are, (i) stoichiometric amount of DMF should be used while the in-situ generation of active electrophile; vilsmeier reagent (chloroiminium ion), (ii) the reaction should involve least possible amount of water/ moisture and (iii) the reaction mixture should not be heated over the optimized condition i.e. 60 ℃ for 3 h. Finally, (A) subunits namely, **1**, **2** and **3** were condensed with the synthesized (A) subunit **5** to yield the desired products; **6**, **7** and **8** (Scheme 3). In the forthcoming discussion, we shall refer **6**, **7** and **8** as **TP**, **T_{CN}P** and **QP** respectively. The condensation reaction was carried out following the Knoevenagel-type condensation reaction at rt. One important issue to be taken care of while the syntheses of fluorescent molecules is that these molecules are sensitive to light. Hence, exposure to light was minimalized using an aluminum foil to cover the reaction flask.

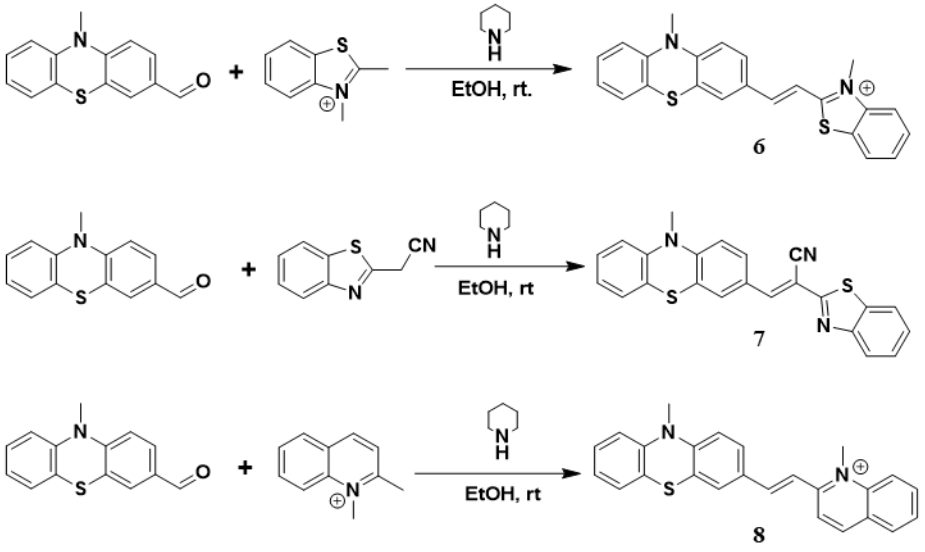

Scheme 3. Facile Knoevenagel-type condensation reactions to synthesize **6**, **7** and **8** respectively

2.5 Results and discussions

The desired condensed products; **6**, **7** and **8** were successfully synthesized and characterized by following, ^{1}H NMR, ^{13}C NMR, and ESI-HRMS analyses. The data has been reported in the appendix section 2.9.

2.6 Photophysical Characterization

The designed and the synthesized molecules namely, **TP**, **T$_{CN}$P** and **QP** were characterized for their spectral profiles i.e. absorbance and emission properties. The data was recorded for 10 µM of each compound in phosphate buffer saline (PBS) buffer at rt condition. Interestingly, **TP** and **QP** exhibited no strong emission in PBS while the cyano analog; **T$_{CN}$P**, exhibited a weak but readable fluoresce signal towards the red wavelength. The observed spectral behavior is regarded as one of the characteristics of an ideal fluorescent probe i.e. an ideal fluorescent molecular sensor should be non-fluorescent or very weakly fluorescent in its free state in solution but when bound to a particular analyte, it should emit an emission signal. This reduces the intervention from the autofluorescence or also referred to as background fluorescence. Fortunately, the three designed molecular probes satisfy this ideal characteristic of an ideal probe.

Hence, these shall be an excellent molecular probe to study important biological phenomena. The challenge is to find out the pertinent target for these molecules. The extensive photophysical examination of these molecular probes with various biological and synthetic analytes have been done in chapter three. The absorption and the emission profiles of the three designed probes; **TP**, **QP** and **T$_{CN}$P** have been demonstrated in Figure 3.

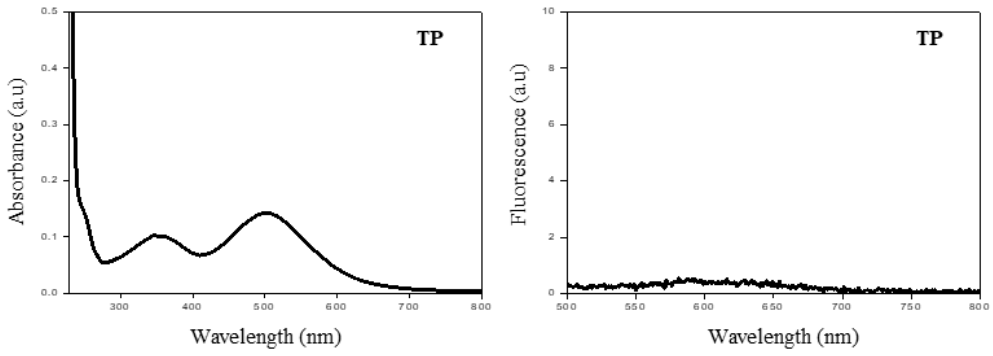

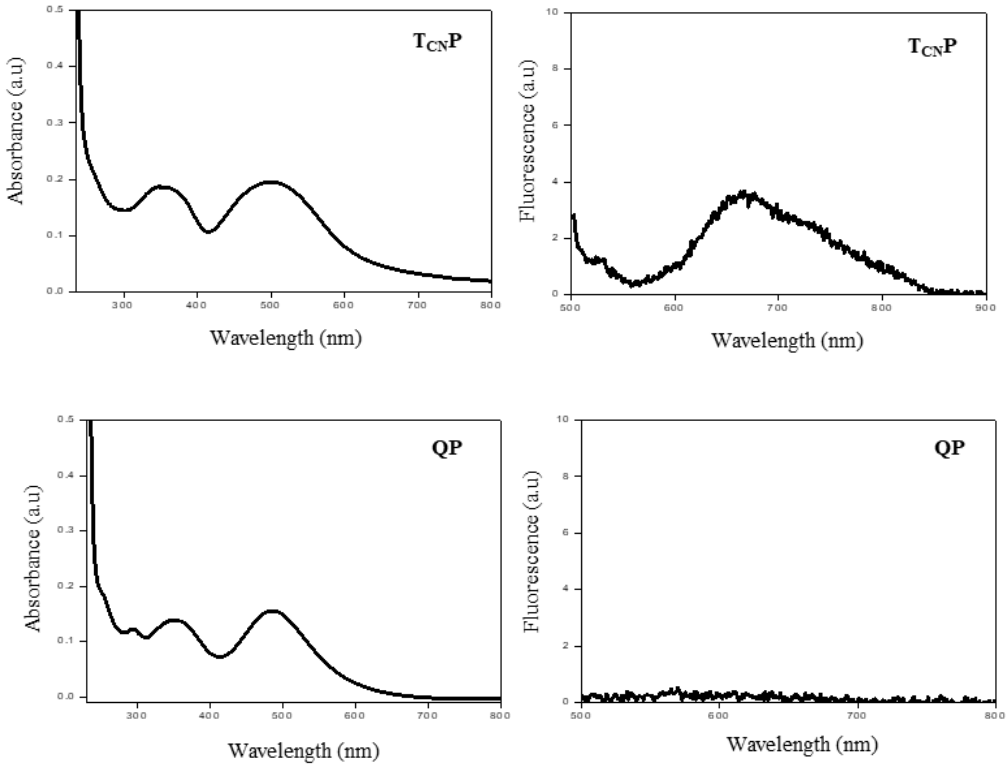

Figure 3. Absorbance and fluorescence spectra of **TP**, **$T_{CN}P$** and **QP** in PBS (10 mM, pH = 7.4)

2.7 Conclusion

We have developed a set of three fluorescent molecules inspired by the already reported structure TC. These molecules are structural analogs of each other in terms of their intrinsic D-π-A architecture. However, the photophysical properties of the synthesized molecules are different which is attributed to the minute structural differences present in their structure. As it is already mentioned, phenothiazine finds a variety of applications in biology and non-biological fields like in materials namely, OLEDS, semiconductors etc. Hence, we speculate that the synthesized phenothiazine-based fluorescent molecules would exhibit chemosensory behavior in pertinent biological systems. Since, these structures are inspired by TC, these may exhibit similar or different interactions with the DNA like TC. Furthermore, different modifications can be done at phenothiazine N and S positions, inspired by the existing FDA approved drugs namely, prochlorperazine (antiemetic) and chlorpromazine (antipsychotic) to develop fluorescent probes to monitor cascades of events in the respective disorders.

2.8 Experimental section

General experimental procedure

All the chemicals, solvents and analytical grade (AR) grade reagents were obtained from Sigma-Aldrich, Tokyo chemical industry (TCI) and Spectrochem and were used as purchased without any further purification. ^{1}H NMR and ^{13}C NMR were performed using Bruker AV-400 spectrometer with chemical shifts reported as parts per million (in *$CDCl_3$ or DMSO d6*, with tetramethylsilane (TMS) as internal standard). Mass spectra was obtained from Agilent 6538 UHD HRMS/Q-TOF spectrometer. Final purification of the compounds was performed using reverse phase chromatography on Shimadzu SPD-M20A HPLC with a single peak collection at 254 nm in the chromatogram. Photophysical characterization was done using Agilent cary series UV-PL spectrometers.

Synthesis of 2, 3-dimethylbenzothiazol-3-ium iodide (**1**)

To a stirred solution of 2-methylbenzothiazole (1 mL, 6 mmol) in MeCN in a high-pressure tube, MeI (2 mL, 40 mmol) was added using a dropper at rt. The reaction mixture was stirred at 40 ℃ for 24 h. The reaction was continuously monitored by thin layer chromatography and after completion of the reaction, the reaction mixture was repeatedly washed with cold diethyl ether. The obtained white precipitate was then filtered and dried to yield an off-white solid compound **1** in quantitative yield. The compound was used for further reactions without any extra purification.

Synthesis of 1, 2-dimethylquinolin-1-ium iodide (**3**)

To a stirred solution of 2-methylquinoline (1 mL, 7 mmol) in MeCN in a high-pressure tube, MeI (2 mL, 40 mmol) was added using a dropper at rt. The reaction mixture was stirred at 40 ℃ for 24 h. The reaction was continuously monitored by thin layer chromatography and after completion of the reaction, the reaction mixture was repeatedly washed with cold diethyl ether. The obtained yellow precipitate was then filtered and dried to yield a dark yellow solid

compound **3** in quantitative yield. The compound was used for further reactions without any extra purification.

Synthesis of 10-methyl-10H-phenothiazine (4)

To a stirred solution of 10H-phenothiazine (500 mg, 2.5 mmol) in dry DMF in a high-pressure tube, NaH (60 mg, 2.5 mmol) was added in lots at 0 ℃. The reaction mixture was stirred for 30 min at 0 ℃ followed by 15 min at rt. To the same solution, MeI (2 mL, 40 mmol) was added using a dropper at rt. The reaction mixture was stirred at 40 ℃ for 24 h. The reaction was continuously monitored by thin layer chromatography and after the completion of the reaction, the reaction mixture was purified by column chromatography using silica get (EtOAc: Hexane,10:90) to yield a white solid compound **4** in average yield (60%). ^{1}H NMR (400 MHz, *DMSO d6*) δppm 3.32 (s, 3H), 6.97 (m, 4H), 7.15 (s, 1H), 7.17 (s, 1H), 7.22 (t, *J* = 15.44, 2H). ^{13}C NMR (100 MHz, *DMSO d6*) δppm 35.5, 115.0, 122.5, 122.9, 127.2, 128.2, 145.8. HRMS (ESI-TOF, $(M+H)^{+}$) Calcd. for $C_{13}H_{11}NS$ 214.0690 found 214.0671.

Synthesis of 10-methyl-10H-phenothiazine-3-carbaldehyde (5)

To a stirred solution of **4** (500 mg, 2.3 mmol) in dry DMF (2 mL, 27 mmol), POCl3 (1.5 mL, 16 mmol) was dropwise added through a septum under N_2 atmosphere at ≤0 ℃. The reaction mixture was stirred under same condition for 40 min before it was brought to rt when the reaction mixture was further stirred for 20 min. The dark red reaction mixture was then heated at 60 ℃ for 3 h. The completion of the reaction was continuously monitored by thin layer chromatography and after the completion of the reaction, the reaction mixture was poured into ice-cold water when a yellowish-brown precipitate of **5** was observed in average yield (62%). The precipitate was filtered and dried. ^{1}H NMR (400 MHz, *DMSO d6*) δppm 3.40 (s, 3H), 7.04 (d, *J* = 7.68, 2H), 7.11 (d, *J* = 8.60, 1H), 7.19 (d, *J* = 7.08, 1H), 7.26 (t, *J* = 15.64, 1H), 9.81 (s, 1H). ^{13}C NMR (100 MHz, *DMSO d6*) δppm 36.1, 115.0, 115.9, 121.6, 122.9, 124.0, 127.4, 127.7, 125.5, 130.9, 131.4, 144.2, 150.9, 191.1. HRMS (ESI-TOF, (M^{+}) Calcd. for $C_{14}H_{11}NOS$ 241.0561 found 241.0933.

Synthesis of 3-methyl-2-(2-(10-methyl-10H-phenothiazin-3-yl) vinyl) benzothiazol-3-ium iodide (**6**)

To a stirred solution of **1**(500 mg, 1.7 mmol) in ethanol (30 mL), piperidine (170 µL, 1.7 mmol) was added dropwise using a micropipette. The reaction mixture was stirred at rt for 20 min. To the same solution, **5** (414 mg, 1.7 mmol) suspended in ethanol was added and the reaction mixture was stirred for 24 h. The reaction was continuously monitored by thin layer chromatography and after the completion of the reaction, the reaction mixture was kept at -20 ℃ for precipitation. The obtained dark blue precipitate was filtered and washed with hexane. The precipitate was re-dissolved in MeCN and filtered through microfilter (0.4 µm) to be injected in reverse phase HPLC for further purification. The obtained pure fractions from HPLC were lyophilized for 24 h to yield a dark blue solid compound **6** in good yield (57 %). ^{1}H NMR (400 MHz, *CDCl$_3$*) δppm 3.31 (s, 3H), 4.35 (s, 3H), 6.62 (d, *J* = 8.60, 1H), 6.82 (d, *J* = 8.08, 1H), 7.03 (d, *J* = 14.80, 1H), 7.13 (d, *J* = 7.52, 1H), 7.23 (t, *J* = 15.48, 1H), 7.47 (m, 1H), 7.15 (m, 2H), 7.58 (m, 1H), 7.76 (m, 2H), 7.98 (m, 2H). ^{13}C NMR (100 MHz, *CDCl$_3$*) δppm 35.7, 36.2, 110.0, 114.2, 114.9, 115.3, 122.2, 123.4, 123.7, 123.8, 127.2, 127.4, 127.7, 127.8, 128.2, 128.3, 129.4, 131.1, 141.5, 143.6, 149.6, 149.7, 160.7, 161.1, 171.8. HRMS (ESI-TOF, (M^+) Calcd. for $C_{23}H_{19}N_2S_2$ 387.0984 found 387.1092.

Synthesis of 2-(benzothiazole-2-yl)-3-(10H-ohenothiazin-3-yl) acrylonitrile (**7**)

To a stirred solution of **2** (500 mg, 2.8 mmol) in ethanol (30 mL), piperidine (283 µL, 2.8 mmol) was added dropwise using a micropipette. The reaction mixture was stirred at rt for 20 min. To the same solution, **5** (690 mg, 2.8 mmol) suspended in ethanol was added and the reaction mixture was stirred for 24 h. The reaction was continuously monitored by thin layer chromatography and after the completion of the reaction, the reaction mixture was kept at -20 ℃ for precipitation. The obtained dark orange precipitate was filtered and washed with hexane. The precipitate was re-dissolved in MeCN and filtered through microfilter (0.4 µm) to be injected in reverse phase HPLC for further purification. The obtained pure fractions from HPLC were lyophilized for 24 h to yield an orange solid compound **7** in good yield (80 %). ^{1}H NMR (400 MHz, *DMSO d6*) δppm 3.42 (s, 3H), 7.04 (m, 2H), 7.15 (d, *J* = 8.68, 1H), 7.21 (d, *J* =7.44, 1H),

7.27 (t, *J* =15.48, 1H), 7.50 (t, *J* = 15.16, 1H), 7.58 (t, *J* = 15.24, 1H), 7.92 (d, *J* = 1.72, 1H), 8.04 (m, 2H), 8.15 (d, *J* = 7.96, 1H), 8.26 (s, 1H). ^{13}C NMR (100 MHz, *DMSO d6*) δppm 36.0, 102.3, 115.2, 115.9, 117.1, 121.4, 122.7, 123.3, 126.5, 126.9, 127.5, 128.6, 131.6, 134.6, 144.1, 147.0, 149.2, 153.5, 164.0. HRMS (ESI-TOF, $(M+H)^+$) Calcd. for $C_{23}H_{16}N_3S_2$ 398.0786 found 398.0739.

Synthesis of 1-methyl-2-(2-(10-methyl-10H-phenothiazin-3-yl) vinyl) quinoline-1-ium iodide (8)

To a stirred solution of **3** (500 mg, 1.7 mmol) in ethanol (30 mL), piperidine (172 µL, 1.7 mmol) was added dropwise using a micropipette. The reaction mixture was stirred at rt for 20 min. To the same solution, **5** (422 mg, 1.7 mmol) suspended in ethanol was added and the reaction mixture was stirred for 24 h. The reaction was continuously monitored by thin layer chromatography and after the completion of the reaction, the reaction mixture was kept at -20 ℃ for precipitation. The obtained dark blue precipitate was filtered and washed with hexane. The precipitate was re-dissolved in MeCN and filtered through microfilter (0.4 µm) to be injected in reverse phase HPLC for further purification. The obtained pure fractions from HPLC were lyophilized for 24 h to yield a dark blue solid compound **8** in good yield (83 %). ^{1}H NMR (400 MHz, *DMSO d6*) δppm 3.41 (s, 3H), 4.55 (s, 3H), 7.04 (m, 2H), 7.09 (d, *J* = 8.40, 1H), 7.22 (d, *J* = 7.52, 1H), 7.27 (t, *J* = 15.48, 1H), 7.76 (d, *J* = 8.36, 1H), 7.82 (d, *J* = 15.76, 1H), 7.93 (t, *J* = 14.92, 2H), 8.16 (m, 2H), 8.32 (d, *J* = 8.00, 1H), 8.53 (d, *J* = 9.00, 2H), 9.00 (d, *J* = 8.92, 1H). ^{13}C NMR (100 MHz, *DMSO d6*) δppm 36.0, 115.2, 115.8, 117.2, 119.7, 121.2, 121.6, 123.2, 123.8, 126.9, 127.4, 128.0 128.5, 129.2, 129.8, 130.4, 131.2, 135.2, 139.7, 143.9, 144.4, 146.6, 148.5, 156.6. HRMS (ESI-TOF, (M^+) Calcd. for $C_{25}H_{21}N_2S$ 381.1420 found 381.1526.

2.9 Appendix

2.9.1 NMR characterization

*10-Methyl-10H-phenothiazine (**4**)*

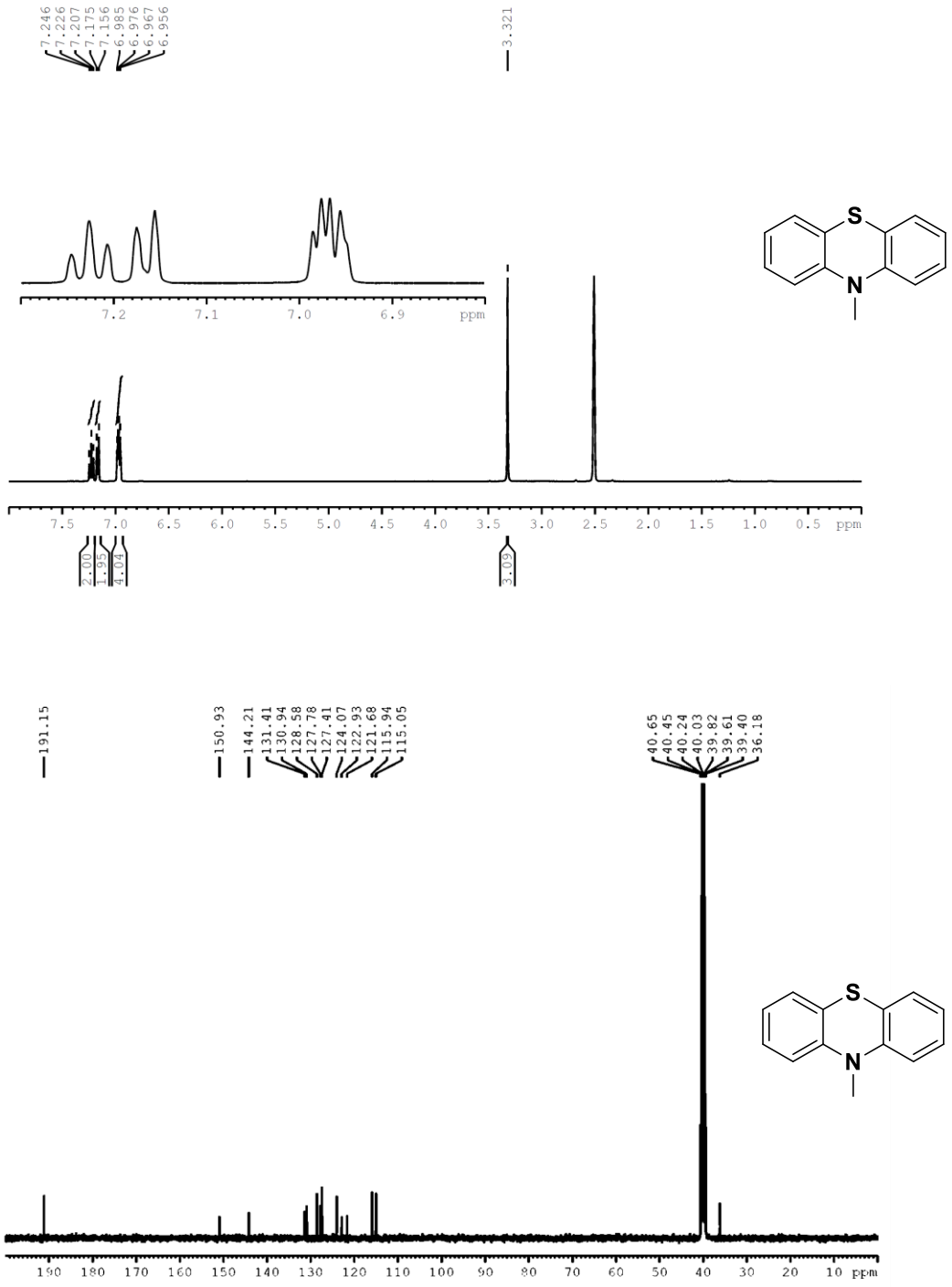

*10-Methyl-10H-phenothiazine-3-carbaldehyde (**5**)*

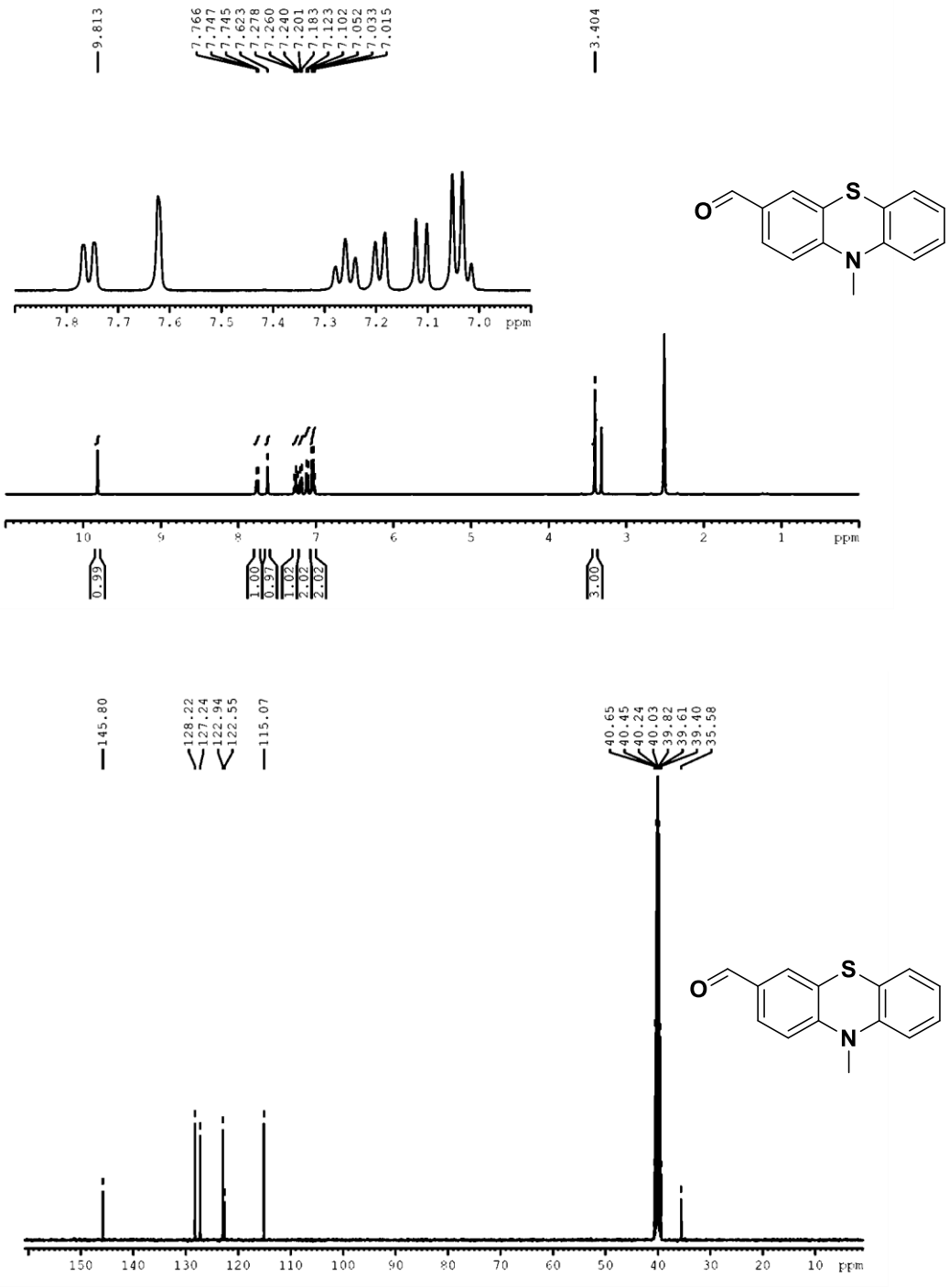

*3-Methyl-2-(2-(10-methyl-10H-phenothiazin-3-yl) vinyl) benzothiazol-3-ium iodide (**6**) or **TP***

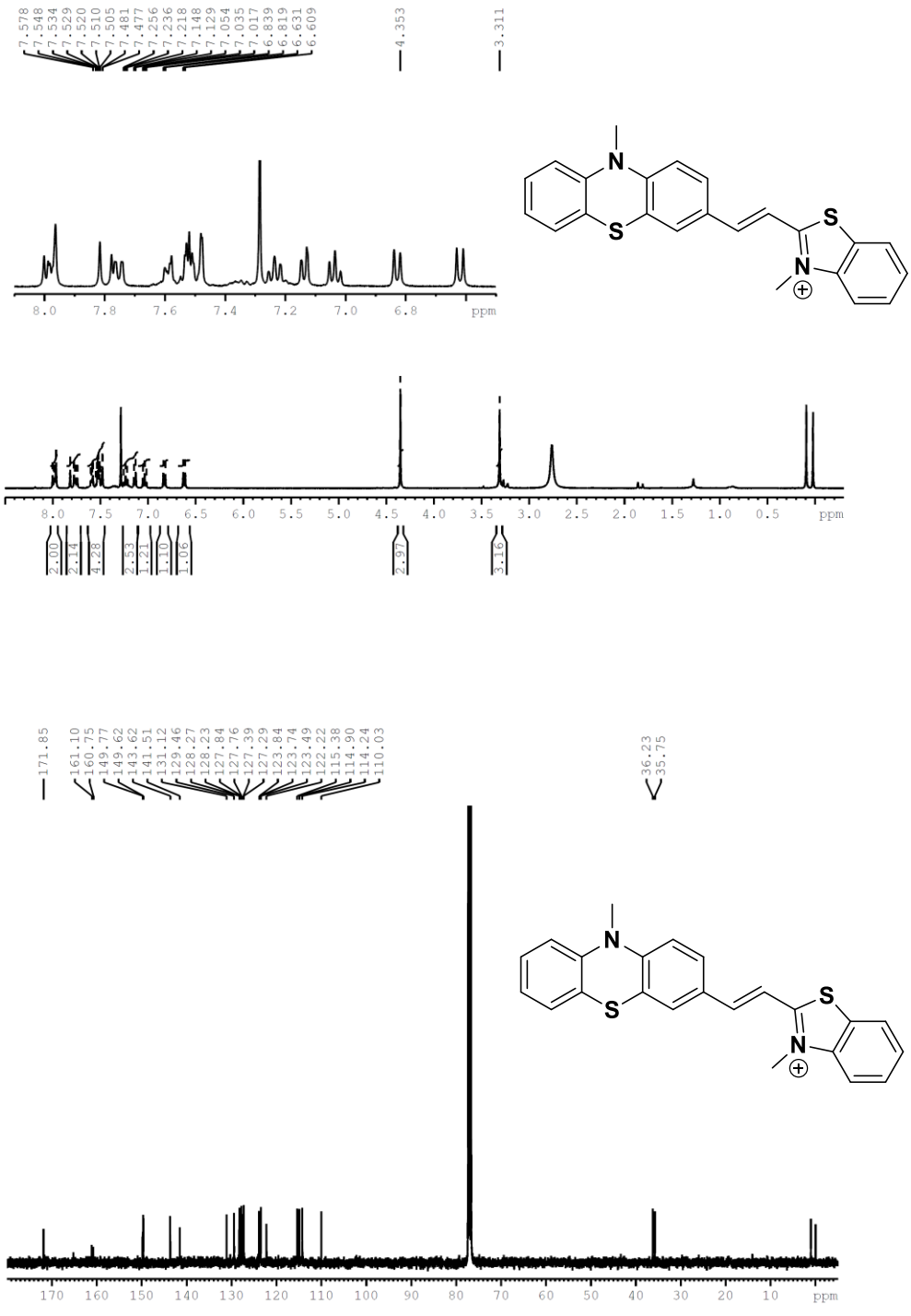

*2-(Benzothiazole-2-yl)-3-(10H-ohenothiazin-3-yl) acrylonitrile (**7**) or* ***$T_{CN}P$***

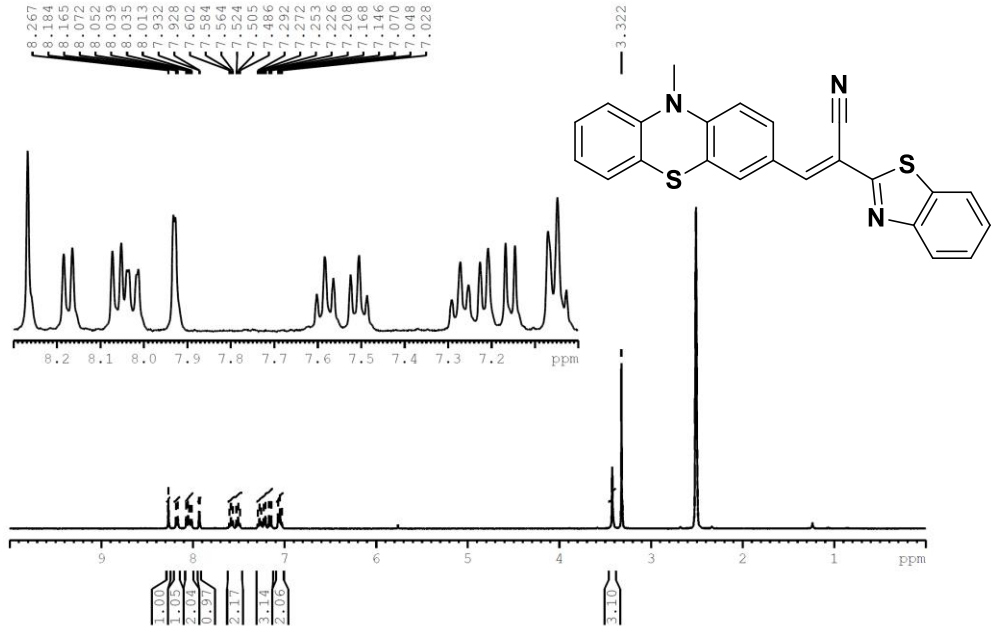

*1-Methyl-2-(2-(10-methyl-10H-phenothiazin-3-yl) vinyl) quinoline-1-ium iodide (**8**) or **QP***

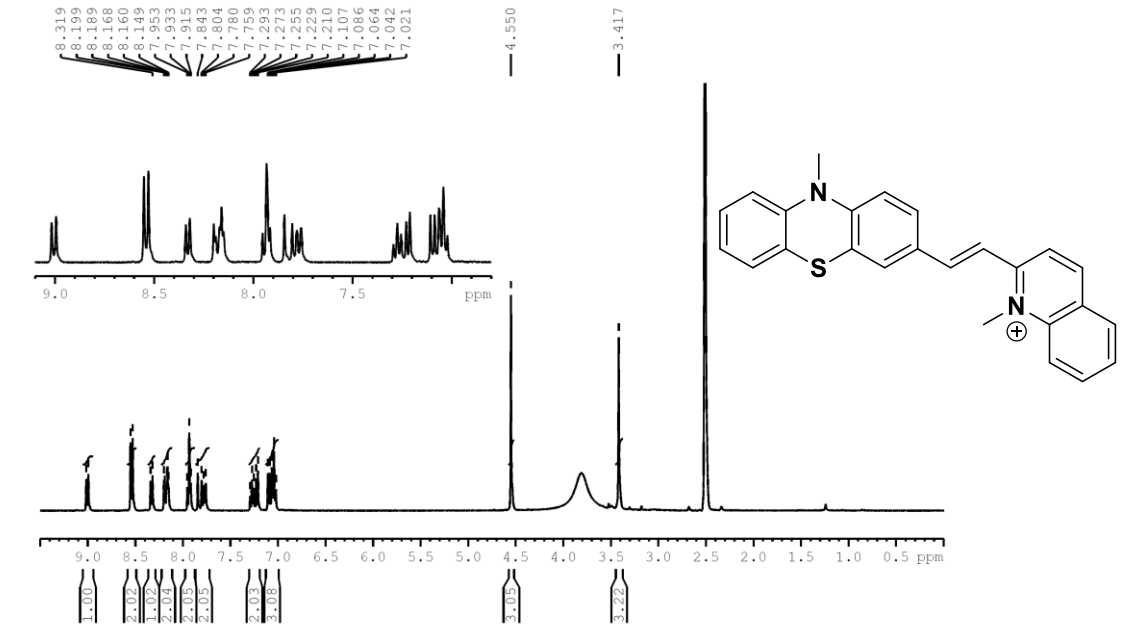

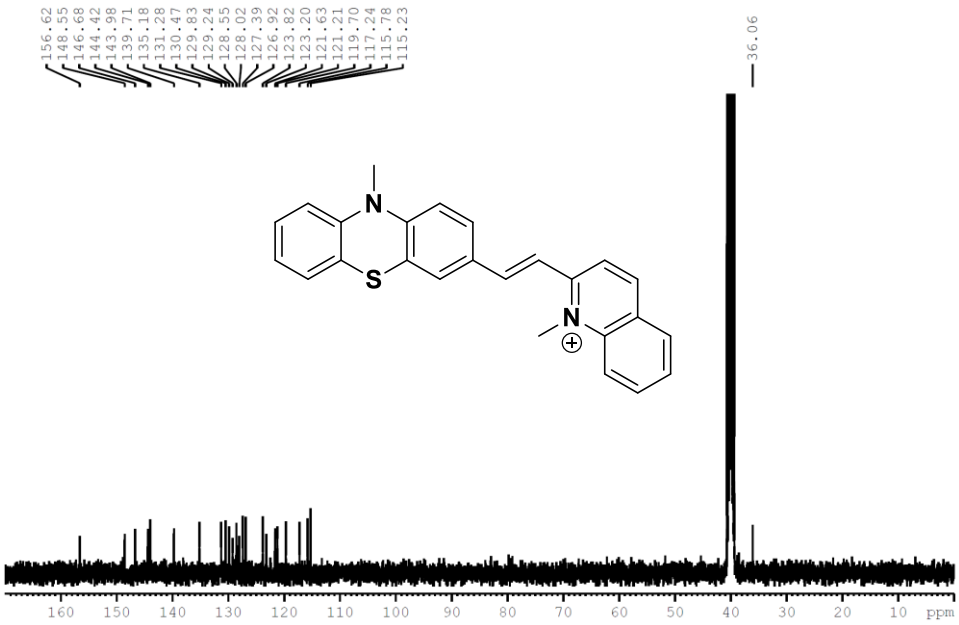

2.9.2 HRMS characterization

*2, 3-Dimethylbenzothiazol-3-ium iodide (**1**)*

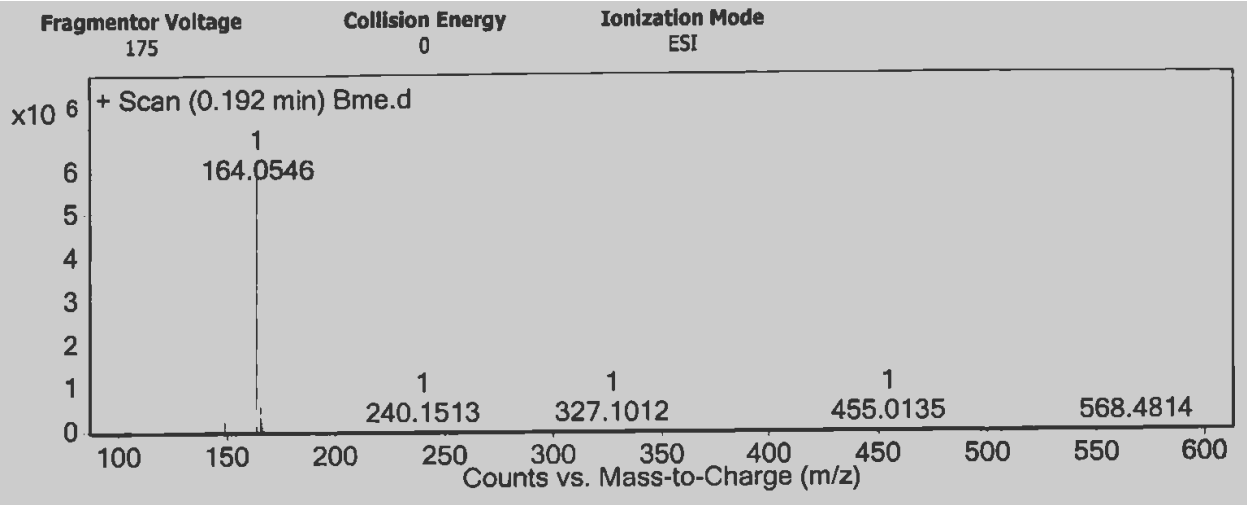

*1, 2-Dimethylquinolin-1-ium iodide (**3**)*

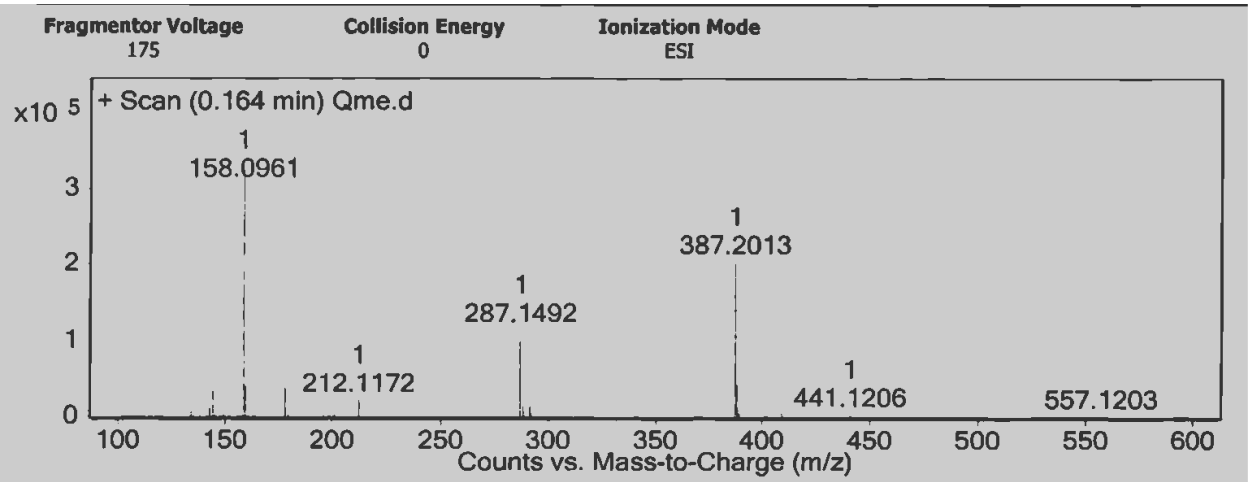

*10-Methyl-10H-phenothiazine (**4**)*

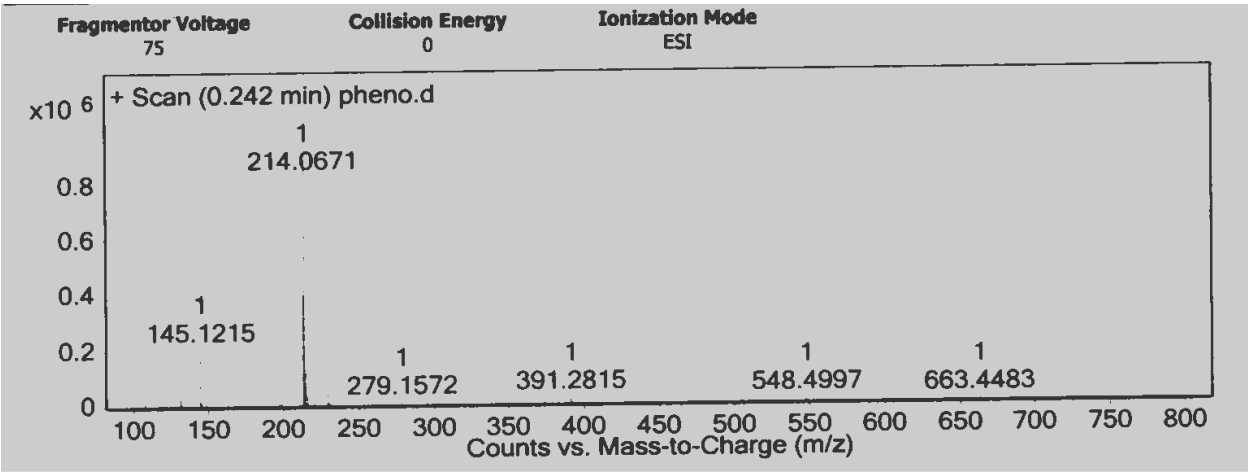

*10-Methyl-10H-phenothiazine-3-carbaldehyde (**5**)*

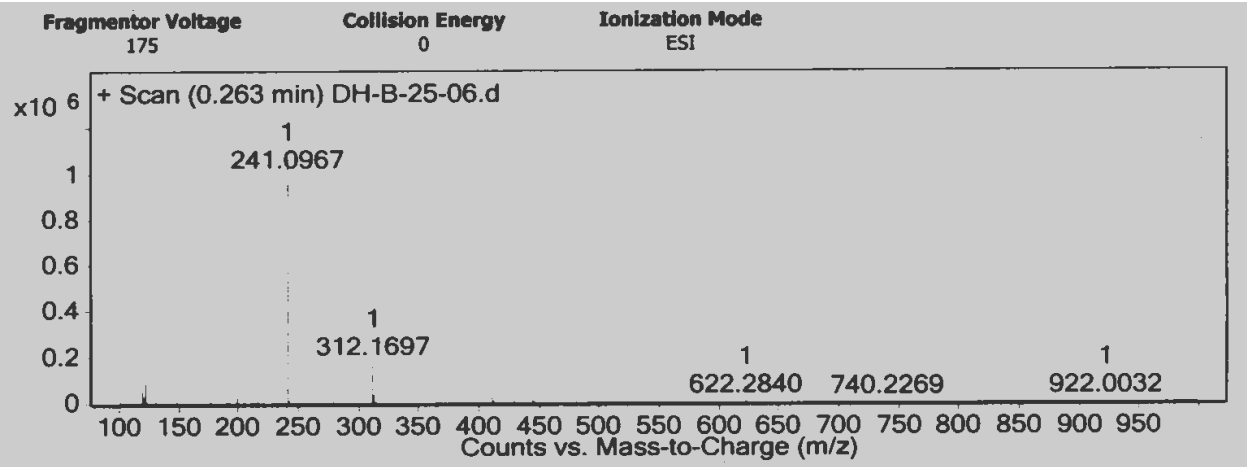

*3-Methyl-2-(2-(10-methyl-10H-phenothiazin-3-yl) vinyl) benzothiazol-3-ium iodide (**6**) or **TP***

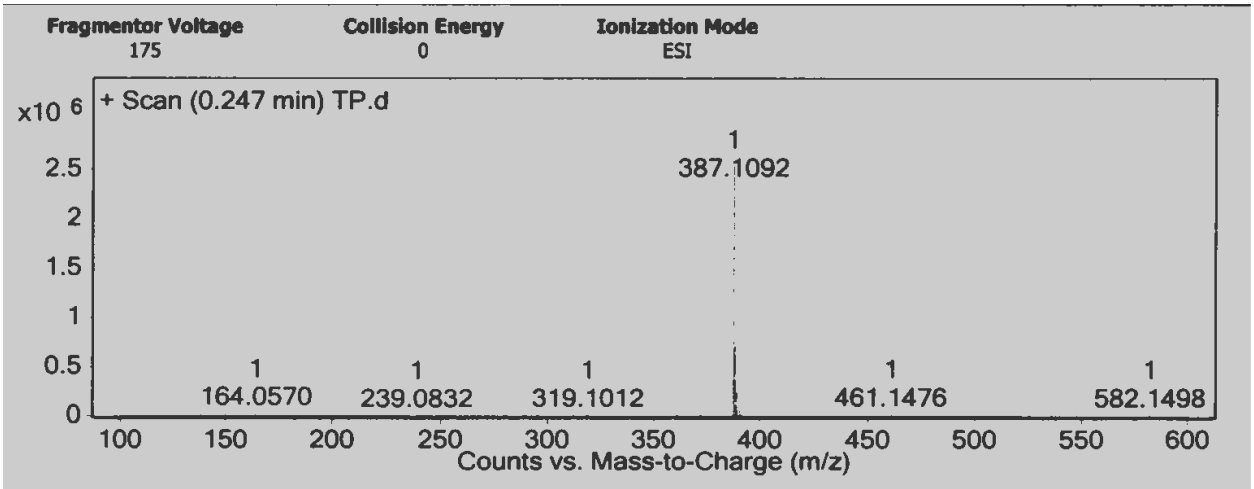

*2-(Benzothiazole-2-yl)-3-(10H-ohenothiazin-3-yl) acrylonitrile (7) or **$T_{CN}P$***

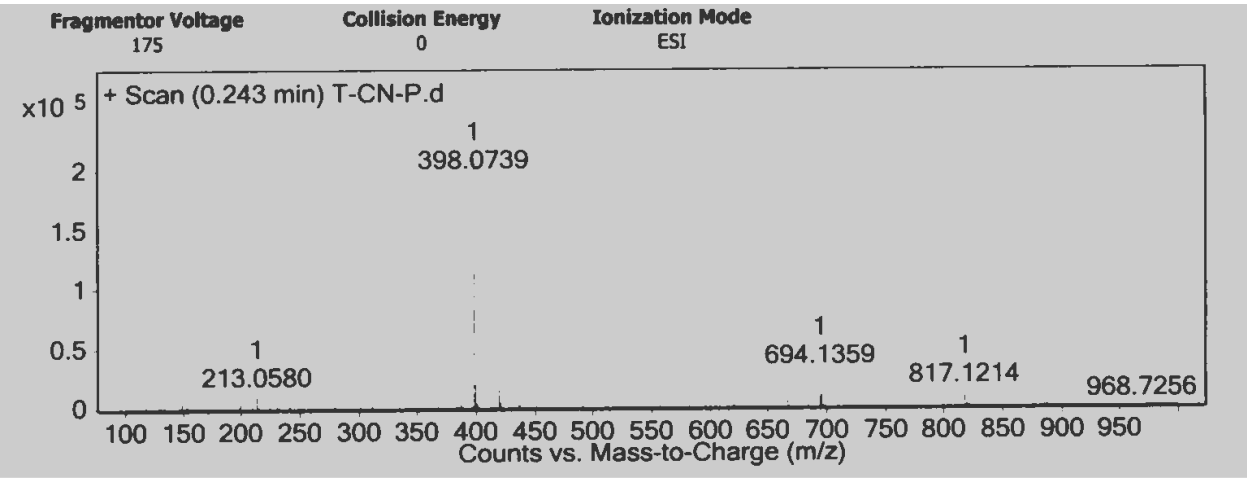

*1-Methyl-2-(2-(10-methyl-10H-phenothiazin-3-yl) vinyl) quinoline-1-ium iodide (**8**) or **QP***

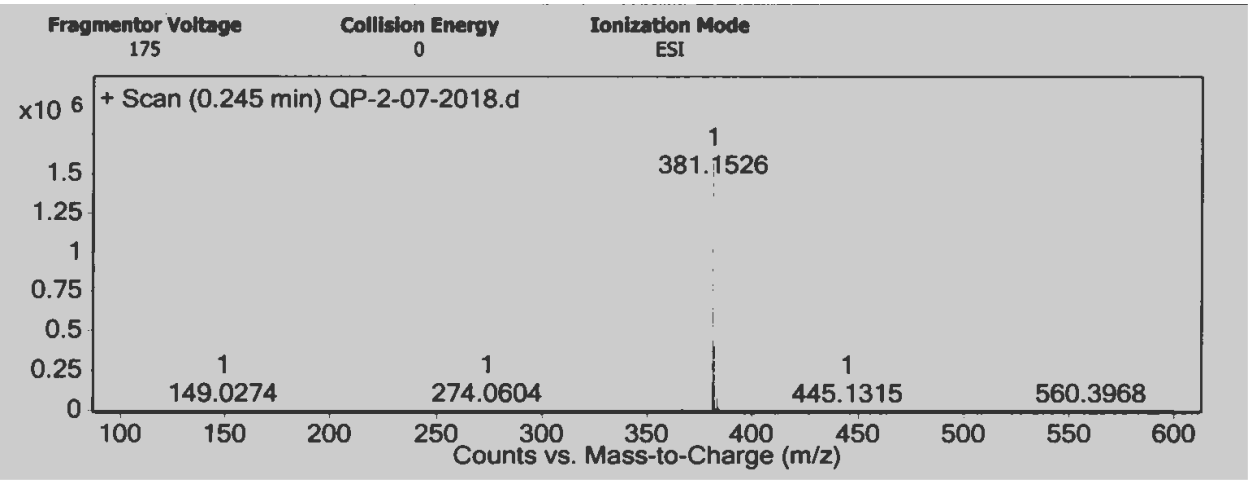

2.10 References

1. Wang, L.; Frei, M. S.; Salim, A.; Johnsson, K., Small-Molecule Fluorescent Probes for Live-Cell Super-Resolution Microscopy. *J. Am. Chem. Soc.* **2019,** *141* (7), 2770-2781.

2. Narayanaswamy, N.; Kumar, M.; Das, S.; Sharma, R.; Samanta, P. K.; Pati, S. K.; Dhar, S. K.; Kundu, T. K.; Govindaraju, T., A Thiazole Coumarin (TC) Turn-On Fluorescence Probe for AT-Base Pair Detection and Multipurpose Applications in Different Biological Systems. *Sci. Rep.* **2014,** *4*, 6476.

3. Rajasekhar, K., Narayanaswamy, N., Murugan, N. A., Kuang, G., Ågren, H., & Govindaraju, T. A high affinity red fluorescence and colorimetric probe for amyloid β aggregates. *Sci. Rep.* **2016,** *6*, 23668.

4. Rajasekhar, K., Narayanaswamy, N., Murugan, N. A., Viccaro, K., Lee, H. G., Shah, K., & Govindaraju, T. Aβ plaque-selective NIR fluorescence probe to differentiate Alzheimer's disease from tauopathies. *Biosens. Bioelectron.* **2017**, *98*, 54-61.

5. Narayanaswamy, N., Das, S., Samanta, P. K., Banu, K., Sharma, G. P., Mondal, N., ... & Govindaraju, T. Sequence-specific recognition of DNA minor groove by an NIR-fluorescence switch-on probe and its potential applications. *Nucleic Acids Res.* **2015**, *43*(18), 8651-8663.

6. Zhang, Y.; Chen, Z.; Song, J.; He, J.; Wang, X.; Wu, J.; Chen, S.; Qu, J.; Wong, W.-Y., Rational design of high efficiency green to deep red/near-infrared emitting materials based on isomeric donor–acceptor chromophores. *J. Mater. Chem. C* **2019,** *7* (7), 1880-1887.

7. Massie, S. P., The Chemistry of Phenothiazine. *Chem. Rev.* **1954,** *54* (5), 797-833.

8. Bernthsen, A., Zur Kenntniss des Methylenblau und verwandter Farbstoffe. *Ber. Dtsch. Chem. Ges.* **1883,** *16* (2), 2896-2904.

9. Mosnaim, A. D.; Ranade, V. V.; Wolf, M. E.; Puente, J.; Antonieta Valenzuela, M., Phenothiazine Molecule Provides the Basic Chemical Structure for Various Classes of Pharmacotherapeutic Agents. *Am. J. Ther.* **2006,** *13* (3), 261-273.

10. Ohlow, M. J.; Moosmann, B., Phenothiazine: the seven lives of pharmacology's first lead structure. *Drug Discov. Today* **2011,** *16* (3), 119-131.

11. Jones, G. "The Knoevenagel Condensation." *Organic Reactions*, 2004; pp 204-559.

12. Sola, M.; Lledos, A.; Duran, M.; Bertran, J.; Abboud, J. L. M., Analysis of solvent effects on the Menshutkin reaction. *J. Am. Chem. Soc.* **1991,** *113* (8), 2873-2879.

A red-NIR selective fluorescent molecular sensor for BSA

Chapter Three - A

Abstract

In this chapter, a D-π-A architecture; **T_{CN}P** has been examined in detail for its selective interactions with bovine serum albumin (BSA). At first, the stability of **T_{CN}P** has been monitored by spectroscopic measurements as a function of varying dielectric constant of different solvents, viscosity and pH conditions. Furthermore, the selectivity of the probe towards BSA has been demonstrated by using a comparative analysis with the other biological or biologically important analytes. Later, statistical analyses (Stern-Volmer, Lippert-Mataga and Benesi-Hildebrand plots) have been utilized to provide useful physical insights about the BSA- **T_{CN}P** system.

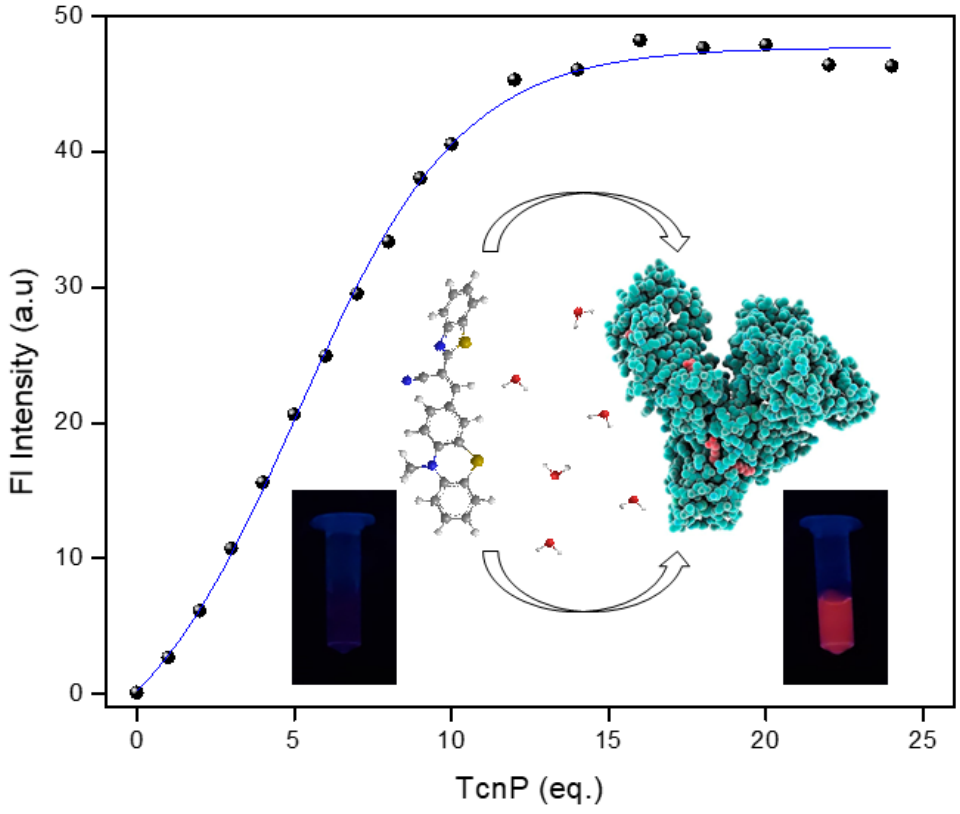

Figure demonstrates that the BSA-**T_{CN}P** system follows a sigmoidal curve. The schematic inside the graph shows that the probe binds to the BSA with a concomitant 'turn-on' red signal

3.1 Introduction

Fluorescence spectral examination of bio-macromolecules such as proteins is significant because, fluorescence spectroscopy can easily probe and monitor proteins' biochemical roles in the living organisms. Intrinsic fluorescence of a protein is due to the presence of three amino acids namely, phenylalanine (F), tyrosine (Y), and tryptophan (W) as already mentioned in chapter one.[1] Among these amino acids tryptophan (W) is more dominant as well as more sensitive to alterations in its micro-environment. Serum albumin protein is one of the most abundant proteins found in the plasma and is present throughout the mammalian kingdom.[2] Albumin is a complex globular protein which has multiple functions in living organisms including; (i) transport of fatty acids in blood plasma, (ii) regulation of osmotic pressure of the circulatory system, (iii) binding to several foreign molecules like drugs and toxins.[3] It is well known from several scholarly reports that there are numerous transport proteins present in the blood plasma however, the unique property of albumin is that it binds reversibly and transports a variety of ligands. During an intravenous administration, serum proteins and DNA are the major targets for the synthetic drugs or bioactive molecules. This characteristic of the albumin proteins prompted significant interests in the study of interaction of foreign (synthesized) molecules with the albumin.

Bovine serum albumin (BSA) is a well characterized and abundant serum albumin which is generated as a by-product of meat industry. Most importantly, BSA is homologous to human serum albumin (HSA) and owing to its abundance and cost effectiveness, several experiments can be performed with BSA and hypotheses can be laid similarly for HSA.[4] The full-length BSA precursor protein is 607 amino acids (AAs) in length. An N-terminal 18-residue signal peptide is cut off from the precursor protein upon secretion, hence the initial protein product contains 589 amino acid residues. An additional six amino acids are cleaved to yield the mature BSA protein (66.5kDa) that contains 583 amino acids.[5] BSA per se exhibits high binding to the drug molecules which can simply be reasoned out by studying the presence of large number of binding sites in its structure. These sites are compartmentalized in three domains namely, I, II and III. Further, these domains are divided in two sub-domains A and B.[6]

The three domains with different surface charge densities impact BSA adsorption on charged surfaces.[5,7] As for example, the presence of both positively charged residues (lysine and

arginine) and negatively charged amino acids (glutamic acid and aspartic acid) on BSA can result in electrostatic interactions with both negatively and positively charged surfaces, respectively.[8-9] Because of the presence of a negatively charged domain, BSA is involved in (a) binding with water, salts, fatty acids, vitamins, and hormones and carries them between tissues and cells, (b) removing toxic substances, including pyrogens, from the medium, (c) solubilizing lipids and is a blocking agent in western blot or enzyme-linked immunosorbent assay applications, and (d) solubilizing other proteins (e.g., labile enzymes). BSA is readily soluble in water and can only be precipitated in the presence of high concentrations of neutral salts such as ammonium sulfate. However, albumin is readily coagulated by heat. So, it is apparent that the BSA can bind a large variety of bioactive molecules by various noncovalent interactions such as hydrophobic, hydrophilic, and ionic interactions. The major binding sites of BSA are localized in subdomains, IIA and IIIA, known as site I and site II. To infer the protein interaction site with small molecules, site marker fluorescent probes are utilized.[10] *In vivo* binding of serum albumin with the small organic molecule and most of the drugs is well known. The drug protein interaction affects the biological activity of the drug. Hence, it is important to study the interaction and behavior of these molecules towards BSA as these molecules could be utilized in pharmacological application. Moreover, BSA can be developed as a potent tool for protein–drug interaction studies and their specific and firm binding with small molecules, drugs and dyes which can be used for drug delivery in future.[11-13] These studies could provide the valuable information on the structural feature that determines the efficiency of drugs. Utilization of sensitive and easy to handle fluorometric techniques for the interaction of fluorescent molecules with BSA is an interesting area of research.

In our present work, we have studied **$T_{CN}P$**, which upon interacting with BSA yields a ‘turn-on’ fluorescence signal in the NIR spectral window. The other two analogues; **TP** and **QP** were discontinued due to their inefficiency to probe any potential analyte.

3.2 Photophysical properties of red-NIR probe

$T_{CN}P$ has been synthesized as a combination of a cyanobenzothiazole unit (D), a phenothiazine unit (A) and a vinyl unit (π-linkage). The D-π-A architecture was designed to obtain a

fluorescent molecular probe in the red-NIR spectral region. **$T_{CN}P$** exhibited favorable solubility in common organic solvents such as methanol (MeOH), ethanol (EtOH), acetonitrile (MeCN), dimethyl sulfoxide (DMSO), chloroform ($CHCl_3$), dichloromethane (DCM), tetrahydrofuran (THF), toluene, but was sparingly soluble in water. Therefore, a stock solution of 1 mM of the compound was prepared in DMSO and used for the experiments. Since phosphate buffer saline (PBS) is commonly used buffer in several biological experiments, all the performed photophysical studies have been done in PBS, by dissolving the appropriate amount of **$T_{CN}P$** stock solution into required volume of PBS.

3.2.1 Effect of solvent polarity

As depicted in the absorption spectrum of the compound (Figure 1a), the λ_{max} value exhibited a bathochromic (towards red wavelength) shift upon increasing the polarity of the solvent i.e. the absorption maximum (λ_{max}) value shifted from 463 nm in toluene to 495 nm in PBS (aqueous environment). The concentration of the probe was kept constant at 10 µM in all solvents. This feature is clearly an indication of the positive solvatochromism. The observed red shift in the absorption spectrum of **$T_{CN}P$** can easily be explained based on the stabilization of the electronic state hypothesis, i.e. if the ground state of the molecule under interest is polar then upon increasing the polarity of the environment, the ground state gets stabilized in terms of its energy

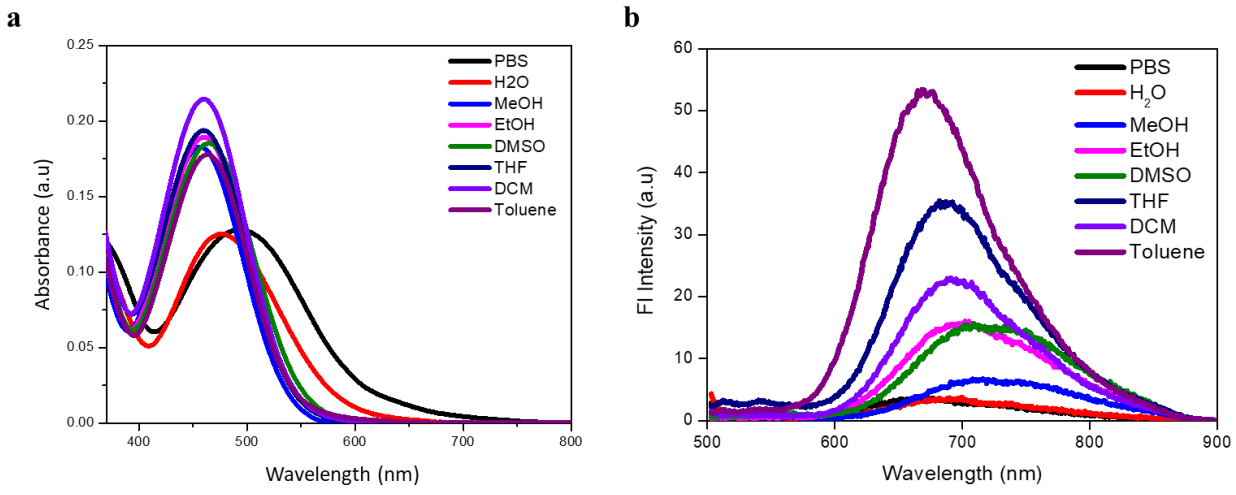

Figure 1 Absorption (a) and emission (b) spectra of **$T_{CN}P$** in different solvents

and consequently, the energy gap between the ground and the excited state would increase leading to transitions corresponding to lower wavelengths (hypsochromic shift). Nonetheless, in our case the shift is towards red which means that the excited state must have been a polar state.

In concordance with the absorption data, fluorescence spectrum of the molecule was also studied in solvents with disparate polarities. As depicted in the emission spectrum (Figure 3a), **$T_{CN}P$** exhibited a decrease in its emission maximum (λ_{em}) when the polarity of the environment was increased i.e. the λ_{em} value shifted from 55 a.u in toluene to 5 a.u in PBS/H_2O (the concentration of the probe was kept constant at 10 µM). Moreover, the probe displayed a significant bathochromic shift in its λ_{em} value ranging from 671 nm in toluene to ~727 nm in MeOH (Figure 1b). The spectral information can also be visualized by the visual signal from the probe dissolved in different solvents (Figure 2). The above experimentally observed data can be explained based on the Lippert-Mataga equation (theory of solvent effects on fluorophore's emission). According to the theory, fluorophores, in general have larger dipole moment in their excited states than their ground states. Following excitation at characteristic λ_{max}, the solvent dipoles reorient or relax around the excited state and as the solvent polarity is increased, this effect becomes larger, resulting in emission at lower energies or higher wavelengths (bathochromic shift).

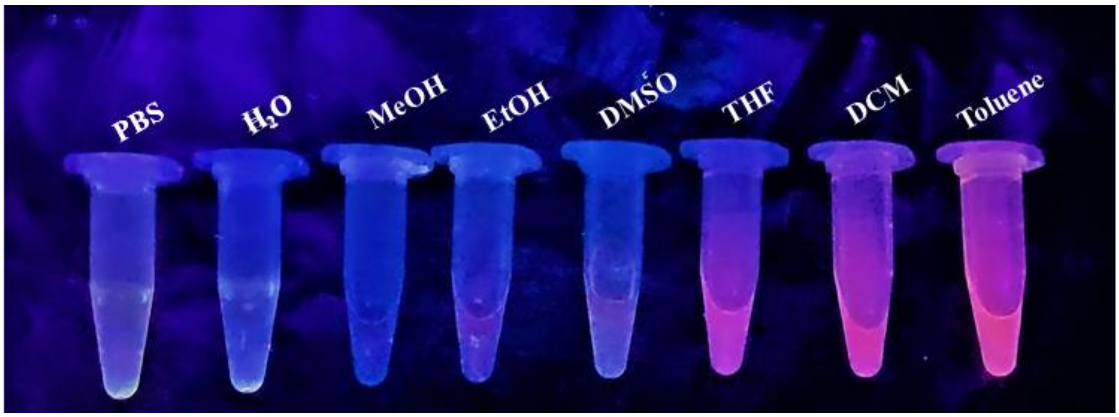

Figure 2 Fluorimetric change in the solution of **$T_{CN}P$** with different solvents

However, in addition to the above explanation, there are many other hypotheses which take several other parameters into account as well. As in our case, the molecule **$T_{CN}P$** has a donor phenothiazine and an acceptor benzothiazole and such a system is most probable to form internal

charge transfer (ICT) state, or a twisted ICT (TICT). Consequently, there exist a charge separation which is even more enhanced upon excitation hence, larger dipole moment in the excited state and longer wavelength shift (towards red) upon interactions with solvents of increasing polarities.

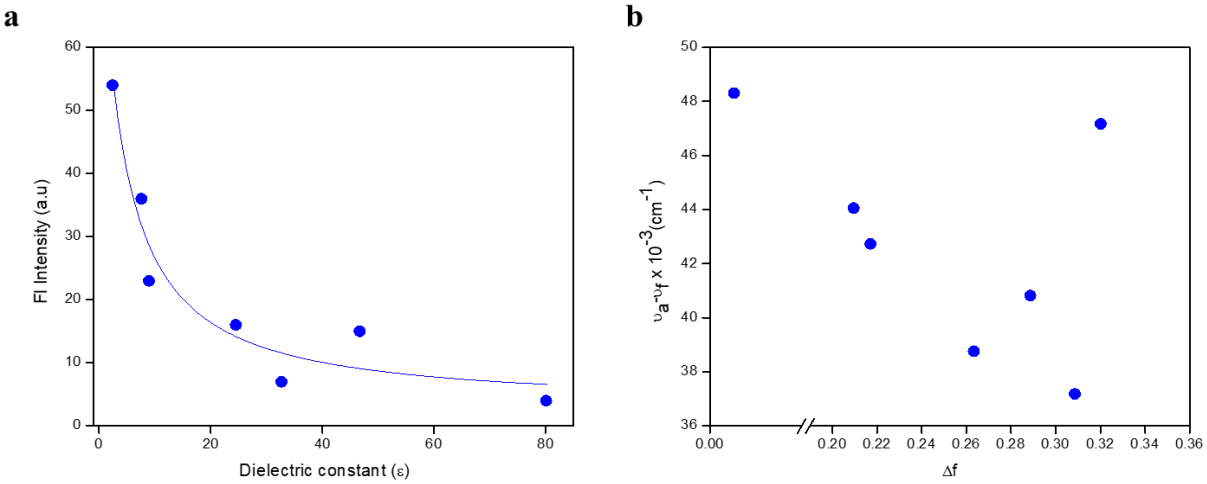

Figure 3 (a) Fluorescence spectrum of **$T_{CN}P$** decays when plotted as a function of increasing dielectric constants i.e. polarity of solvents (b) the Lippert-Mataga plot depicting the dependence of **$T_{CN}P$** photo-physics on solvent properties

It has been reported in the literature that Lippert-Mataga analysis provides a reliable means to examine the specific solvent effect on the photo-physics of the fluorescent probe.[14]

$$\nu_A - \nu_B = {}^{2}/_{hc} \frac{\left({}^{\varepsilon - 1}/_{2\varepsilon + 1} - {}^{n^2 - 1}/_{2n^2 + 1}\right)(\mu_E - \mu_G)^2}{a^3}$$

Where, *h* is the Planck's constant, c is the speed of light, *a* is the radius of the cavity in which the fluorophore resides, n is the refractive index of the solvent and ε is the dielectric constant o the solvent. ν_A and ν_F are the wave numbers (cm^{-1}) of absorption and fluorescence. Hence, we have constructed a Lippert-Matage plot (Figure 3b) to understand the solvent effects on the designed

probe; **T$_{CN}$P**. It is clear from the plot that **T$_{CN}$P** follows a non-linear behavior with the increasing polarizabilities of the solvents (plotted on the X-axis). A linear Lippert plot demonstrates no specific interactions of the probe with the solvents. On the contrary, **T$_{CN}$P** is expected to exhibit specific interactions with different solvents and hence, a non-linear Lippert plot corroborates it.

As a simple structure, α-cyanostilbene is usually employed as a building block while constructing an AIE fluorogen.[15] Interestingly, a part of **T$_{CN}$P** contains a similar moiety i.e. cyanobenzothiazole which should impart AIE characteristics to the overall molecule. Thus, we carried out a simple absorption and fluorescence study in a mixture of DMSO and H_2O, with increasing concentration of H_2O from 0 to 100 % (stock solution was prepared in DMSO). As depicted in the absorption spectrum (Figure 4a), **T$_{CN}$P** displayed a slight bathochromic shift in its λ_{max} value ranging from 465 nm in 100 % DMSO to 475 nm in 100 % H_2O besides a slight decrement in the absorption intensity till 50 % H_2O (v/v) which dropped rapidly after 50 % H_2O (v/v). This can be reasoned out based on the fact that **T$_{CN}$P** is sparingly soluble in water and increasing the concentration of water in DMSO helps the molecule in forming aggregates. This aggregation process reduces the number of molecules available for light absorption.

A similar but more informative result was obtained from the fluorescence spectrum of the same samples (Figure 4b). A solution of **T$_{CN}$P** (10 μM) in DMSO emits in the NIR region with λ_{em} ~ 690 nm. Upon gradually increasing the water percentage in DMSO (till 50 % water (v/v)),

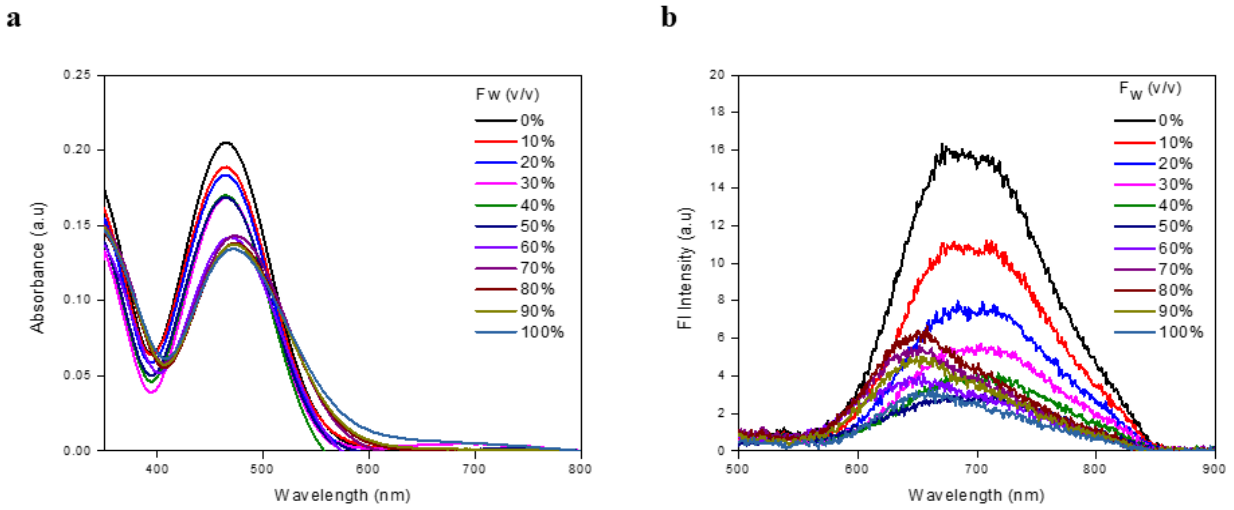

Figure 4 (a) Absorption (b) fluorescence spectra of **T$_{CN}$P** exhibiting TICT and AIE behavior with increasing water fraction (v/v) in DMSO monitored at λ_{ex}= 480 nm

the fluorescence spectrum of **T_{CN}P** exhibited a linear decease in the fluorescence intensity and nearly non-emissive at 1:1 DMSO: H2O mixture. This may be attributed to the formation of TICT state which is known to weaken the fluorescence intensity owing to its non-radiative decay.[16]

With further increase in the water percentage in DMSO solution (≥ 60 % water (v/v)), the fluorescence intensity of **T_{CN}P** increased slightly and the λ_{em} value exhibited a hypsochromic shift to 649 nm from the pristine 690 nm in DMSO. The fluorescence intensity increased till 80 % water (v/v) and decreased again upon further addition of water till the water percentage reached 100 %. The unusual increase in the fluorescence intensity of the molecule with increasing percentage of water from about 50 % to 80 % can be explained in a way that the molecule must have aggregated to form invisible nanoparticles and that the increment in the fluorescence is due to AIE phenomenon. To illustrate, a plot of fluorescence intensity versus

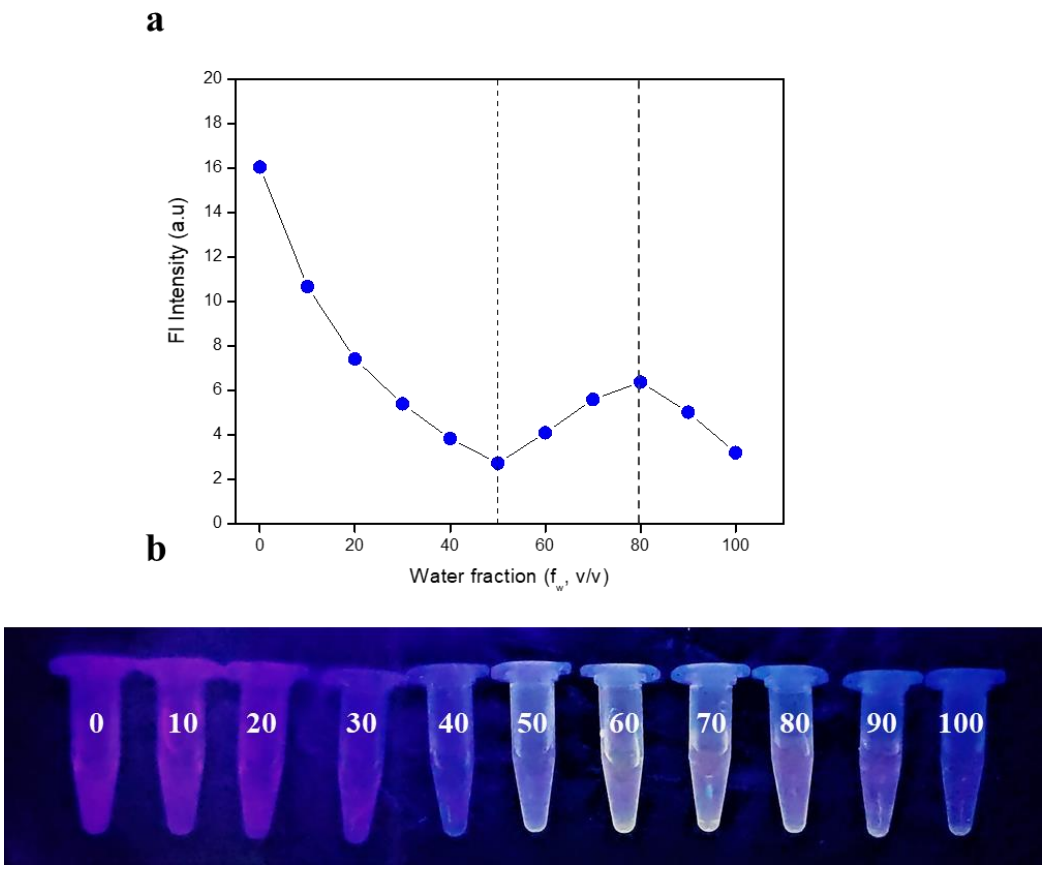

Figure 5 (a) Plot of change in the emission intensity of **T_{CN}P** with increasing water fractions (v/v) in DMSO (b) fluorimetric changes in the vials containing **T_{CN}P** with increasing water fractions (v/v) in DMSO

water percentage has been constructed below (Figure 5a) besides a fluorimetric change in the same solutions in the UV chamber (Figure 5b). In the Figure 5b, it can easily be visualized that the red color of the probe in DMSO alone and in initial fractions shifts to yellowish in the middle when the water fraction is around 60 to 80 %. Finally, the color disappears when the water fraction reaches 100 % which is primarily due to poor solubility of probe in water.

3.2.2 Effect of viscosity

Many cellular and organismal functions are linked to the viscosity of their micro-environment.[17] Besides, on a macroscopic scale, viscosity changes in blood plasma as well as lymphatic fluids have been linked with numerous disease states. Hence, in-depth investigation of viscosity on microscopic scale is important. Nonetheless, conventional methods like mechanical viscometer are cumbersome and inefficient while performing real-time viscosity measurement.[18] In this regard, fluorescent probes have been designed to monitor microscopic alterations in the viscosity in biological systems.

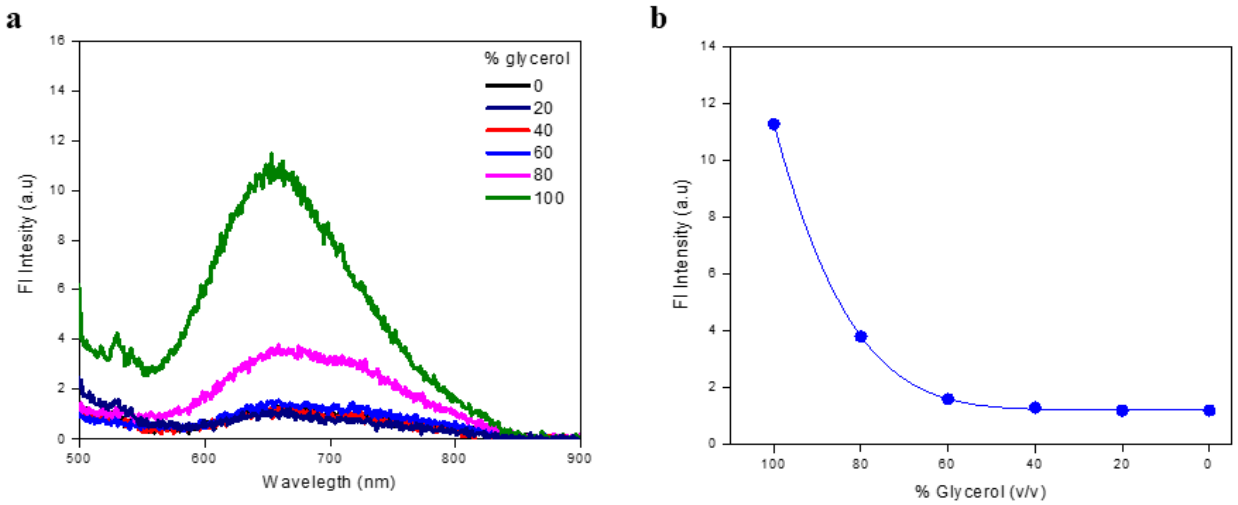

Figure 6 (a) Fluorescence spectrum of **$T_{CN}P$** with increasing fraction (v/v) of glycerol in PBS monitored at λ_{ex}= 480 nm (b) Illustration of decay of the emission intensity with increasing glycerol fractions in water monitored at λ_{em}= 655 nm

It is already discussed in the preceding sections that **$T_{CN}P$** exhibits the formation of TICT state in solvents due to which it shows a characteristic dual emission (weak signal in the fluorescence

spectrum) and reduction in its emission intensity due to non-radiative decay from the TICT state. As far as viscosity is considered, TICT formation rate decrease with the increasing viscosity of the micro-environment of the molecule. To validate this hypothesis, we constructed a plot of fluorescence intensity of the compound in PBS (10 μM) as a function of increasing viscosity (we have used glycerol, Figure 6a and 6b). Upon monitoring the fluorescence intensity of the molecule, we did not observe any increment till 60 % glycerol in PBS while the fluorescence intensity only slightly increased (2 times) when the percentage of glycerol was raised to 80 %. Finally, at 100 % glycerol, the fluorescence intensity of **T_{CN}P** was observed to increase by about 5 times of the solution containing **T_{CN}P** with only PBS. Moreover, at 60 % glycerol, the dual emission of the molecule could be observed which disappeared at 100 % concentration of glycerol. These above observations are the direct consequences of the fact that the TICT peak is highly dependent on the viscosity of the solvent. Higher viscosity tends to minimize the TICT peak intensity while increases the peak intensity corresponding to the locally excited sate (LE). The reverse is true for the solvent polarity. The data showed that even till 60 % of the glycerol, the TICT peak was not suppressed which implies that **T_{CN}P** is able to undergo molecular rotation till 60 % glycerol medium with least difficulty. At last, the TICT peak completely disappeared at 100 % glycerol which implies that the molecule is present in a restricted environment and there are a smaller number of non-radiative decay pathways available. Hence, more fluorescence than that in PBS only.

3.2.3 Effect of pH

Many fluorescent molecular probes are capable of undergoing ionization upon varying the pH of the solution, and one of the ionic states of a compound often have different fluorescence characteristics from the unionized form.[19] The effect of pH upon the fluorescence of a compound is thus of considerable importance, and a knowledge of the changes in fluorescence brought about by pH changes in the medium can be valuable from several aspects. It is a well-known fact that the pH inside a typical human cell varies from 5 (in the lysosomes) to 7 (in the cytosol) and to 8 (in mitochondria).[20] Thus, to evaluate the stability of our probe towards different pH environments, we monitored the absorbance and emission profiles of **T_{CN}P** as a function of varying pH on the x-axis (Figure 7a). As depicted from the plots, **T_{CN}P** exhibited quite a stable

behavior towards a wide range of pH (1-14) conditions (Figure 7b). This result implies that the designed probe can be used as a marker inside any mammalian cell without undergoing any undesired molecular transformation upon altering pH environment.

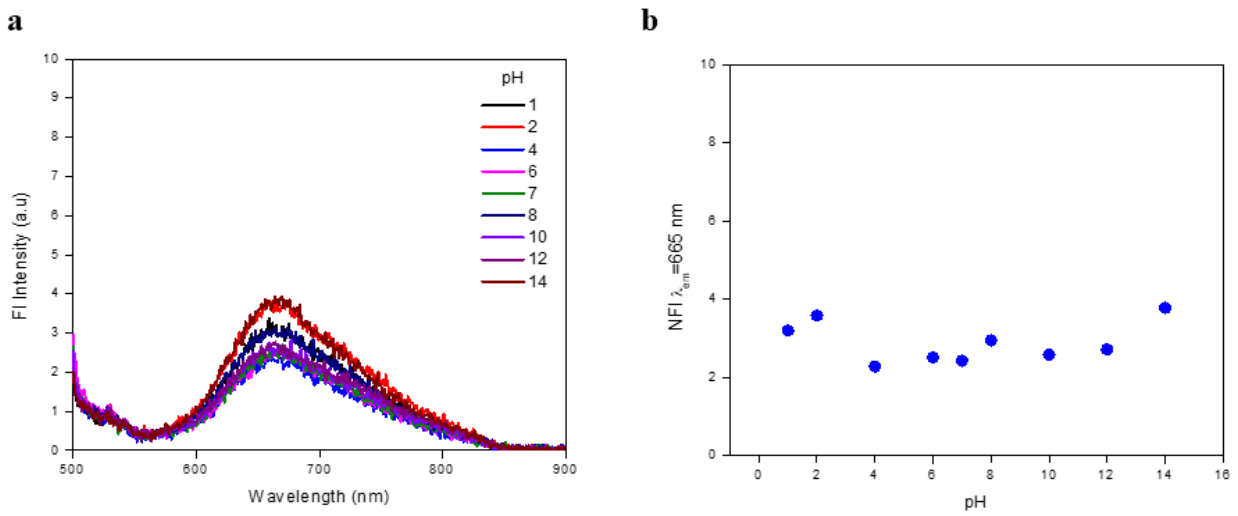

Figure 7 (a) Fluorescence spectrum of **T_{CN}P** with increasing pH (b) Illustration of stability of the probe in a wide range of pH (monitored at λ_{ex}= 480 nm)

3.2.4 Selective switch-on NIR signal transduction with BSA

The designed red-NIR emissive; **T_{CN}P** was examined for its sensory properties with several biological and biologically significant inorganic species. The experimental data corresponding to the fluorescence spectra were plotted to compare the significant changes in the signal transduction of the molecule with the examined analytes (Figure 8). It is quite clear from the spectral plots that **T_{CN}P** selectively interacts with BSA in comparison with the other tested analytes. Though the emission intensity yielded upon BSA-**T_{CN}P** interactions is low but certainly the observed difference could not be ignored.

Since the tested analytes were either inorganic anionic species or biologically potent DNA canonical and non-canonical structures, none of them could be employed for a direct and reasonable comparison with the selective signal from BSA. BSA is a high molecular mass globular protein which offers multiple interactions at different sites in its ternary structure. Hence, we examined our probe with similar globular proteins namely, pepsin, trypsin and

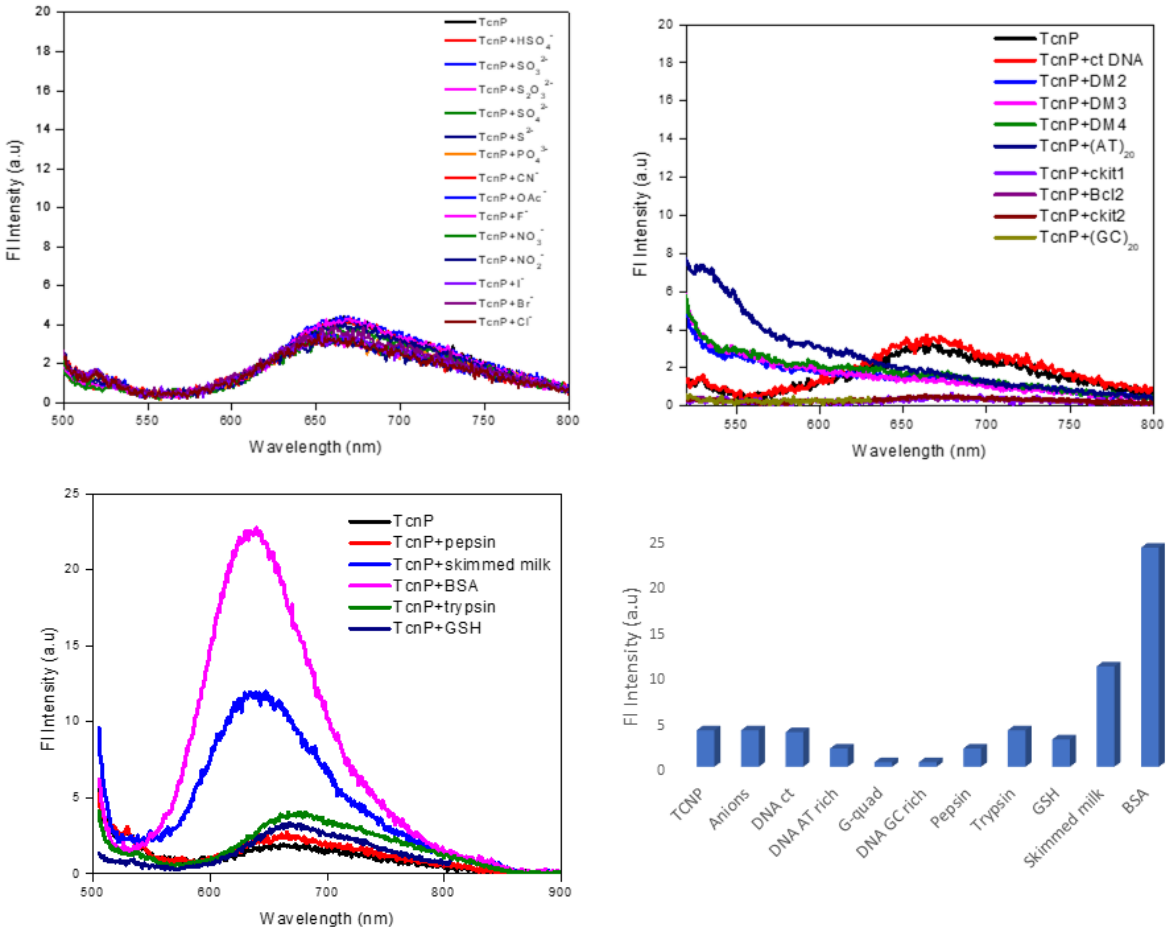

Figure 8 Fluorescence spectra of **$T_{CN}P$** with diverse biological or biologically potential analytes and preferential detection of BSA in comparison with other analytes monitored at λ_{ex}= 480 nm

especially skimmed milk, which is a concoction of several proteins and peptides much like BSA. As depicted in the emission plot of **$T_{CN}P$** with these proteins (Figure 8), **$T_{CN}P$** selectively binds to BSA in comparison to the remaining two globular proteins. Interestingly, **$T_{CN}P$** interacted with the skimmed milk as well but the signal intensity displayed in the plot is lesser (2 times) than in the case of BSA. Thus, a valid point to be made here is that both BSA and skimmed milk interact with **$T_{CN}P$** but differ only in their signal output. Moreover, the observed data can also be projected in a different way which is; both BSA and skimmed milk provides suitable hydrophobic environment to the probe which is why the emission intensity increase from the basal state in PBS alone to the characteristic intensities shown in Figure 8. Polar solvents are known to quench the emission by predisposing the probe molecules to form TICT state and decay in a non-radiative way. Upon addition of the hydrophobic proteins; BSA and skimmed

milk, the polarity of the solution decreases and thus, the emission intensity of the probe increases. The extent to which this process occurs depends on the interactions and several other parameters which are prerogative of the system. In our case, BSA interacts more with the fluorescent molecular probe **$T_{CN}P$** while skimmed milk interacts less strongly in comparison to BSA.

3.2.5 Spectral studies with BSA

3.2.5.1 Titration of $T_{CN}P$ with BSA

It has already been mentioned that the designed probe interacts well with BSA. However, this effect can be evaluated by titrating the probe with increasing concentration of BSA, monitored by fluorescence signal (Figure 9a). At 1:1 stoichiometry, **$T_{CN}P$** exhibited a 6-order increment in its emission intensity besides a concomitant hypsochromic shift in its λ_{em} value which shifted from ~679 nm in PBS alone to 637 nm in PBS with BSA. Further, upon titrating the probe (50 µM) with increasing concentration of BSA (0 µM to 110 µM), similar result was observed. As the concentration of BSA increased, each time the λ_{em} value of the probe shifted towards blue wavelength with of course increase in its emission intensity. The increment in the emission intensity of the probe has already been justified based on the introduction of hydrophobicity in the solution while the hypsochromic shift in the emission maximum value may indicate toward the confinement of the probe in one of the several hydrophobic pockets in BSA.

3.2.5.2 Titration of BSA with $T_{CN}P$

An alternate study can be done to examine the effect of **$T_{CN}P$** on the photophysical properties of the protein; BSA. To obtain such information, a titrimetric analysis was performed with a constant concentration of BSA (2 µM) and varying concentration of the probe (0 µM to 50 µM). Upon increasing the concentration of **$T_{CN}P$**, the absorbance of BSA at 278 nm increased in linear correlation with the probe's concentration while the emission recorded at 345 nm exhibited a regular decrease in its intensity besides slight hypsochromic shift (Figure 10a).

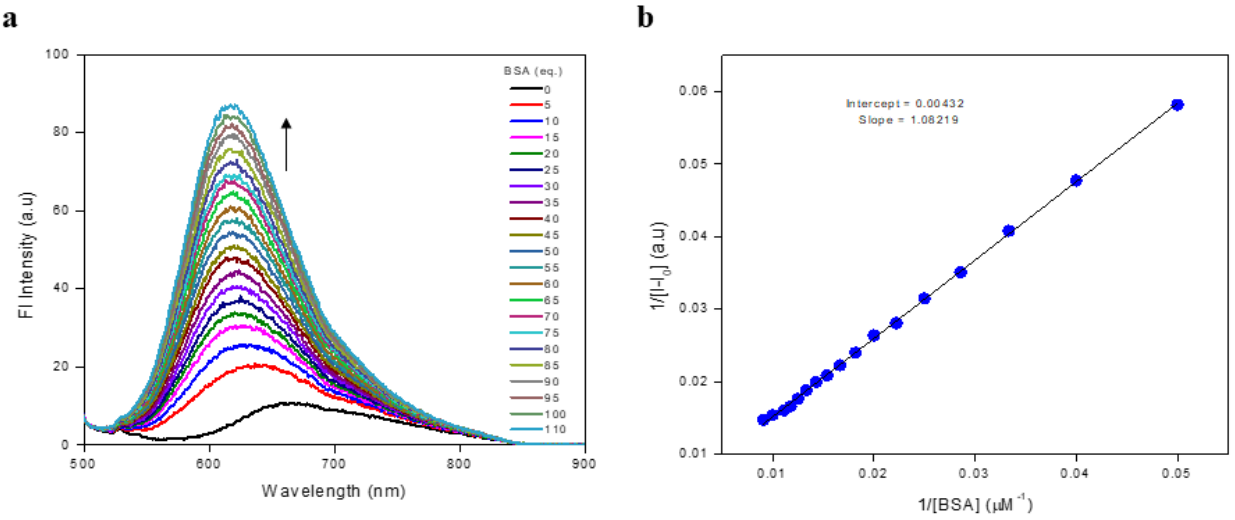

Figure 9 (a) Fluorescence spectrum of **$T_{CN}P$** with increasing concentration of BSA monitored at λ_{ex}= 480 nm (b) Benesi-Hildebrand plot of **$T_{CN}P$** fluorescence intensity versus the reciprocal of the concentration of BSA to yield a linear correlation indicating 1:1 complex stoichiometry

The observed data can be explained as follows; the absorption peak of BSA at 278 nm is characteristic of the microenvironment around tyrosine and tryptophan residues. The observed increment in the absorption intensity of BSA at 278 nm as a function of **$T_{CN}P$** concentration can be a possible outcome of the alteration in the polarity of the microenvironment of the aromatic amino acid residues in BSA (namely, tyrosine and tryptophan).

Furthermore, the intrinsic fluorescence intensity of the BSA at 345 nm exhibited a regular decrease upon titration with the increasing concentration of **$T_{CN}P$** (Figure 10b). This observation corroborates well with the absorption data. Intrinsic fluorescence of BSA is characteristic of the present tryptophan and tyrosine residues, and any alteration (e.g. binding of the probe in the hydrophobic pockets of BSA) in their microenvironment affects the protein's emission at ~350 nm. Since our probe is interacting with BSA (as proved earlier), the emission at 345 nm is quenched regularly as the concentration of the compound increases.

3.2.5.3 Quenching of BSA spectral signal

A fluorescence titration of BSA with increasing concentration of **$T_{CN}P$** demonstrated the quenching effect of the probe, monitored at 345 nm (Figure 10b). In literature, quenching

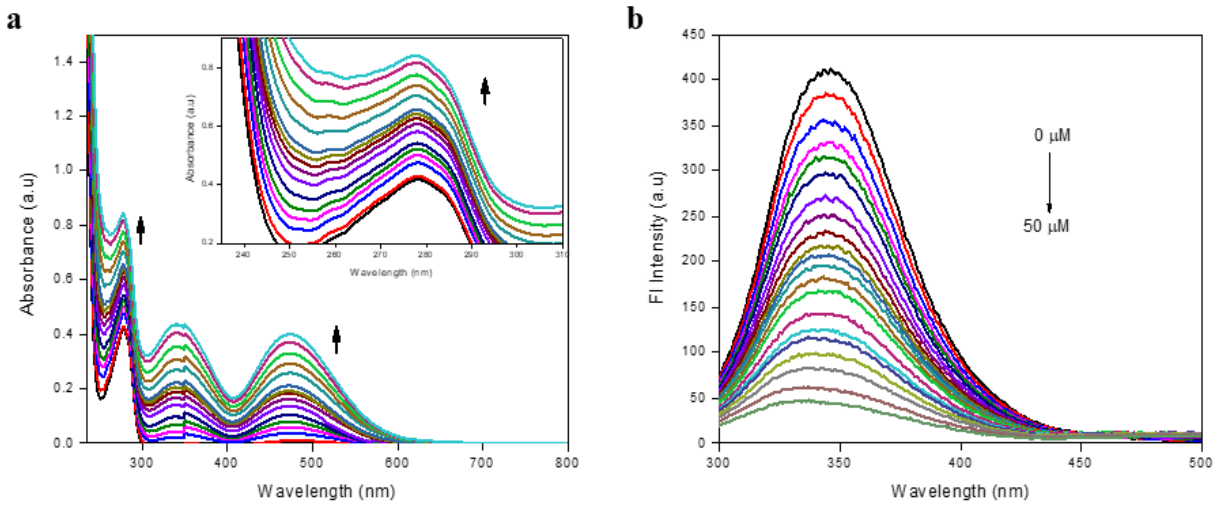

Figure 10 (a) Absorbance spectrum of BSA at 278 nm with increasing concentration of **T_{CN}P** (b) intrinsic fluorescence of BSA monitored at 345 nm with increasing concentration of **T_{CN}P**

mechanism either follow static quenching (i.e. ground state complex formation) or dynamic (collisional) quenching. During dynamic quenching, the quencher (**T_{CN}P**) diffuses to the fluorophore (BSA tyrosine and tryptophan residues) in excited state and returns to the ground state without any emission of the photon. In static quenching on the other hand, a non-fluorescent complex is formed between the two species. The mode of quenching can be determined by plotting the Stern-Volmer equational parameters (Figure 11).

$$I/I_0 = 1 + K_q\tau_q[Q] = 1 + K_{SV}[Q]$$

Where, I and I_0 are the steady state fluorescence intensities in the presence and absence of the quencher respectively. K_{SV} is the Stern-Volmer quenching constant and τ_q is the average life time of the protein without the quencher. [Q] is the concentration of the quencher; **T_{CN}P**. At higher concentrations of the probe, the plot deviated from the straight line which indicated complex quenching mechanism. However, evaluation of the Stern-Volmer quenching constant was done by carefully selecting the region of linearity. The calculated parameters are tabulated in Table 1.

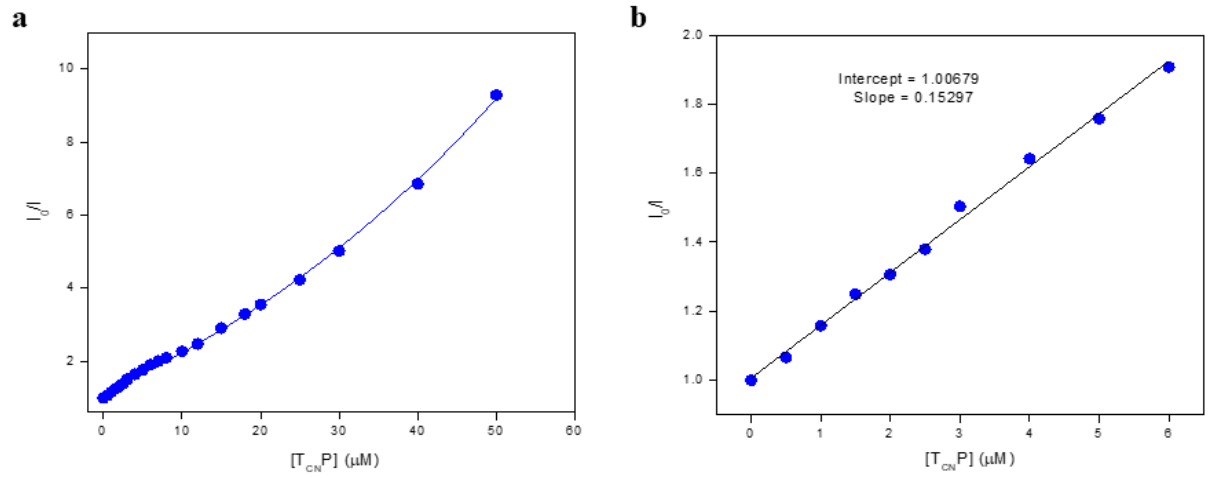

Figure 11 (a) Stern-Volmer plot of BSA at 345 nm with increasing concentration of **T_{CN}P** (b) linear fitting of the Stern-Volmer data points to evaluate the value of quenching constant

As per the literature, the collisional quenching constant of various kinds of quencher with biopolymer is of the order of 10^{10} M^{-1} s^{-1}, while the calculated value in our case has the order of 10^{5} M^{-1} s^{-1}. This implies that the possible mechanism employed in our case of BSA-**T_{CN}P** system must be static quenching.

To further validate this result, absorption plot of BSA with increasing concentration of **T_{CN}P** (Figure 10a) was constructed. As discussed in the previous section, changes at 278 nm (characteristic of BSA) clearly indicates that the probe and BSA are interacting at ground state level which has been monitored by the alterations in the UV band of BSA. Hence, static quenching is a possible mechanism employed in our system.

System	τ_0	K_{SV}	K_q
T_{CN}P-BSA	10^{-8} s	1.53 x 10^{5} M^{-1}	1.53 x 10^{13} $M^{-1}s^{-1}$

Table 1 Evaluated values of the Stern-Volmer equational parameters

3.2.6 Binding stoichiometry and affinity of $T_{CN}P$ with BSA

To evaluate the binding stoichiometry for the BSA-**$T_{CN}P$** interactive system, a fluorescence plot corresponding to the titrimetric analysis of the probe (50 µM) with increasing concentration of BSA was constructed (Figure 9a). The observed data points were fitted in the Benesi-Hildebrand equation to plot $1/[I-I_0]$ versus 1/[BSA]. A linear correlation was observed which implies a ratiometric (1:1) formation of a complex between the probe and BSA (Figure 9b). Further, the data points were fitted using a straight-line equation (y= mx + c) to yield the equilibrium constant value of 5.37 μM^{-1}.

$$^1/_{I-I_0} = {}^1/_{I_1-I_0} + \left({}^1/_{I_1-I_0}\right)\left({}^1/_{K[BSA]}\right)$$

Where, I_0, I and I_1 are the emission intensities in the absence, intermediate and infinite concentrations respectively. K is the Benesi-Hildebrand equilibrium constant and [BSA] is the concentration of the protein. The above experimental result was corroborated with another fluorescence titrimetric analysis. In order to calculate the stoichiometry of the interacting systems, two titrimetric analyses were done; one with constant probe and increasing BSA concentration and second with constant BSA and increasing concentration of **$T_{CN}P$**. finally, both the spectra were plotted in one frame and the observed data points were individually fitted in linear equation format. The intersection of the two lines yielded the stoichiometry of the complex (Figure 12a). The result was similar to the above observed result (1:1 stoichiometry).

A sigmoidal curve was obtained while plotting the titrimetric analysis of BSA (10 µM) with increasing concentration of **$T_{CN}P$** monitored ~615 nm (Figure 12b). The curve exhibited an initial increase followed by a saturation stage after 10 µM of **$T_{CN}P$**. The observation indicates as well as indirectly validates the 1:1 stoichiometry of the complex, as was calculated from the Benesi-Hildebrand plot.

System	K_b	n
T_{CN}P-BSA	1.49 x 10^5 M^{-1}	1.03

Table 2 Evaluated values of the Stern-Volmer equational parameters

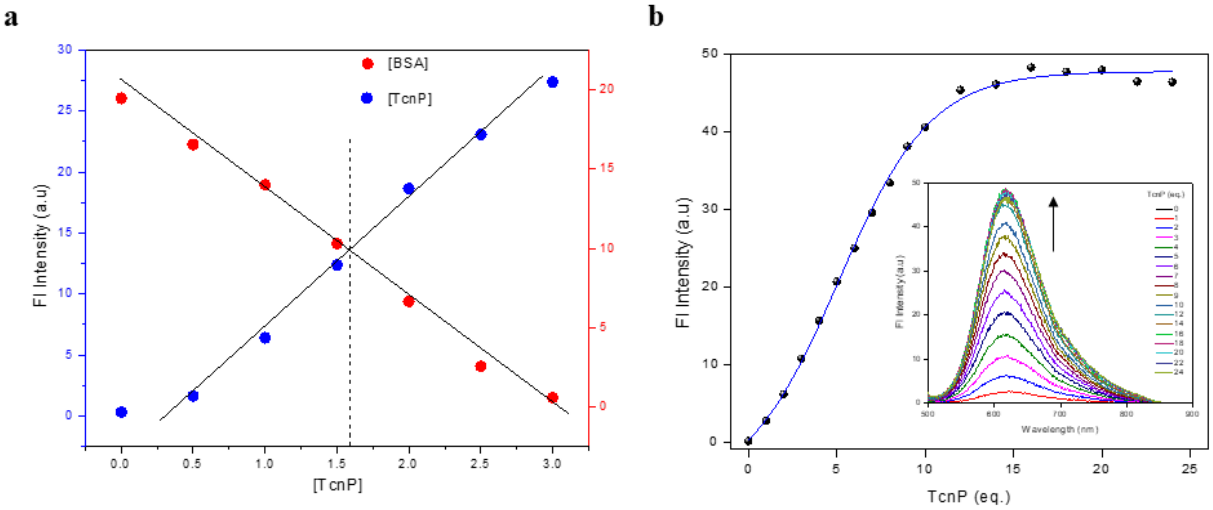

Figure 12 (a) Fluorescence titration with **T_{CN}P**-BSA system to obtain the stoichiometry of the bound complex (b) saturation curve obtained from the fluorescence spectrum of increasing concentration of **T_{CN}P** with 10 µM of BSA, monitored at 665 nm

During a typical case static quenching, relation between the fluorophore (BSA) emission intensity at 354 nm and the quencher (**T_{CN}P**) concentration can be correlated by a modified Stern-Volmer equation. A construction of a simple plot of log [$(I-I_0)/I$] versus log [**T_{CN}P**] would provide information about the binding constant as well as number of binding sites (Figure 13).

$$\log\left[{}^{I_o - 1}/_{I}\right] = logK_b + nlog[Q]$$

Where, I_0 and I are the fluorescence intensities in the absence and presence of the probe. K_b is the binding constant and n is the number of binding sites on the protein for a molecule of our probe. The evaluated parameters have been listed in Table 2. The high value of binding constant implies strong interactions between BSA and the probe; **T_{CN}P** while n=1 indicates that there is indeed a 1:1 binding between BSA and the designed probe.

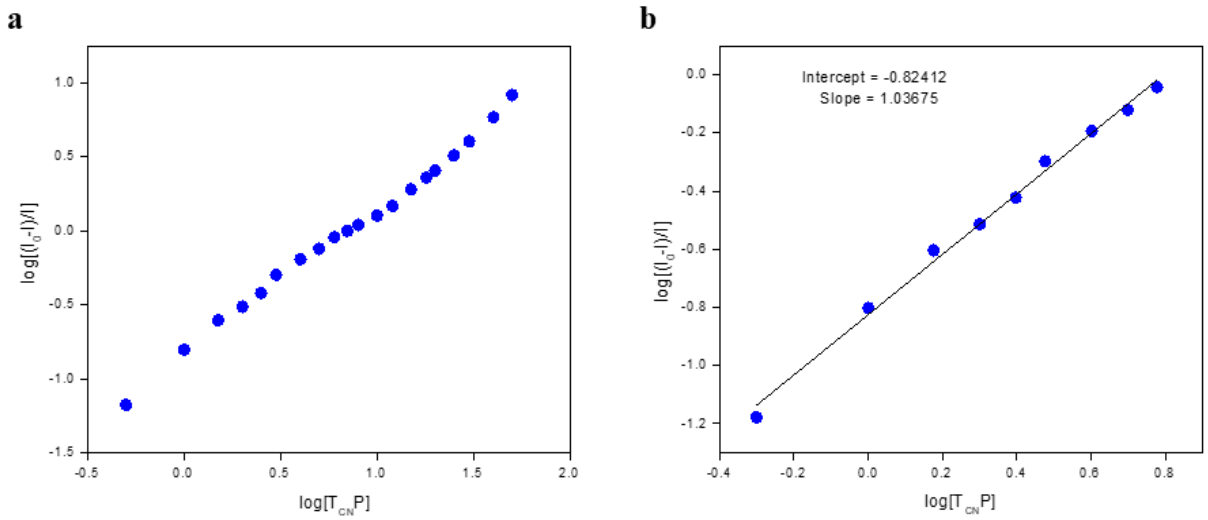

Figure 13 (a) Modified Stern-Volmer plot for the intrinsic fluorescence of BSA at 354 nm measure upon increasing concentration the probe (b) linear fitting of the data points obtained from (a)

3.2.7 Mode of T_{CN}P binding to BSA

Guanidine hydrochloride (GnHCl) is an ionic solute commonly used for denaturation of proteins.[21,22] GnHCl exhibits a specific denaturation pattern with BSA.[23] Initially, when the concentration of GnHCL is below 1.4 M, domain III gets reversibly denatured while inducing minimum alterations in the other domains. However, when the concentration of GnHCL is in between 1.4 M to1.8 M, domain II is irreversibly denatured while domain I starts its reversible denaturation at this concentration range. A further increase in the concentration of GnHCl (i.e. >3 M) leads to complete denaturation of BSA. Therefore, studying the affect in the fluorescence intensity signal of the **T_{CN}P** (10 μM) bound BSA (10 μM) complex with varying concentrations of GnHCl (0.2 M to 5 M) would provide a useful insight into the nature of binding mode of **T_{CN}P** with BSA. In this context, a plot of fluorescence intensity corresponding to the denatured

BSA-**TCNP** system, monitored at 612 nm (normalized to one) versus the concentration of GnHCl has been constructed (Figure 14a). As depicted from the graph, the emission intensity followed quite a linear correlation till the concentration of GnHCl was 1.4 M and drops down to almost basal fluorescence from 1.4 M to 2 M. This indicates that the designed probe interacts particularly with domain II. A further decrease in the emission intensity with increasing concentration of GnHCl indicates the complete denaturation of BSA consequently, non-availability of any residual sites for interaction. As a control, fluorescence intensity of **TCNP** at 660 nm was also monitored with the increasing concentration of GnHCl (Figure 14b).

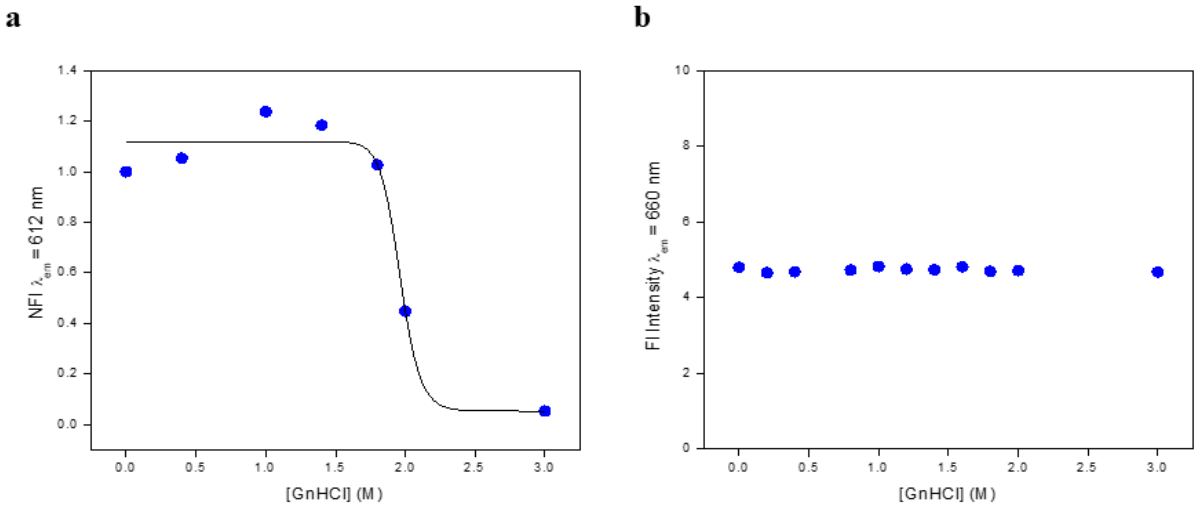

Figure 14 (a) Fluorescence intensity of BSA-**TCNP** complex versus the increasing concentration of GnHCl, monitored at 612 nm (b) fluorescence intensity of **TCNP** versus the increasing concentration of GnHCl, monitored at 660 nm

To further validate our experimental result, BSA-**TCNP** complex was subjected to varying pH conditions (particularly towards acidic scale, Figure 15a) and a plot of emission intensity at 615 nm versus decreasing pH was constructed (Figure 15b). The three domains of BSA exhibit distinct denaturation patterns of their tertiary structures as a function of pH.[24] When the pH is lowered from pH 7 to pH 3, domain II of BSA loses its tertiary structure and is transformed to the molten globule state (secondary structure intact); however, domains I and III retain their tertiary structure. Since, the denatured BSA-**TCNP** complex showed a sharp decrease in fluorescence intensity upon decreasing the pH from 7.4 to 3, it can be concluded that **TCNP** is

mainly localized in domain II (drug binding site I) of BSA and the tertiary structure of domain II is critical for the binding of the probe to BSA.

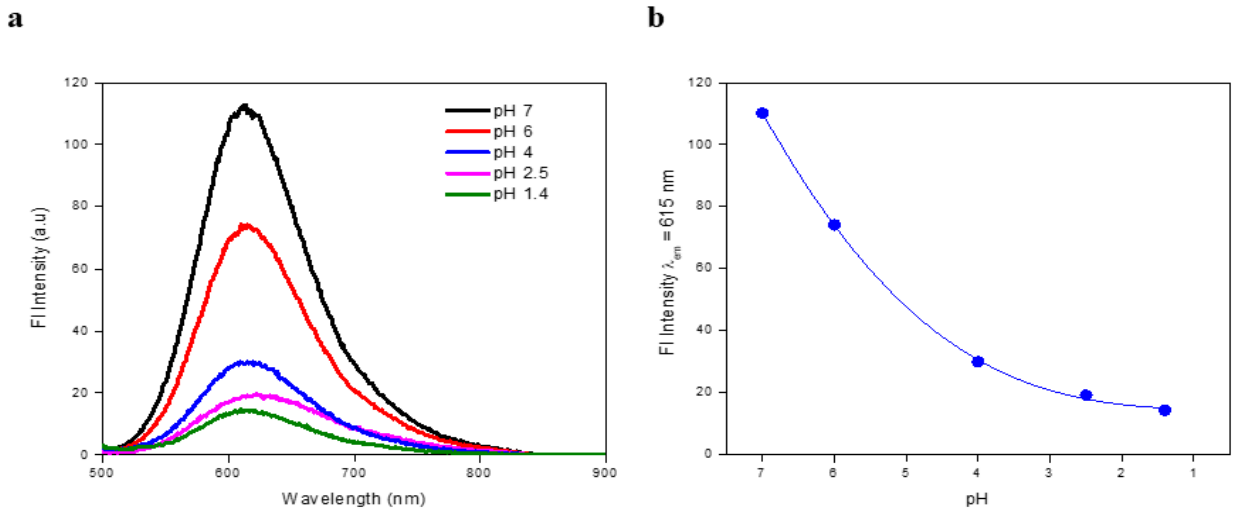

Figure 15 (a) Fluorescence intensity of BSA-**T_{CN}P** complex at different pH solutions (b) fluorescence intensity of BSA-**T_{CN}P** versus the decreasing pH, monitored at 615 nm

3.3 Conclusion

During the studies performed in this chapter, **T_{CN}P** has been employed extensively in demonstrating its interactions with the biological target; BSA using spectroscopic techniques. From the studies, it can be concluded that the designed probe interacts with BSA with high binding affinity as compared to the other examined analytes. Particularly, **T_{CN}P** with the tryptophan and tyrosine amino acid residues as confirmed by the quenching of the intrinsic emission of BSA upon titration with the probe at 345 nm. Statistical analyses including Stern-Volmer plots were constructed to evaluate the 1:1 stoichiometry of the BSA- **T_{CN}P** complex. These findings can be utilized in developing the field of pharmacokinetics and pharmacodynamics as a valuable tool.

3.4 Experimental section

3.4.1 Materials

$T_{CN}P$ was synthesized and purified as discussed in detail in chapter two. Bovine serum albumin (BSA) was purchased from Sigma Aldrich and used without any further purification. PBS buffer was prepared in milli-q water. All the solvents employed in the studies were either HPLC or spectroscopic grade.

3.4.2 Instrumentation

The absorption and fluorescence spectra were recorded in Agilent Cary series spectrometer. Incubation was carried out in Innova incubator. During the studies, the concentration of the probe and other analytes were kept in micromolar range to avoid any aggregation and reabsorption effect. All the experiments were performed by preparing fresh solution at rt.

3.4.3 Procedure

Stock solution of **$T_{CN}P$** was prepared in DMSO due to poor solubility of the probe in PBS (10 mM, pH = 7.4). However, the experiments were performed in PBS without any additional fraction of DMSO except for the addition of the stock solution of the probe. The stock solution of BSA was prepared in milli-q water. For the validation of the results, experiments were performed in triplicates.

*3.4.3.1 Titration of **$T_{CN}P$** with BSA*

Fluorescent titration was performed at a constant concentration of the probe (50 µM) in PBS (10 mM, pH = 7.4) with increasing concentration of BSA (0 µM to 110 µM). The fluorescence signal intensity was monitored between 600 nm to 700 nm when the system was excited at 480 nm.

3.4.3.2 Titration of BSA with ***$T_{CN}P$***

On the contrary to the above titrimetric analysis, fluorescent titration this time was performed at a constant concentration of the BSA (2 µM) in PBS (10 mM, pH = 7.4) with increasing concentration of **$T_{CN}P$** (0 µM to 50 µM). The fluorescence signal intensity was monitored between 300 nm to 400 nm when the system was excited at 278 nm.

3.4.3.3 Mode of ***$T_{CN}P$*** *binding to BSA*

GnHCl stock solution was prepared in milli-q water. The denaturation of BSA was carried out by dissolving the protein in PBS with GnHCl followed by an incubation period of 10 h at rt. To the denatured protein, **$T_{CN}P$** (10 µM) was added and the fluorescence spectrum was measured. For the pH dependent mechanism, different pH solutions were added to the BSA- **$T_{CN}P$** (1:1) complex and the fluorescence spectrum was monitored and plotted.

3.5 References

1. Eftink, M. R., Intrinsic Fluorescence of Proteins. In *Topics in Fluorescence Spectroscopy: Volume 6: Protein Fluorescence*, Lakowicz, J. R., Ed. Springer US: Boston, MA, 2000; pp 1-15.

2. Peters, T., Serum Albumin. In *Advances in Protein Chemistry*, Anfinsen, C. B.; Edsall, J. T.; Richards, F. M., Eds. Academic Press: 1985; Vol. 37, pp 161-245.

3. Rosenoer, V. M.; Oratz, M.; Rothschild, M. A., *Albumin: Structure, function and uses*. Elsevier: 2014.

4. Steinhardt, J.; Krijn, J.; Leidy, J. G., Differences between bovine and human serum albumins. Binding isotherms, optical rotatory dispersion, viscosity, hydrogen ion titration, and fluorescence effects. *Biochemistry* **1971,** *10* (22), 4005-4015.

5. Majorek, K. A.; Porebski, P. J.; Dayal, A.; Zimmerman, M. D.; Jablonska, K.; Stewart, A. J.; Chruszcz, M.; Minor, W., Structural and immunologic characterization of bovine, horse, and rabbit serum albumins. *Mol. Immunol.* **2012,** *52* (3), 174-182.

6. Carter, D. C.; Ho, J. X., Structure of Serum Albumin. In *Advances in Protein Chemistry*, Anfinsen, C. B.; Edsall, J. T.; Richards, F. M.; Eisenberg, D. S., Eds. Academic Press: 1994; Vol. 45, pp 153-203.

7. McClellan, S. J.; Franses, E. I., Effect of concentration and denaturation on adsorption and surface tension of bovine serum albumin. *Colloids Surf. B Biointerfaces* **2003,** *28* (1), 63-75.

8. Servagent-Noinville, S.; Revault, M.; Quiquampoix, H.; Baron, M. H., Conformational Changes of Bovine Serum Albumin Induced by Adsorption on Different Clay Surfaces: FTIR Analysis. *J. Colloid Interface Sci.* **2000,** *221* (2), 273-283.

9. Kudelski, A., Influence of electrostatically bound proteins on the structure of linkage monolayers: adsorption of bovine serum albumin on silver and gold substrates coated with monolayers of 2-mercaptoethanesulphonate. *Vib. Spectrosc.* **2003,** *33* (1), 197-204.

10. Tayyab, S.; Sharma, N.; Mushahid Khan, M., Use of Domain Specific Ligands to Study Urea-Induced Unfolding of Bovine Serum Albumin. *Biochem. Biophys. Res. Commun.* **2000,** *277* (1), 83-88.

11. Liu, T.-Y.; Chen, S.-Y.; Liu, D.-M.; Liou, S.-C., On the study of BSA-loaded calcium-deficient hydroxyapatite nano-carriers for controlled drug delivery. *J. Control. Release* **2005,** *107* (1), 112-121.

12. Lu, J.; Chen, Q.; Ding, X.; Wen, J.; Zhang, Y.; Li, H.; Xu, Y.; Liu, F.; Chen, S.-S.; Sun, S., BSA modified, disulfide-bridged mesoporous silica with low biotoxicity for dual-responsive drug delivery. *Microporous Mesoporous Mater.* **2019,** *278*, 257-266.

13. Zhang, J.; Ren, X.; Tian, X.; Zhang, P.; Chen, Z.; Hu, X.; Mei, X., GSH and enzyme responsive nanospheres based on self-assembly of green tea polyphenols and BSA used for target cancer chemotherapy. *Colloids Surf. B Biointerfaces* **2019,** *173*, 654-661.

14. Wang, L.; Yin, S., State-specific electrostatic potential descriptors for estimating solvatochromic effects. *J. Mol. Model.* **2019,** *25* (3), 60.

15. Yu, C. Y.; Xu, H.; Ji, S.; Kwok, R. T.; Lam, J. W.; Li, X.; Krishnan, S.; Ding, D.; Tang, B. Z, Mitochondrion-Anchoring Photosensitizer with Aggregation-Induced Emission Characteristics Synergistically Boosts the Radiosensitivity of Cancer Cells to Ionizing Radiation. *Adv. Mater.* **2017,** *29* (15), 1606167.

16. Wang, L.; Chen, X.; Xia, Q.; Liu, R.; Qu, J., Deep-Red AIE-Active Fluorophore for Hypochlorite Detection and Bioimaging in Live Cells. *Ind. Eng. Chem. Res.* **2018,** *57* (23), 7735-7741.

17. Turitto, V., Blood viscosity, mass transport, and thrombogenesis. *Prog. Hemost. Thromb.* **1982,** *6*, 139.

18. Haidekker, M. A.; Theodorakis, E. A., Molecular rotors—fluorescent biosensors for viscosity and flow. *Org. Biomol. Chem.* **2007,** *5* (11), 1669-1678.

19. Lakowicz, J. R., *Principles of fluorescence spectroscopy*. Springer Science & Business Media: 2013.

20. Wu, M. M.; Llopis, J.; Adams, S.; McCaffery, J. M.; Kulomaa, M. S.; Machen, T. E.; Moore, H.-P. H.; Tsien, R. Y., Organelle pH studies using targeted avidin and fluorescein–biotin. *Chem. Biol.* **2000,** *7* (3), 197-209.

21. Monera, O. D.; Kay, C. M.; Hodges, R. S., Protein denaturation with guanidine hydrochloride or urea provides a different estimate of stability depending on the contributions of electrostatic interactions. *Protein Sci.* **1994,** *3* (11), 1984-1991.

22. Rajasekhar K, Achar CJ, Govindaraju T. A red-NIR emissive probe for the selective detection of albumin in urine samples and live cells. *Org. Biomol. Chem.* **2017**, *15* (7), 1584-8.

23. Ahmad, B.; Ahmed, M. Z.; Haq, S. K.; Khan, R. H., Guanidine hydrochloride denaturation of human serum albumin originates by local unfolding of some stable loops in domain III. *BBA-Proteins Proteom.* **2005,** *1750* (1), 93-102.

24. Dockal, M.; Carter, D. C.; Rüker, F., Conformational transitions of the three recombinant domains of human serum albumin depending on pH. *J. Biol. Chem.* **2000,** *275* (5), 3042-3050.

Differential sensing of oxidized BSA from BSA in far red-NIR window

Chapter Three - B

Abstract

In this chapter, a D-π-A architecture; **$T_{CN}P$** was examined for its differential interactions with bovine serum albumin (BSA) and the oxidized BSA. At first, the stability of the designed probe was monitored by several spectroscopic measurements in the presence of the oxidant; H_2O_2. Furthermore, a comparative analysis of the probe towards the pristine and oxidized form of BSA was demonstrated by majorly using fluorescence spectroscopic measurements. Finally, the rate of oxidation of BSA and its effect on the interactions between the oxidized BSA and **$T_{CN}P$** was studied.

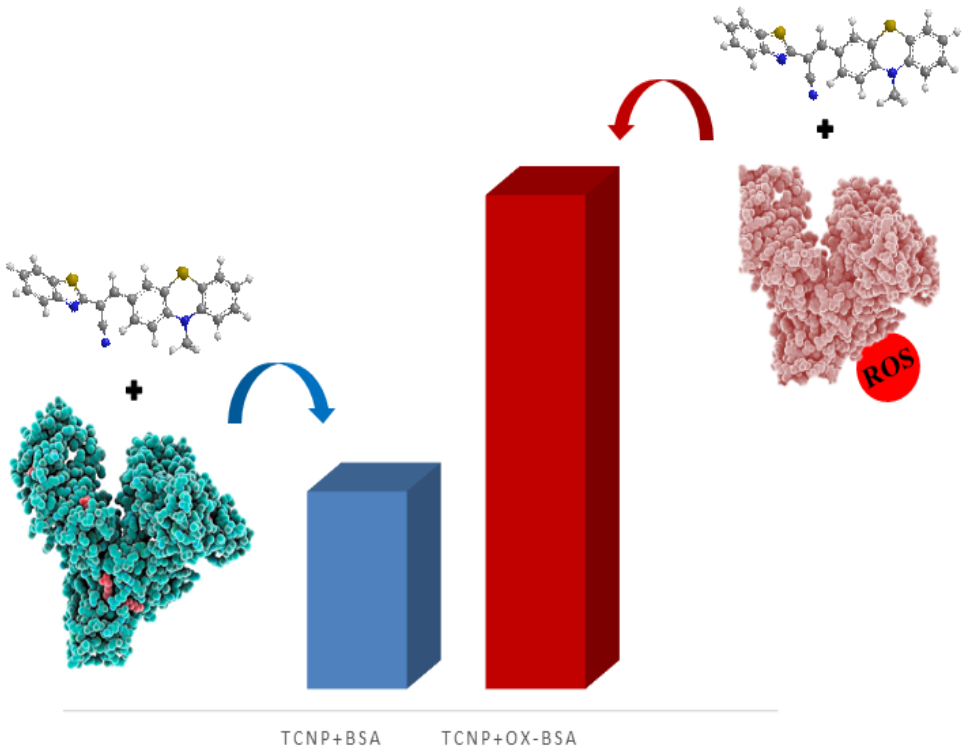

Figure is an illustration of the potential of **$T_{CN}P$** to sense the two forms of BSA namely, the pristine state (left) and the oxidized state (right) in a differential manner

3.1 Introduction

Protein oxidation has gained a lot of impetus in past few decades. Today, it has become an even more important area of research for these oxidized proteins have been characterized as potent biomarkers for certain human disorders.[1-4] BSA (% reduced) tends to be lower in patients with various diseases or conditions such as hepatic disease[5], diabetes[6], renal disease[7], temporomandibular joint disorders[8], aging[9], and tiredness or fatigue.[10] Although many clinical studies have reported changes of BSA (% reduced) in various clinical conditions, little is known regarding its pathophysiological significance. It is almost unquestionable that the posttranslational modifications (PTMs) caused by oxidative damage from reactive oxygen (ROS) and nitrogen species (RNS) on protein integrity is responsible for many pathologies and biological aging.[11-12] However, there is a significant difficulty in identifying important PTMs through in vivo approaches because of protein turnover and repair events.[13] Another reason is related to the potential chemical instability of these oxidative modifications. In vitro oxidation experiments have made important contributions to mechanistic studies and in identifying 'novel' protein oxidation products.[14-18] Nowadays, mass spectrometry (MS) has become the technique of choice for the qualitative detection of protein PTMs besides the conventional immunochemical detection through enzymes and antibodies.[19] In fact, MS analysis allows an unambiguous assignment of the nature and location of the change within a protein sequence. More recently, several independent reports have focused on identifying specific oxidation targets under conditions of metal-catalyzed oxidation (MCO), recognized as a site-specific mechanistic reaction. For example, two histidine residues namely, His-13 and His-14, were found to be target residues in the human and mouse β-amyloid peptide (β-AP) under conditions of site-specific MCO.[17,20]

Moreover, shortly after the MS analysis of α-Syn (protein biomarker in Parkinson's disease) subjected to MCO, methionine was observed to be the most susceptible amino acid residue to be oxidized.[21] However, fluorescence spectroscopy has ever been the most powerful and sensitive tool for studying any biologically potential phenomenon. Thus, if a fluorescent probe which could interact with the oxidized protein species and consequently transduce a signal output is developed then a lot of problems would be resolved. It may also be possible that a completely new area of research evolves from this event.

In our present work, we have developed a synthetic fluorescent probe; **$T_{CN}P$** for studying its interactions with the oxidized form of BSA through fluorescence spectroscopy. Further, during our studies, we have observed that the designed probe interacts differently with BSA and oxidized form of BSA. The difference was monitored and critically examined through series of spectroscopic measurements.

3.2 Structural analysis of BSA and oxidized BSA

The secondary structure of BSA includes 67% helix, 10% turn, and 23% extended chain, with 17 disulfide bridges supporting a triple-domain configuration with nine loops arranged in the order long-short-long.[22-23] BSA is known to be one of the most important plasma antioxidants in protecting key cellular and regulatory proteins.[24] This antioxidant capacity correlates with the large quantity and high turnover of BSA, as well as the high reactivity of BSA sulfhydryl groups with oxidant species. Oxidative modifications of albumin are responsible for different biological properties, the study of these changes being a topic of great interest. To gain insights into the structural changes, Domingues et al. analyzed the tryptic digests of oxidized BSA using different conditions and a MS-based approach (matrix-assisted laser desorption/ ionization (MALDI)-MS and MALDI-MS/MS) combined previously with off-line nano-LC (observations are summarized in Table 1).[12]

This approach allowed them to identify specific sites of oxidative modification, as well as the time-course evaluation of these changes on albumin. Upon oxidation of BSA, significant increase in the number of carbonylation on the protein sites was observed which, as experimentally observed, resulted either from amino acid oxidation or polypeptide backbone cleavage or both. The authors also reported that even though all the amino acid residues are prone to oxidation, the major effects were observed in cysteine, lysine, methionine, tryptophan, arginine, proline, histidine and tyrosine. Besides the expected oxidation products, the authors have also reported some of the unusual oxidized products like lactone formation from oxidized tryptophan residues, carbamylation in oxidized lysine residues etc. In their course of study, the authors have performed a time-dependent oxidation of BSA to provide better insight about the effect of increasing oxidation rate on the three domains of BSA namely, I, II and III. As observed from MS analyses of the kinetics of BSA oxidation, number of oxidized amino acid residues increased with time resulting in the concomitant alterations in the protein structure each time.

PRISTINE BSA	OXIDIZED BSA	OXIDATION 30 min	OXIDATION 2 h
TYROSINE	AMINOTYROSINE	1	4
TYROSINE	QUINONE	1	3
METHIONINE	ISOCYANTE	1	-
TRYPTOPHAN	OXOLACTONE	1	1
HISTIDINE	ASPARGINE	-	1
HISTIDINE	ASPARTIC ACID	-	2
PROLINE	PYRROLIDONE	-	2
PROLINE	PYROGLUTAMIC ACID	-	1
LYSINE	AMINOADIPIC ACID	1	6
LYSINE	ALLYSINE	2	15
CYSTEINE	OXOALANINE	-	1
ARGININE	GLUTAMIC SEMIALDEHYDE	1	1

Table 1 Comparative analysis of post oxidation effects on BSA as a function of time. Adopted from Domingues et. al. work, 2009

The authors noticed that when the concentration of the oxidant (H_2O_2) was kept same, time was the determining factor while on the contrary when time was kept as a constant parameter, higher concentration of the oxidant could oxidize larger number of amino acid residues than the milder conditions. In conclusion, the report suggested that there exists no linearity in the protein oxidation either with time of the concentration of the oxidant, rather the event has been observed to proceed through a step-ladder mechanism.

3.3 Photophysical examination of the $T_{CN}P$-oxidized BSA complex

In order to test the probe's potential to interact with the oxidized BSA, the pristine state of BSA was subjected to a common oxidant; H_2O_2. Following a certain incubation period (in concordance with Domingues et. al.), the absorbance and fluorescence signal output were monitored throughout the experiments to evaluate the desired changes upon **$T_{CN}P$**-oxidized BSA complex formation. The experiments were performed at rt and most importantly at cellular pH conditions (pH = 7.4) in PBS buffer (10 mM).

3.3.1 Effect of oxidation on $T_{CN}P$

H_2O_2 is a powerful oxidant. Thus, it is quite probable that this oxidant may even oxidize the probe besides the protein itself. Hence, in order to examine any kind of effect of H_2O_2 on the emission signal of the probe, a concentration-dependent analysis of **$T_{CN}P$** (10 µM, PBS 10 mM, pH = 7.4) with the increasing concentration of H_2O_2 was carried out and a plot of absorbance and emission signal intensities of the probe versus the concentration of the oxidant was constructed (Figure 1a and 1b). As clearly demonstrated by figure 1b, the increasing concentration had least effect on the emission intensity of the probe which in a way implies that there are no undesired effects yielded upon the oxidation of the probe itself. This would prevent any faulty examination of the observations obtained from the oxidized BSA and pristine **$T_{CN}P$**.

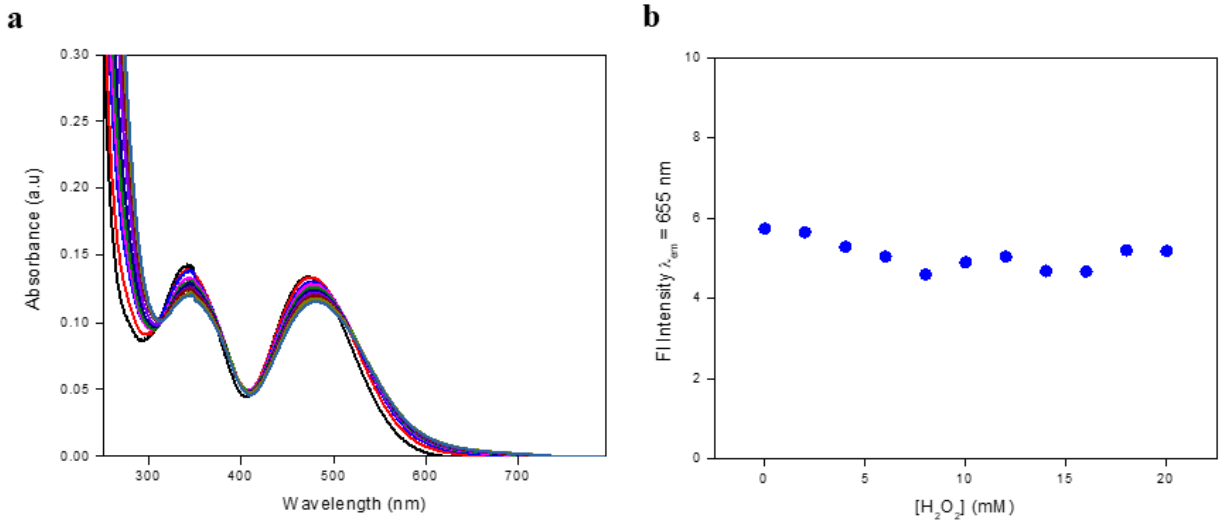

Figure 1 (a) Absorbance and (b) fluorescence spectra of **$T_{CN}P$** as a function of [H_2O_2] monitored at λ_{ex} = 480 nm and λ_{em} = 665 nm

3.3.2 Effect of oxidation on BSA

As a proof of principle, the protein oxidation in the presence of H_2O_2 was studied through absorption and fluorescence spectroscopic techniques, with the emission spectrum monitored at 345 nm. The study has been done in concordance with the report on BSA oxidation by Domingues et al. The concentration of BSA was kept constant at 2 µM and so was that of H_2O_2 (2 equivalents) and the time-dependent changes in the structure of pristine BSA were evaluated (Figure 2a and 2b). As observed from the spectroscopic signals, the absorption band of the protein around 280 nm exhibited a hyperchromic shift besides an increasing distortion in the band signal. The changes in this band indicates changes in the microenvironment around tryptophan or tyrosine residues. Moreover, the emission band of the pristine BSA at 345 nm displayed a gradual decrement under the same conditions. The is in concordance with the observed absorption data and the report by Domingues et al. According to the report, changes in the BSA spectroscopic signal post-oxidation were monitored till 3 hours.

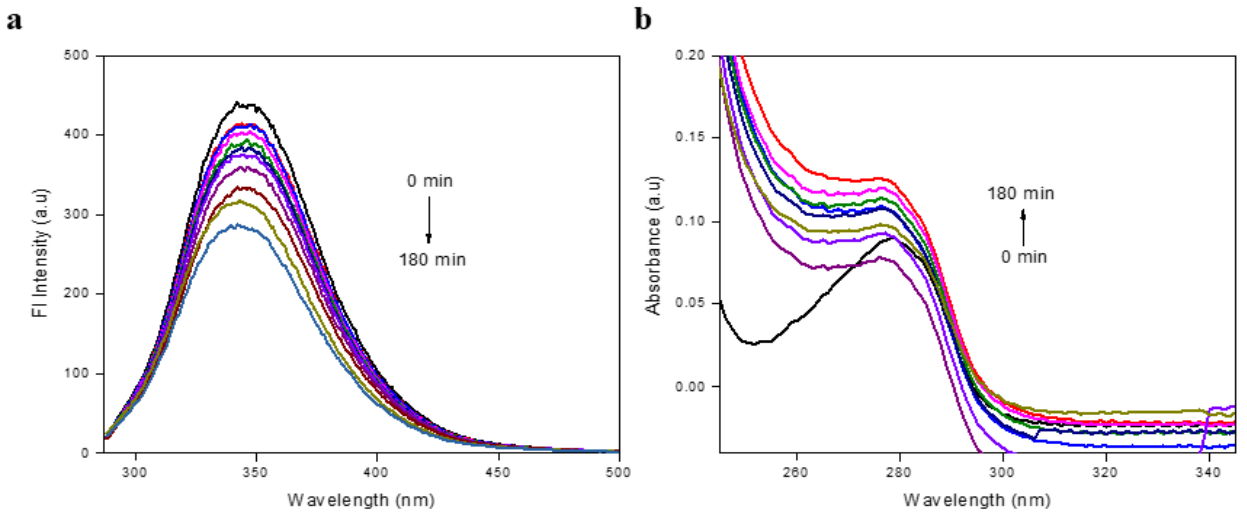

Figure 2 (a) Fluorescence and (b) absorbance spectra of BSA, pre-incubated with H_2O_2, plotted as a function of time at λ_{ex} = 278 nm and λ_{em} = 345 nm

3.3.3 Differential switch-on NIR signal transduction from $T_{CN}P$ bound BSA and oxidized BSA complexes, respectively

A preliminary experiment was first performed to test the actual potential of the designed probe to detect the oxidized form of BSA. **$T_{CN}P$** exhibits strong interaction with BSA which has already been estimated in the preceding chapter nonetheless, it can only be projected as a differentially sensor if it detects oxidized BSA with similar or a different spectroscopic signal transduction. As hypothesized by Domingues et al., amino acid residues and hence the 3-D structural organization of BSA is altered upon the introduction of an oxidant. Hence, **$T_{CN}P$** which exhibited 1:1 binding with BSA may not actually be able to bind to the oxidized form of BSA. In order to answer this interesting yet unanswered question, **$T_{CN}P$** (10 µM, PBS 10 mM, pH = 7.4) was incubated with the pre-oxidized BSA (10 µM, PBS 10 mM) besides the pristine form of BSA (10 µM, PBS 10 mM) and H_2O_2 in PBS alone as potential controls. Following a 10 min incubation period at rt, the samples were examined for any spectroscopic changes using absorption and fluorescence spectroscopies mainly (Figure 3a and 3b). As already discussed in section 3.3.1, there was only the basal fluorescence from the probe and probe in the presence of the oxidant. Moreover, the emission signal output from the BSA- **$T_{CN}P$** complex was in concordance with the earlier performed studies in the earlier chapter. However, the interesting observation made was the comparative emission signal transduction (i) from the BSA- **$T_{CN}P$** complex and most importantly, (ii) the oxidized BSA- **$T_{CN}P$** complex. The absorption spectrum, nonetheless, displayed the changes only at 278 nm while the absorption band (around 480 nm) from the probe remained unaltered.

From the above set of experimental observations, it can be analyzed that the designed probe; **$T_{CN}P$** indeed exhibits differential interactions with the two forms of BSA. The absorption spectrum in this case provided less informative results while on the contrary, fluorescence spectrum clearly marked the difference between the two complexes; BSA- **$T_{CN}P$** and the oxidized BSA- **$T_{CN}P$**. The fluorescence spectrum exhibited an increase in the intensity of emission from the oxidized BSA-**$T_{CN}P$** complex (approx. 2 times) besides a slight bathochromic shift of 2 nm. This clearly indicates that the designed probe; **$T_{CN}P$** interacts more strongly with the oxidized form of BSA in comparison with the pristine BSA, monitored at same temperature, solvent, pH, viscosity, slit width, and pressure conditions.

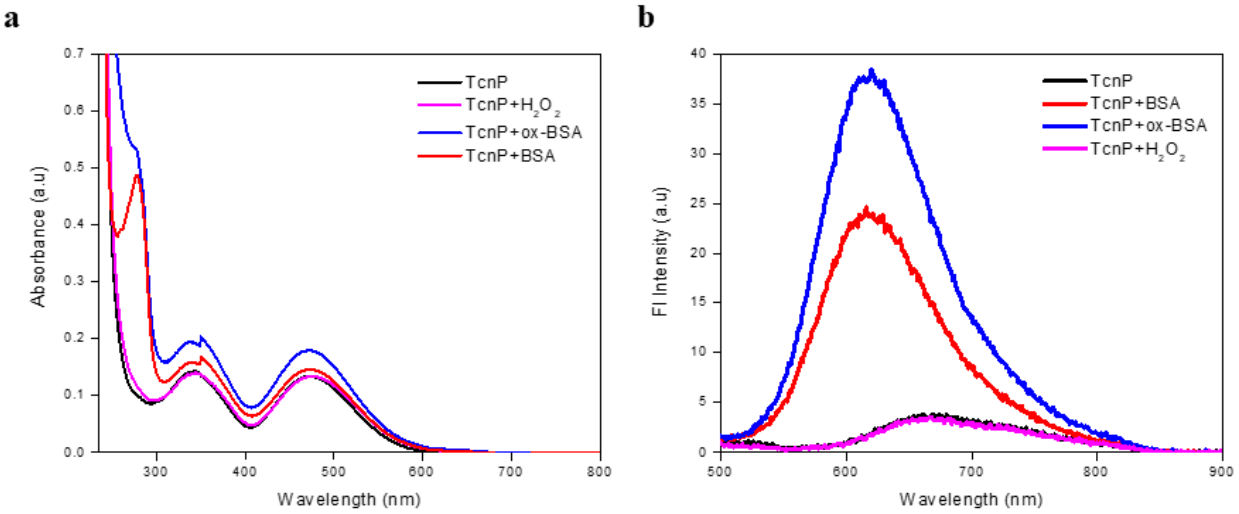

Figure 3 Differential detection of pristine and oxidized form of BSA by **TCNP** examined by (a) absorbance and (b) fluorescence spectroscopic techniques with emission signal monitored at λ_{ex} = 480 nm and λ_{em} = 665 nm

3.3.4 Effect of rate of oxidation on oxidized BSA-TCNP complex

As Domingues et al. reported that the oxidation of BSA is indeed a function of time and that the rate of oxidation proceeds through a step ladder function instead of regular linear correlation, a set of BSA samples (10 µM each) with same concentration of the oxidant were prepared at different time intervals (10 min, 1 h, 2 h and 3 h respectively). Upon completion of the incubation time, **TCNP** (10 µM) was added to every sample and fluorescence signal was monitored at λ_{ex} = 480 nm (Figure 4a and 4b). Interestingly, the fluorescence signal intensity exhibited an increase from 10 min to 1 h of pre-oxidized BSA with **TCNP** while it decreased gradually after 1 h till 3 h of oxidation incubation period.

This can be understood if a simple hypothesis is put forth. Initially, the designed probe; **TCNP** interacts with the oxidized BSA which is similar to the case of pristine BSA protein. These interactions are majorly between the probe and the aromatic amino acid residues which form a hydrophobic pocket in BSA. Upon different extent of oxidation of BSA, the 3-D structure of the protein changes as a result, the binding sites in the three domains; I, II and III suffer drastic transformation spatially. Since, the protein oxidation is not a linear correlation with time, the trend in the experimental observation cannot simply be commented. Some more insightful

studies in future, may help in developing a clear understanding of the true mechanism behind the differential emission output from the oxidized BSA-**T_{CN}P** complex as function of time.

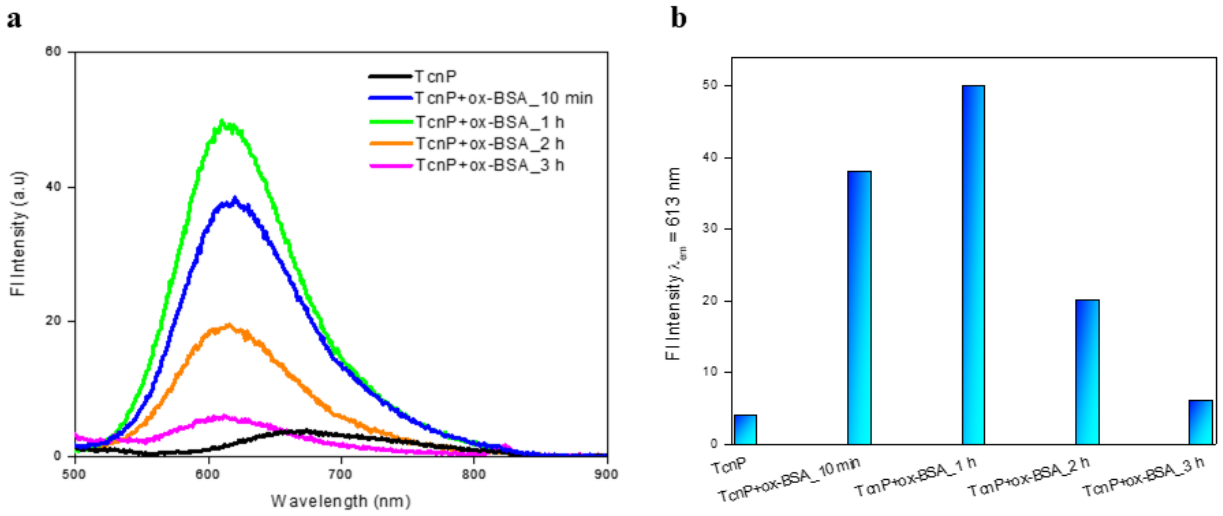

Figure 4 (a) Fluorescence spectrum of **T_{CN}P** with oxidized BSA, pre-incubated with H_2O_2 for different time intervals (b) bar graph illustration of the different intensity of emission of **T_{CN}P** with rate of oxidation of BSA

3.4 Conclusion

In this particular chapter, we have demonstrated the utility of **T_{CN}P** as a differential sensor of pristine and oxidized form of BSA. The probe differentiates the two forms of BSA by transducing disparate emission intensities with a slight bathochromic shift of 2 nm in the case of oxidized BSA. Moreover, the intensity from the bound complex has been shown to be a function of extent of oxidation of protein. The exact mechanism is yet to be studied but some insightful studies in future may provide a better idea behind the observed phenomenon.

3.5 Experimental section

3.5.1 Materials

$T_{CN}P$ was synthesized and purified as discussed in detail in chapter two. Bovine serum albumin (BSA) was purchased from Sigma Aldrich and used without any further purification. PBS buffer was prepared in milli-q water. H_2O_2 (35 % w/w) was purchased from Sigma Aldrich. All the other solvents employed in the studies were either HPLC or spectroscopic grade.

3.5.2 Instrumentation

The absorption and fluorescence spectra were recorded in Agilent Cary series spectrometer. During the studies, the concentration of the probe and other analytes were kept in micromolar range to avoid any aggregation and reabsorption effect. All the experiments were performed by preparing fresh solution at rt. Incubation of the protein with the oxidant was performed in Innova incubator.

3.5.3 Procedure

Stock solution of **$T_{CN}P$** was prepared in DMSO due to poor solubility of the probe in PBS (10 mM, pH = 7.4). However, the experiments were performed in PBS without any additional fraction of DMSO except for the addition of the stock solution of the probe. The stock solution of BSA was prepared in milli-q water. For the validation of the results, experiments were performed in triplicates.

3.5.3.1 Oxidation of BSA

Oxidation of BSA in PBS was carried out by dissolving appropriate volume of H_2O_2 from a stock solution of 35 % (w/w). The sample was stored in dark and covered all the time to avoid any external interference. The measurements were done at the same hour for the life-time of in situ generated hydroxyl radical is very low.

3.5.3.2 Oxidation of $\boldsymbol{T_{CN}P}$

The oxidation of the probe was done in a similar manner as in the case of BSA.

3.6 References

1. Dalle-Donne, I.; Giustarini, D.; Colombo, R.; Rossi, R.; Milzani, A., Protein carbonylation in human diseases. *Trends Mol. Med.* **2003,** *9* (4), 169-176.

2. Masudo, R.; Yasukawa, K.; Nojiri, T.; Yoshikawa, N.; Shimosaka, H.; Sone, S.; Oike, Y.; Ugawa, A.; Yamazaki, T.; Shimokado, K., Evaluation of human nonmercaptalbumin as a marker for oxidative stress and its association with various parameters in blood. *J. clin. Biochem. Nutr.* **2017**, 17-5.

3. Nakatani, S.; Yasukawa, K.; Ishimura, E.; Nakatani, A.; Toi, N.; Uedono, H.; Tsuda, A.; Yamada, S.; Ikeda, H.; Mori, K., Non-mercaptalbumin, Oxidized Form of Serum Albumin, Significantly Associated with Renal Function and Anemia in Chronic Kidney Disease Patients. *Sci. Rep.* **2018,** *8* (1), 16796.

4. Fujii, R.; Ueyama, J.; Aoi, A.; Ichino, N.; Osakabe, K.; Sugimoto, K.; Suzuki, K.; Hamajima, N.; Wakai, K.; Kondo, T., Oxidized human serum albumin as a possible correlation factor for atherosclerosis in a rural Japanese population: the results of the Yakumo Study. *Environ. Health Prev. Med.* **2018,** *23* (1), 1-1.

5. Watanabe, A.; Matsuzaki, S.; Moriwaki, H.; Suzuki, K.; Nishiguchi, S., Problems in serum albumin measurement and clinical significance of albumin microheterogeneity in cirrhotics. *Nutrition* **2004,** *20* (4), 351-357.

6. Suzuki, E.; Yasuda, K.; Takeda, N.; Sakata, S.; Era, S.; Kuwata, K.; Sogami, M.; Miura, K., Increased oxidized form of human serum albumin in patients with diabetes mellitus. *Diabetes Res. Clin. Pract.* **1992,** *18* (3), 153-158.

7. Soejima, A.; Matsuzawa, N.; Hayashi, T.; Kimura, R.; Ootsuka, T.; Fukuoka, K.; Yamada, A.; Nagasawa, T.; Era, S., Alteration of redox state of human serum albumin before and after hemodialysis. *Blood Purif.* **2004,** *22* (6), 525-529.

8. Tomida, M.; Ishimaru, J.-I.; Hayashi, T.; Nakamura, K.; Murayama, K.; Era, S., The redox states of serum and synovial fluid of patients with temporomandibular joint disorders. *Jpn. J. Physiol.***2003,** *53* (5), 351-355.

9. Era, S.; Kazuo, K.; Imai, H.; Nakamura, K.; Hayashi, T.; Sogami, M., Age-related change in redox state of human serum albumin. *BBA-Protein Struct. Molec. Enzym.* **1995,** *1247* (1), 12-16.

10. Imai, H.; Hayashi, T.; Negawa, T.; Nakamura, K.; Tomida, M.; Koda, K.; Tajima, T.; Koda, Y.; Suda, K.; Era, S., Strenuous exercise-induced change in redox state of human serum albumin during intensive kendo training. *Jpn. J. Physiol.* **2002,** *52* (2), 135-140.

11. Beal, M. F., Oxidatively modified proteins in aging and disease. *Free Radic. Biol. Med.* **2002,** *32* (9), 797-803.

12. Guedes, S.; Vitorino, R.; Domingues, R.; Amado, F.; Domingues, P., Oxidation of bovine serum albumin: identification of oxidation products and structural modifications. *Rapid Commun. Mass Spectrom.* **2009,** *23* (15), 2307-2315.

13. Schöneich, C.; Williams, T. D., Cu (II)-catalyzed oxidation of β-amyloid peptide targets His13 and His14 over His6: detection of 2-Oxo-histidine by HPLC-MS/MS. *Chem. Res. Toxicol.* **2002,** *15* (5), 717-722.

14. Bridgewater, J. D.; Lim, J.; Vachet, R. W., Transition Metal− Peptide Binding Studied by Metal-Catalyzed Oxidation Reactions and Mass Spectrometry. *Anal. Chem.* **2006,** *78* (7), 2432-2438.

15. Davies, K.; Delsignore, M.; Lin, S., Protein damage and degradation by oxygen radicals. II. Modification of amino acids. *J. Biol. Chem.* **1987,** *262* (20), 9902-9907.

16. Dubinina, E.; Gavrovskaya, S.; Kuzmich, E.; Leonova, N.; Morozova, M.; Kovrugina, S.; Smirnova, T., Oxidative modification of proteins: oxidation of tryptophan and production of dityrosine in purified proteins using Fenton's system. *Biochemistry* **2002,** *67* (3), 343-350.

17. Inoue, K.; Garner, C.; Ackermann, B. L.; Oe, T.; Blair, I. A., Liquid chromatography/tandem mass spectrometry characterization of oxidized amyloid beta peptides as potential biomarkers of Alzheimer's disease. *Rapid Commun. Mass Spectrom.* **2006,** *20* (5), 911-918.

18. Temple, A.; Yen, T.-Y.; Gronert, S., Identification of specific protein carbonylation sites in model oxidations of human serum albumin. *J. Am. Soc. Mass Spectrom.* **2006,** *17* (8), 1172-1180.

19. Finch, J. W.; Crouch, R.; Knapp, D.; Schey, K., Mass spectrometric identification of modifications to human serum albumin treated with hydrogen peroxide. *Arch. Biochem. Biophys.* **1993,** *305* (2), 595-599.

20. Kowalik-Jankowska, T.; Ruta, M.; Wiśniewska, K.; Łankiewicz, L.; Dyba, M., Products of Cu (II)-catalyzed oxidation in the presence of hydrogen peroxide of the 1–10, 1–16 fragments of human and mouse β-amyloid peptide. *J. Inorg. Biochem.* **2004,** *98* (6), 940-950.

21. Wang, X.; Brown, D. R., Synuclein proteins and their roles as metal binding proteins. In *Metals and Neurodegeneration*, Research Signpost: 2010; pp 177-210.

22. Brown, J. R., Serum albumin: amino acid sequence. In *Albumin: Structure, Function and Uses*, Elsevier: 1977; pp 27-52b.

23. Peters Jr, T., Serum albumin. In *Advances in protein chemistry*, Elsevier: 1985; Vol. 37, pp 161-245.

24. Wratten, M. L.; Sereni, L.; Tetta, C., Oxidation of albumin is enhanced in the presence of uremic toxins. *Ren. Fail.* **2001,** *23* (3-4), 563-571.